EUROPEAN COMMISSION

European Research Area

CArbon-14 Source Term

CAST

Final report on ^{14}C release from zirconium alloy in highly alkaline conditions (D3.17)

Author(s):

Sébastien Caes, Frank Druyts and Wouter Van Renterghem

Date of issue of this report: 20/11/2017

The project has received funding from the European Union's Seventh Framework Programme for research, technological development and demonstration under grant agreement no. 604779, the CAST project'		
Dissemination Level		
PU	Public	**x**
RE	Restricted to the partners of the CAST project	
CO	Confidential, only for specific distribution list defined on this document	

CAST – Project Overview

The CAST project (CArbon-14 Source Term) aims to develop understanding of the potential release mechanisms of carbon-14 from radioactive waste materials under conditions relevant to waste packaging and disposal to underground geological disposal facilities. The project focuses on the release of carbon-14 as dissolved and gaseous species from irradiated metals (steels, Zircaloys), irradiated graphite and from ion-exchange materials as dissolved and gaseous species.

The CAST consortium brings together 33 partners with a range of skills and competencies in the management of radioactive wastes containing carbon-14, geological disposal research, safety case development and experimental work on gas generation. The consortium consists of national waste management organisations, research institutes, universities and commercial organisations.

The objectives of the CAST project are to gain new scientific understanding of the rate of re-lease of carbon-14 from the corrosion of irradiated steels and Zircaloys and from the leaching of ion-exchange resins and irradiated graphites under geological disposal conditions, its speciation and how these relate to carbon-14 inventory and aqueous conditions. These results will be evaluated in the context of national safety assessments and disseminated to interested stakeholders. The new understanding should be of relevance to national safety assessment stakeholders and will also provide an opportunity for training for early career researchers.

For more information, please visit the CAST website at:
http://www.projectcast.eu

CAST		
Work Package: 3	CAST Document no. :	Document type:
Task: 3.3	CAST-2017-D3.17	R
Issued by: SCK•CEN		Document status:
Internal no. :		Final

Document title
Final report on ^{14}C release from zirconium alloy in highly alkaline conditions

Executive Summary

Due to its long half-life (5730 years) and its high mobility in the geosphere and biosphere, ^{14}C is a critical radionuclide in the safety assessment of the geological disposal of high level nuclear waste. The international project CAST (Carbon-14 Source Term), which is partially funded through the Euratom Seventh Framework Programme, aims at understanding the generation and release of ^{14}C containing species by corrosion or waste degradation processes in conditions relevant for waste packaging and geological disposal. The aim of the work at SCK•CEN in the framework of Work Package 3 of the CAST project was to investigate the release of ^{14}C from Zircaloys representative for the claddings of the fuel of Belgian nuclear power plants and the ^{14}C speciation in a cementitious environment, which is relevant for the Belgian Supercontainer design, as perceived for the geological disposal of high level waste.

Both irradiated and unirradiated Zircaloy-4 samples, representative of the fuel cell claddings of Belgian nuclear power plants, were studied at the SCK•CEN.

The unirradiated sample was a rod of Zircaloy-4 which was cut in smaller pellets. The total nitrogen content of this sample showed the presence of 17 to 25 µg/g in the bulk, which is 2 to 4 times lower than the 40 to 80 µg/g expected from the specification sheets. As the activation of ^{14}N ($^{14}N(n,p)^{14}C$) is the most probable production of ^{14}C in Zircaloy-4, the concentration after irradiation should be lower. Calculation showed that the ^{14}C activity would be 13300 to 19600 Bq/g of irradiated Zircaloy-4.

The irradiated sample was the upper part of a fuel cell cladding originating from Belgian nuclear reactors. It was also cut in smaller pieces to perform corrosion tests and

metallography analysis. γ-ray spectrometry revealed that the activity was mainly emitted by ^{106}Ru, ^{60}Co, ^{144}Ce, ^{137}Cs, ^{125}Sb, ^{95}Zr and ^{95}Nb.

Metallography analysis was performed on both irradiated and unirradiated samples to analyse the influence of radiation on the metallic structure. The structure of the unirradiated sample possessed defects such as dislocation lines. Precipitates were also present and the main ones were identified as Laves phases, composed of $Zr(Fe,Cr)_2$. A second type of precipitates with a needle- or platelet-like structure was found with a possible ZrC phase. Two different irradiated samples were analysed by TEM: the cladding representative of samples used for the static corrosion tests and the end-plug representative of samples used for the accelerated corrosion tests. The rolling process needed to produce the cladding induced texture. It results in a narrow lath structure, that is different from the structure in the unirradiated Zircaloy-4, but dislocation lines are still present. The main effect of the neutron irradiation was the presence of small dislocation loops. The structure of the end-plug part is different from the cladding (no rolling process) and equiaxed grains are present. The Laves phase precipitates were still present and, due to neutron activation, a low amorphisation of those precipitates was observed.

To obtain information on the behaviour of Zircaloy-4 in real geological conditions, static corrosion tests were performed. Accelerated corrosion tests were performed to obtain some indication of the corrosion mechanism and the light carbon molecules formation in a shorter reaction time. A saturated portlandite $Ca(OH)_2$ aqueous solution was used, with a pH close to 12.5, which is representative for the geological disposal conditions. In order to increase the corrosion rate, 0.5 M of $CaCl_2$ was also added to the electrolyte solution inducing pitting corrosion. This addition of chloride was only done for some accelerated corrosion tests.

The vial for the static corrosion tests was composed of a PEEK liner-coated steel vial possessing an internal volume of 50 cm^3 filled with 35 cm^3 of electrolyte. After closing the test cell airtightly with a lid, the whole setup was stored behind a lead wall for 195 days.

The vial for the accelerated corrosion tests contained three electrodes immersed in the electrolyte under anaerobic conditions at room temperature and atmospheric pressure. The reference electrode was an Ag/AgCl home-made electrode, the counter electrode was a

platinum one while the working electrode was the unirradiated or irradiated Zircaloy-4 sample embedded in a resin and polished to obtain a fresh non-oxidized surface. A metallic wire glued on the back of the sample (before resin embedding) was used for electrical connection. After assembly, a gas tightness tests revealed a very small decrease of the pressure from 1.1 to 1.07 bar which is negligible for our tests.

Before starting the accelerated corrosion tests, polarisation curves were recorded to have information on the electrochemical behaviour of the Zircaloy-4 samples. Even if those curves were only recorded once, irradiation seemed to induce some difference in the sample behaviour such as the stabilisation of the passivation layer or the shift of the corrosion potential to more a reductive potential. The addition of chloride led to a huge increase of the current at a potential called pitting potential, where the pitting corrosion appears. Based on these curves, specific potentials were chosen to perform the accelerated corrosion tests.

Carbon speciation was analysed by total organic / inorganic carbon content (TIC/TOC), ion chromatography (IC) and liquid scintillation counting (LSC) for the liquid phase and by gas chromatography for the gas phase. Unfortunately, it was difficult to obtain reliable information of the total inorganic and organic compounds in solution due to the very low expected concentration of carbon-based compounds coming from corrosion process and due to the presence of some contamination, which were very difficult to avoid. The activity of ^{14}C was also difficult to obtain due to the presence of other radionuclides and due to the low concentration of ^{14}C released during corrosion. A separation from all other radionuclides should be performed to be able to determine the ^{14}C activity.

Concerning the analysis of the gas phase by GC, no carbon-based compounds could be detected after the accelerated corrosion tests in saturated portlandite, while a big peak of methane was observed in the presence of chloride. For the static corrosion tests, methane, ethene and maybe CO_2 were produced. Methane is the main carbon-based gas present in the gas phase. Considering the gas production, an approximation of the corrosion rate was calculated and led to 57 to 84 nm per year which looks very high compared to the conservative corrosion rate of 20 nm per year.

List of Contents

1 Introduction

In the safety assessment of the geological disposal of high level nuclear waste, ^{14}C is a critical radionuclide because of its long half-life (5730 years) and its high mobility in the geosphere and biosphere. ^{14}C will be released from the waste as a result of corrosion or waste degradation processes. The speciation of ^{14}C will depend on the speciation of its precursor (it is generally assumed that the main precursor of ^{14}C is ^{14}N, but there are ^{14}C production pathways with ^{13}C and ^{17}O as precursors) and the chemical conditions in the repository. The question also arises whether the chemical bond of the precursor is maintained during irradiation.

The international project CAST (Carbon-14 Source Term), which is partially funded through the Euratom Seventh Framework Programme, aims at understanding the generation and release of ^{14}C containing species in conditions relevant for waste packaging and geological disposal. The project is focusing on ^{14}C releases from irradiated metals (steels and zirconium alloys), irradiated graphite, and spent ion-exchange resins, as dissolved and gaseous species. The results of these studies will be transferred to the national programmes where they will be used for further development of the national safety cases. Within the CAST project, Work Package 3 focuses on irradiated Zircaloys (Zircaloy-2, Zircaloy-4 and M5) representative of the fuel cell claddings of nuclear power plants.

The aim of the work at SCK•CEN in the framework of Work Package 3 of the CAST project was to investigate the release of ^{14}C from Zircaloys representative for the claddings of the fuel of Belgian nuclear power plants and the ^{14}C speciation in a cementitious environment, which is relevant for the Belgian Supercontainer design, as perceived for the geological disposal of high level waste. To achieve this, we designed static and accelerated corrosion tests, and we obtained irradiated reference material representative for the fuel cladding at end-of-life in the Belgian power plants. The static tests consisted of exposing the sample to a representative environment (anaerobic, high pH) for several months without applying any potential, while in the shorter accelerated tests an electrochemical setup was used to fix the potential of the sample at a more anodic value than the corrosion potential, in order to accelerate the corrosion processes. This report gives an overview of the entire

experimental programme carried out at SCK•CEN in the framework of WP3 of the CAST project. It contains information on the samples (both unirradiated and irradiated), the properties of the samples, the results from the corrosion tests, and the results from the speciation studies.

2 Method

2.1 *Materials*

SCK•CEN has at its disposal both unirradiated and irradiated Zircaloy-4 (Zry-4) samples. In this section we will discuss the properties and history of these samples.

2.1.1 Unirradiated material

The unirradiated sample is a 98 mm long rod with a diameter of 12 mm (Figure 1) from which samples were cut in small discs for the accelerated corrosion tests.

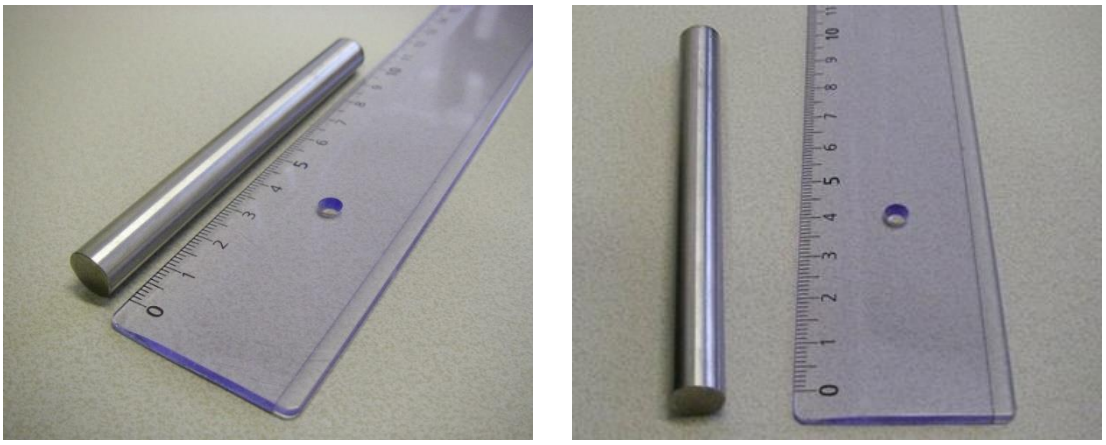

Figure 1. The unirradiated Zircaloy-4 specimen before cutting.

The chemical composition of this sample is given in Table 1. This information is obtained from the 'Material quality control certificate' [ASTM, 2002]. As the amount of nitrogen in the sample is not known accurately, it was measured experimentally. Indeed, the

determination of the initial nitrogen content in metals is desirable to realistically estimate the ^{14}C production after irradiation campaigns.

Table 1. Chemical composition of an unirradiated Zircaloy-4 specimen.

wt.%				µg/g					
Sn	Cr	Fe	Zr	C	Hf	Si	W	O	N
1.2-1.7	0.07-0.13	0.17-0.24	Bal.	270	100	120	100	1000-1400	<50

2.1.2 Irradiated material

Irradiated materials are representative for end-of-life conditions in nuclear power plants (claddings of the fuel) and thus offer the advantage of a realistic input of ^{14}C release into the national safety cases (WP6). The Zircaloy-4 specimens originate from Belgian nuclear reactors (Tihange and Doel) and the (cutting) scheme of the cladding (reference F-6678) used for the CAST project is shown in Figure 2. First, a cladding piece that was in contact with the fuel was chosen for corrosion analyses (Figure 2). Nevertheless, the dose rate of this sample was too high (up to 10 mSv/h at 10 cm) to be easily handled.

For this reason, the upper part of the fuel tube, called F6678-R4, was chosen for the corrosion tests, even if the contact dose rate (through a LaCalhene box) still reached 8 mSv/h.

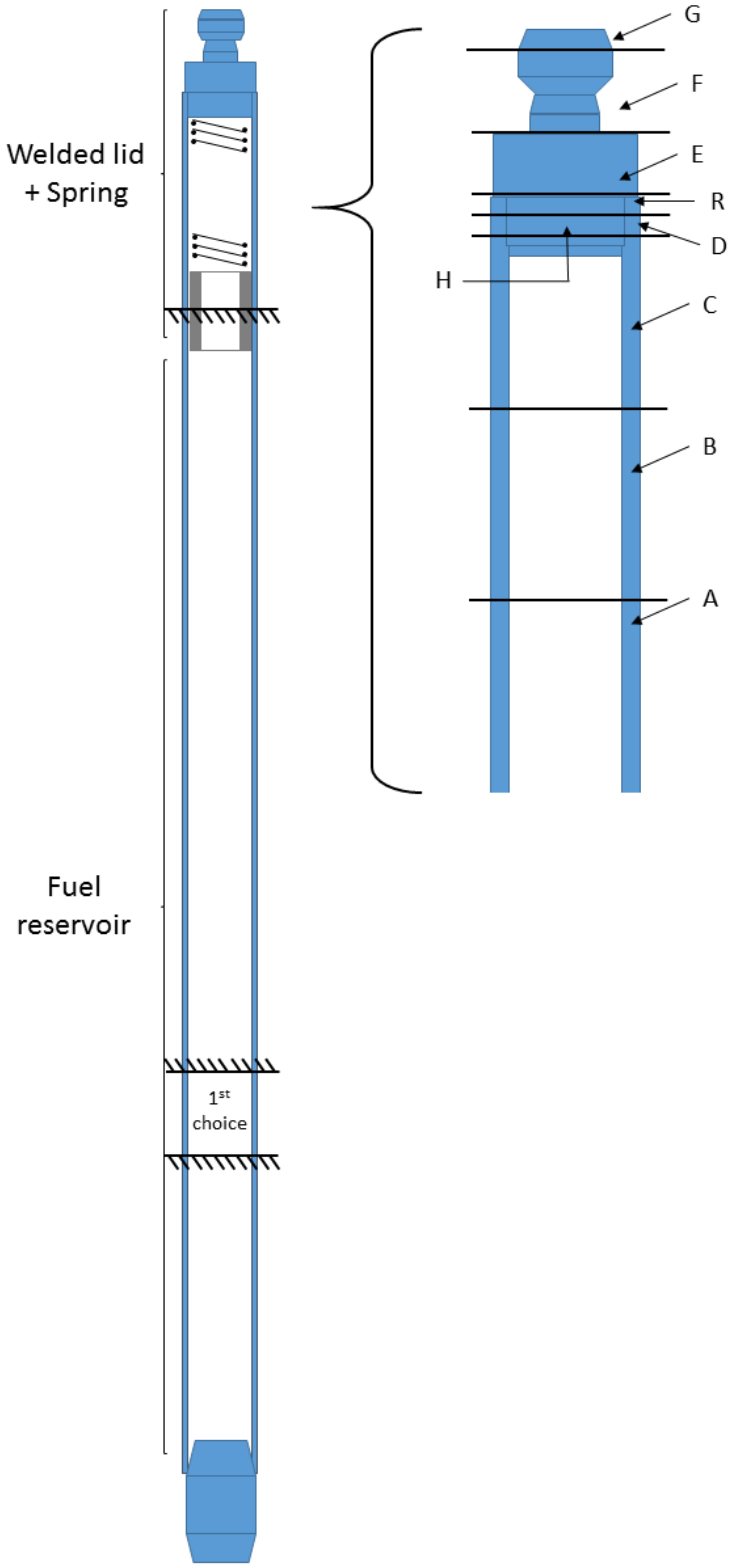

Figure 2. Cutting scheme of the Zircaloy-4 cladding (the letters in the right drawing indicate the indices of the sub-pieces cut from the sample as mentioned in Figure 4 and Table 2).

2.1.2.1 Cutting samples

The upper part of the fuel tube was cut in a hot-cell to obtain a piece possessing a height of 80 mm (Figures 2 and 3(A)). A plenum and a spring present inside this cut piece were removed before cutting them in smaller pieces, which were used for corrosion tests (Figure 3(B)).

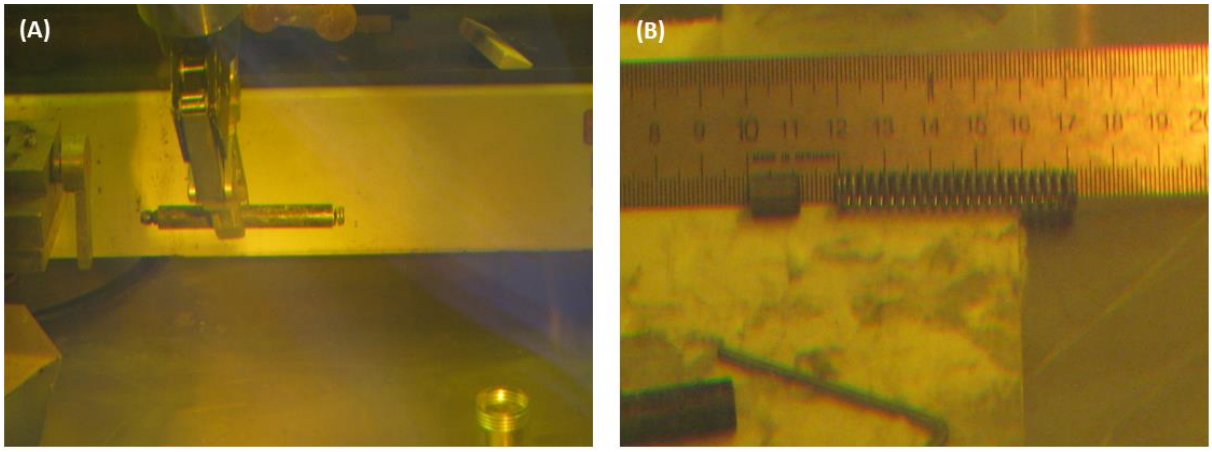

Figure 3. Picture of (A) the F6678-R4 sample before cutting and (B) the spring and the plenum present inside the Zircaloy-4 cladding.

As shown in Figure 2 and Figure 4, sample F6678-R4 was cut in smaller pieces for the corrosion tests. Dimensions of the cut pieces are described in Table 2. Pieces A, B and C were used for static tests and piece E, the thicker disk, was used for the accelerated corrosion tests.

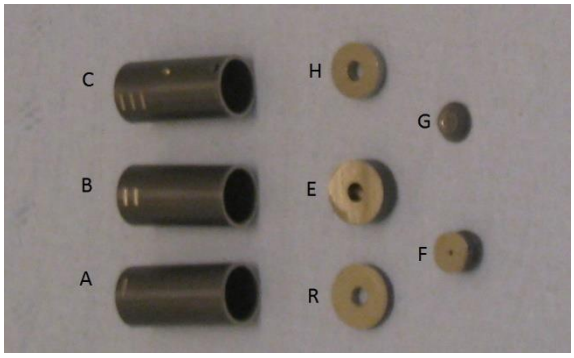

Figure 4. Photographs of the cut F6678-R4 Zircaloy-4 cladding.

Table 2. Dimensions and weight of cut F6678-R4 Zircaloy-4 samples.

Sample	Dimensions (mm)			Weight (g)
	Length	Inner diameter	Outer diameter	
F6678-R4-A	20.87	8.4	9.62	2.3251
F6678-R4-B	20.18	8.4	9.63	2.2374
F6678-R4-C	20.3	8.4	9.64	2.2499
F6678-R4-D	1.9	8.4	9.64	0.2114
F6678-R4-E	4.32	~0.5	9.66	1.8334
F6678-R4-F	4.18	~0.5	~6	0.6216
F6678-R4-G	1.93	~0.5	~6	0.2271
F6678-R4-H	2.74	~2.8	~8.35	0.7734
F6678-R4-R	1.97	~3	9.66	0.7795

A 'cooking' step was performed on these samples to decrease their activity. This procedure consisted of washing the Zircaloy-4 pieces in 8 M nitric acid under reflux for 6.5 hours, followed by rinsing in 1 M nitric acid. After this treatment and after drying, the measurement of the activity (Table 3) shows that the contact dose rate was acceptable to work in a fume hood.

Table 3. Contact dose rate of cut Zircaloy-4 sample after the cooking step (14/07/2016).

Sample	Contact dose rate (µSv/h ; 14/07/2016)
F6678-R4-A	900
F6678-R4-B	450
F6678-R4-C	400
F6678-R4-D	190
F6678-R4-E	270
F6678-R4-F	110
F6678-R4-G	60
F6678-R4-H	180
F6678-R4-R	170

2.2 Nitrogen content analysis

The nitrogen content of unirradiated samples was measured by using an inert gas fusion method with a LECO TC436 model analyser. The sample was cut into a small cube of ~0.5 g and stored in acetone until the analysis. Before the sample analysis, at least 3 nitrogen blanks were measured and the results were normalised with the blanks. The instrument was calibrated using two certified reference materials of different concentration: AR649 with a nitrogen concentration of 44 µg/g and an oxygen concentration of 1200 µg/g (Alpha Ressources) and AR503-653 with a nitrogen concentration of 70 µg/g (LECO). These references were used to check the lowest point, the linearity of the calibration and the calibration factor to be applied. The reported lower limit of detection of the method is approximately 1 µg/g for N.

For the analysis, the sample was placed inside a graphite crucible and held between the upper and lower electrodes of an impulse furnace. A high current passed through the crucible, increasing the inner temperature (> 2500 °C), which eventually led to the melting of the sample. Gaseous compounds generated in the furnace were released into a flowing inert gas stream (argon or helium). The gas stream was sent to an appropriate infrared detector: a thermal conductivity detector for the analysis of nitrogen. At least four replicates were realized for each sample.

2.3 γ-ray spectrometry

For γ-ray spectrometry analyses, two HPGe detectors were used, one from Canberra and one from Ortec. The HPGe-detectors were energy and efficiency calibrated over an energy range of 60 to 2000 keV using a γ-ray reference solution with a mixture of 10 different radionuclides. The ORT1 detector was calibrated using a 9ML01ELMA60 (2014) standard solution from LEA (Laboratoire Etalons d'Activité). The CAN2 detector was calibrated using a 12ML01ELMA60 standard source from LEA.

2.4 *Metallographic analysis*

2.4.1 Samples preparation

Two samples were provided for the microstructure analysis of the Zircaloy-4: an unirradiated Zircaloy-4 rod and an irradiated F6678-R4-R sample, which contained both material from the cladding and the end plug. A sample was prepared from both end plug and cladding.

The activity of the irradiated sample was relatively low and its preparation was performed in a fume hood.

A slice of about 0.6 mm thick was cut from the samples with a Struers Accutom 50 cutting instrument. This slice was mechanically polished on SiC paper with grit sizes 500, 1200 and 4000. When the thickness of the slice was reduced below 0.3 mm, five discs of 3 mm in diameter were punched out of the slice. These discs were then polished further on SiC paper until the thickness was reduced to 0.1 mm.

The final step in the sample preparation was electrochemical double jet polishing with a Struers Tenupol-3 instrument. The electrolyte used consisted of 5% perchloric acid and 95% methanol. The polishing electrolyte was cooled to -30 °C and a voltage of 25 V was applied. The samples used for SEM analysis were polished for 10 seconds, while the samples used for TEM analysis were polished until perforation.

The TEM is a JEOL 3010 microscope operating at 300 kV. Bright field, dark field and selected area electron diffraction were used to determine the defect structure and precipitates. Energy dispersive X-ray spectroscopy (EDS) was applied for the qualitative determination of the composition of the precipitates. It should be noted that during the EDS measurement a small amount of carbon is deposited on the surface of the sample. Moreover, when analysing small precipitates, it could not be avoided that part of the signal is generated in the steel adjacent to or on top or below the precipitate. Therefore, it is not possible to obtain a quantitative composition of the observed precipitates and carbides, but qualitative statements are possible. It should be noted that the EDS detector is not shielded and radiation from the sample is detected. However, because of the low activity of the samples,

the increase in background radiation is minimal and qualitative measurements could still be performed.

The SEM is a JEOL JSM 6610 microscope used for the determination of the grain size. Even though the polishing conditions may not be optimal to reveal the grain structure, it was possible to determine the grain structure under the electron beam of the SEM. The best results were obtained in the back-scattered electron (BSE) images, where the contrast is mainly induced by the atomic weight. Light elements scatter fewer electrons than heavy elements and are darker in the BSE images.

2.4.2 Grain size determination

The grain size of each material was determined from the BSE images of the samples after electrochemical polishing for 10 s. The grain size is determined in accordance with the ASTM standard E112-95. The grain size number (G) is defined as:

$$N=2^{G-1} \quad (1)$$

Where N is the number of grains per inch² at a magnification of 100× which equals the number of grains per mm² at a magnification of 1× divided by 15.50. This number is obtained by placing a circle of a known diameter on the BSE images and by counting the number of grains within the circle. The grains that intersect the circle count for half a grain. As the SEM images were calibrated, the actual diameter of the circle could be determined and the average grain size could be calculated. This value is used to calculate the number of grains per mm² and the grain size number.

2.5 *Corrosion experiments*

Two types of corrosion tests were performed at SCK•CEN: (i) static corrosion tests (leaching tests) to investigate a more realistic corrosion behaviour and associated ^{14}C release

and speciation, and (ii) accelerated corrosion tests (polarised corrosion tests) with an applied potential, which mainly serves for preliminary speciation determination. These corrosion tests were performed under anaerobic and highly alkaline conditions to mimic geological disposal conditions.

2.5.1 Choice of the electrolyte

During the WP2 and WP3 technical meeting in Switzerland (27-28 May 2015), a solution of NaOH at pH 12 at room temperature was recommended for the static tests. However, all participants were allowed to use their own electrolyte. For this reason SCK•CEN decided to use a saturated portlandite $Ca(OH)_2$ solution for its experiments. The main reason is that portlandite is more representative for the Belgian waste repository design. The artificial pore water was prepared in a glove box under anaerobic conditions and degassed with nitrogen to reduce the risk of dissolving environmental $^{14}CO_2$, which would lead to an artefact. The risk of calcite ($CaCO_3$) precipitation cannot be excluded, as shown in our calculations (see Appendix 1). Indeed a concentration of 12.6 µg/L of CO_3^{2-} is enough to enhance $CaCO_3$ precipitation.

A second type of electrolyte was used exclusively for the accelerated (polarised) corrosion tests in addition to pure portlandite pore water. This electrolyte was the same as described above, with the addition of 0.5 M of $CaCl_2$ (1 M of chloride) in order to promote pitting corrosion. The idea was to increase the production of carbon species, making their detection easier.

2.5.2 Description of corrosion setups and sampling (gas and liquids)

2.5.2.1 Static corrosion tests

Static corrosion tests, also called leaching corrosion tests, were carried out with irradiated samples, in order to have a realistic view on the ^{14}C release rate and ^{14}C speciation.

Figure 4 shows a diagram of the experimental setup. The Zircaloy-4 sample was placed in contact with portlandite pore water (pH ~12.5) inside a PEEK liner inserted in a steel vial. Figure 5 shows photographs of the steel vials before and after assembly. The internal volume of the steel vials was 50 cm³. The vials were filled with 35 mL of saturated portlandite ($Ca(OH)_2$) pore water, before adding the Zircaloy-4 sample. Afterwards, the lid was screwed to the vial to make it airtight. All these manipulations were performed in a glove bag in a nitrogen atmosphere to ensure anaerobic conditions. The glove bag is shown in Figure 6.

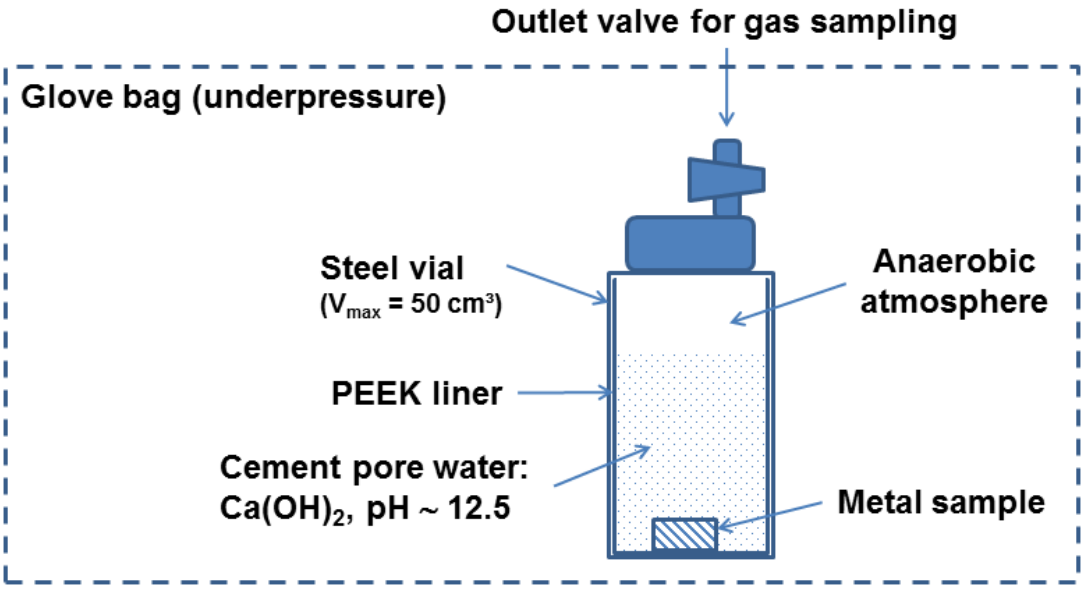

Figure 4. Layout of the static test setup in a glove bag under inert atmosphere.

Figure 5. Photographs of the static test setups (A) before assembly and (B) after assembly.

Figure 6. The glove bag placed in a fume hood.

Following the static tests, which lasted for approximately 6.5 months (195 days), gas and liquid samples were taken and analysed for carbon species. The gas sampling was performed with a 500 µL gas tight syringe with a 5 cm long needle (Figure 7). After sampling 500 µL of gaseous phase from the test cell, the needle was stuck into a septum and the syringe was entirely placed in a small solid transport box, in order to avoid displacement

of the syringe's piston. The syringe was then transferred to a gas chromatograph for analysis (for a description of the gas chromatograph, see Section 2.6.1). After taking the gas samples, the lid of the test cell was removed and liquid samples were taken for further analyses (liquid scintillation counting, ion chromatography, TIC/TOC).

Figure 7. Gas tight syringe with removable needle.

2.5.2.2 Accelerated corrosion tests

Accelerated corrosion tests, also called polarised corrosion tests, were performed with both unirradiated and irradiated samples. The tests consisted of two parts. In a first phase, polarisation curves were recorded in order to examine the electrochemical behaviour of the samples in the investigated environment. Then, in a second phase, a pre-determined potential (derived from the polarisation curve) that would result in accelerated, active corrosion, was applied to the sample.

Manufacturing of the electrodes

The working electrode was manufactured by gluing a steel wire, serving as an electrical connection, to the back of the cut Zircaloy-4 samples (Figure 8(A)). The glue used was a conductive silver epoxy (type CW2400, Circuitworks). Then, the specimens were embedded in a resin under a fume hood (Figure 8(B)). Finally, specimens were mechanically wet-ground, with successively finer SiC papers, down to 500 grit, and then cleaned with double distilled water and finally left to dry in an argon atmosphere (Figure 8(C)).

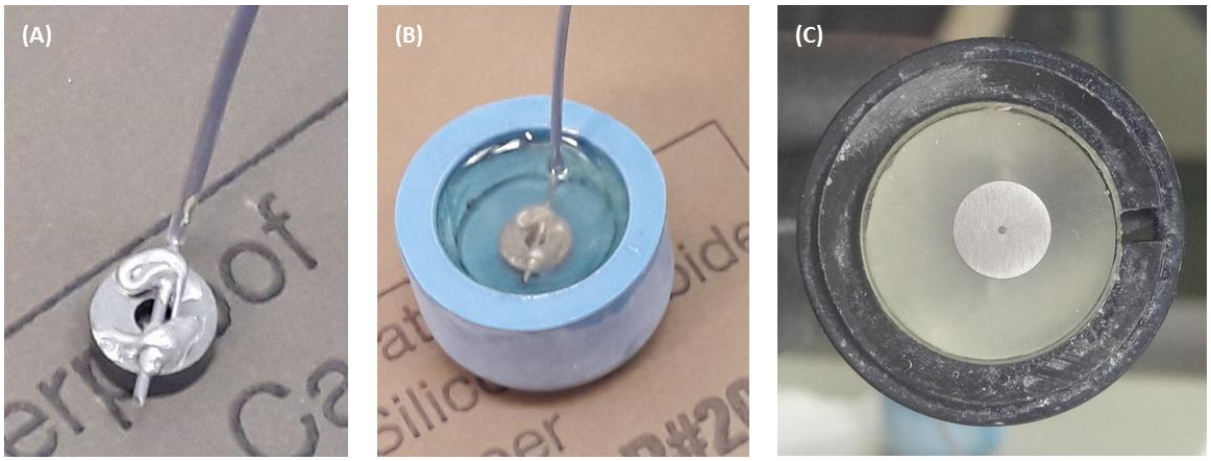

Figure 8. Preparation of the irradiated Zircaloy-4 sample (F6618-R4-E) for the accelerated corrosion tests. (A) Gluing step, (B) embedding step and (C) polishing step.

Electrochemical cells

The test cell consisted of a glass vial with an internal volume of approximately 1450 mL and containing three electrodes attached to the lid: (1) the working electrode (Zircaloy-4 sample), (2) the platinum counter electrode, and (3) the in-house made Ag/AgCl reference electrode. These electrodes constitute a traditional three-electrode setup described in the general literature on electrochemistry [TAIT, 1994]. Figure 9 shows a schematic representation of the test setup and Figure 10 shows a photograph of the test cell equipped with the three electrodes.

The gas tightness of the cell was checked by using rubber sealing between the cell lid and cell body and filling the cell with helium. The pressure in the glass cell was set to 1.1 bar. During the tightness test, which lasted for two months, the cell pressure and ambient pressure and temperature were monitored (experimental setup in Figure 11). The results are shown in Figure 12. After two months, the pressure inside the cell had decreased from 1.10 to 1.07 bar, which is negligible considering the short duration of each test (a few hours to a few days). The sharp intermediate drop in pressure indicates sensor replacement.

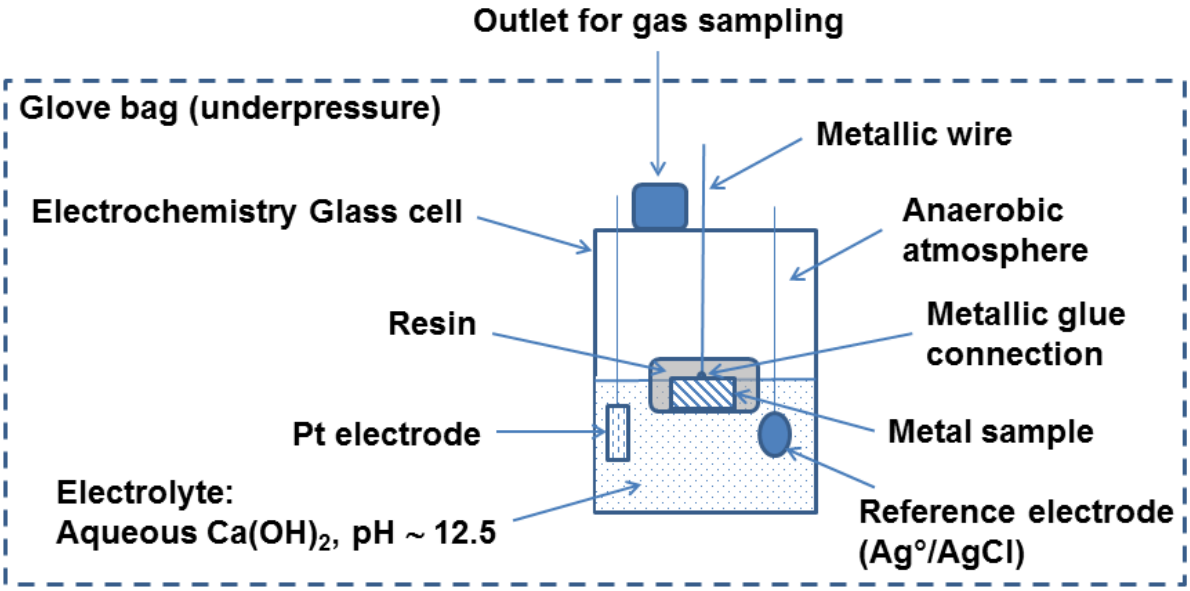

Figure 9. Layout of the accelerated corrosion test setup in a glove bag under inert atmosphere.

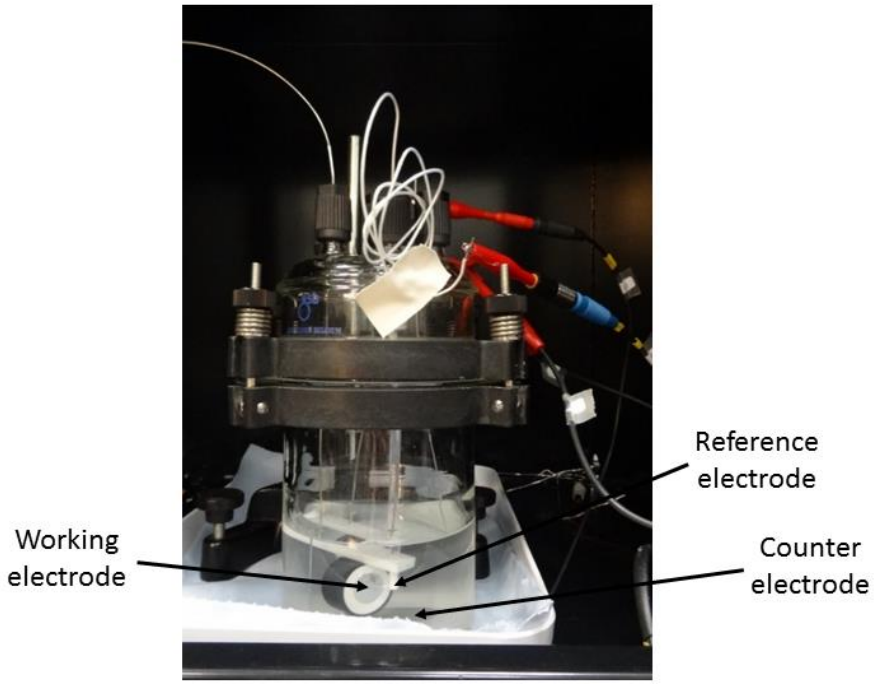

Figure 10. Photograph of the accelerated corrosion test setup.

Figure 11. Accelerated corrosion test cell setup.

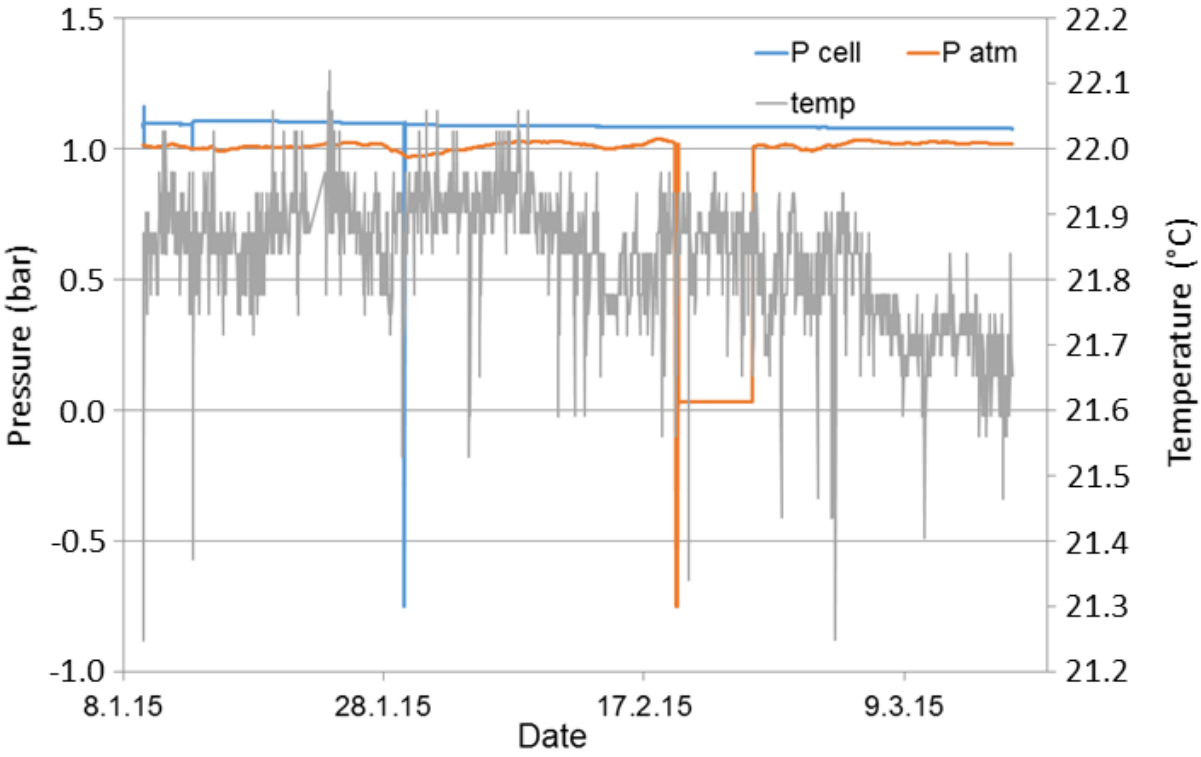

Figure 12. Temperature, internal- and external pressure profile during the gas tightness test.

2.6 *Determination of carbon speciation*

2.6.1 Technique used to analyse gases – Gas chromatography

To determine ^{14}C speciation, a gas chromatography system type Shimadzu GC-2010 Plus, tailor-made to our needs, was used (Figure 13). The gas sample can be injected manually ('1' on Figure 13) or automatically ('2' on Figure 13). In general, the main components of a GC system are an injector, a column and a detector (Figure 14), while the injected sample is transported through the system by a carrier gas.

Figure 13. Gas Chromatograph used for the determination/separation of ^{14}C gases produced from corrosion experiments. (1) Manual injection and (2) Auto sampling.

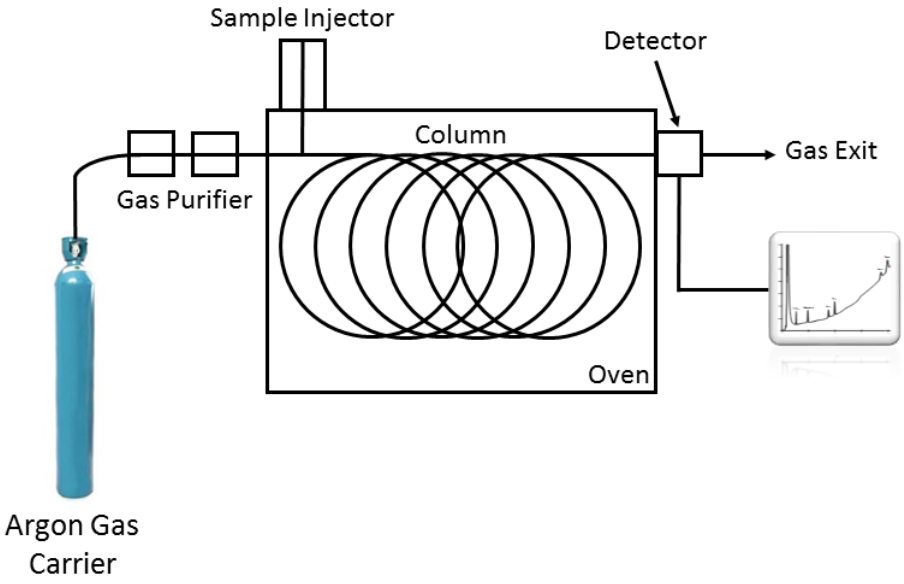

Figure 14. General scheme of a gas chromatograph.

The carrier gas used was pure Argon (N7.5, Air Products). To remove any residual impurities (H_2O, H_2, O_2, N_2, NO, NH_3, CO, CO_2 and CH_4), this gas passes through two gas purifiers (VICI Valco Instruments Co. Inc.) before entering the GC column.

The injector used is a split/splitless injector (Figure 15). The gas sample is introduced into the quartz liner of the injector with a syringe and through a septum. At the same time, the carrier gas flows through the column, out of the septum purge and out of the split when the split mode is used. In these conditions, only a fraction of the sample is injected into the column, depending on the split ratio (the split ratio is the ratio between the column flow and the total flow). In contrast, in splitless mode, the entirety of the sample reaches the column.

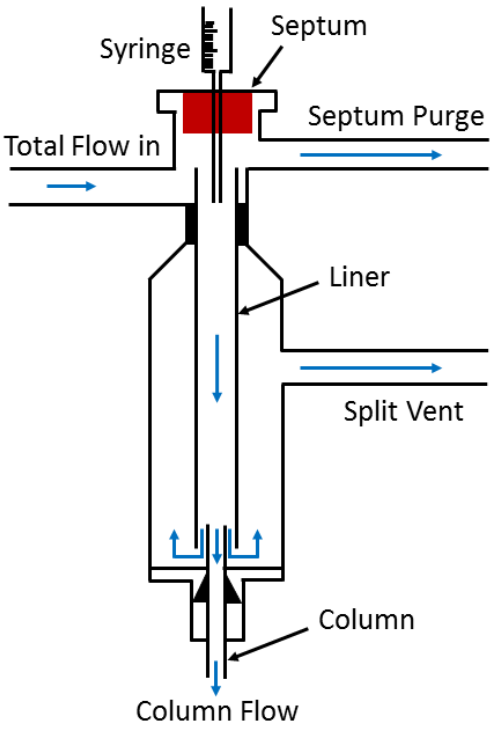

Figure 15. Scheme of a split/splitless GC injector.

Two columns are available at SCK•CEN: a ShinCarbon ST composed of high surface area carbon molecular sieves (Figure 16) and a SH-RTX-1 which is a non-polar column composed of dimethyl polysiloxane. The first column has been developed for separating permanent gases, such as N_2, O_2, CO or CO_2, and mixtures of permanent gases and low hydrocarbons rapidly, without cryogenic cooling. It is a micropacked column with dimensions of 2 m length x 1.27 mm outer diameter x 1 mm inner diameter. The second column is a more universal one. It is a capillary column with dimensions of 30 m length x 0.53 mm inner diameter. The results presented in this report were obtained with the ShinCarbon ST column.

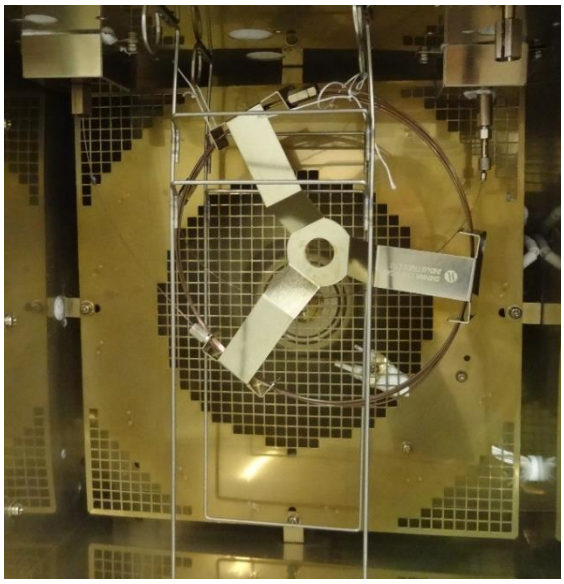

Figure 16. Picture of the ShinCarbon ST column in the furnace of the GC.

Detectors include a Flame Ionisation Detector (FID), a Barrier Discharge Ionisation Detector (BID), and a Pulsed Discharge Helium Ionisation Detector (PDHID). The operation of the FID is based on the detection of ions formed during combustion of organic compounds in a hydrogen flame. The generation of these ions is proportional to the concentration of organic species in the sample gas stream. The response of a FID is semi-universal: all hydrocarbons can be detected. The FID has a detection limit of approximately 1 µg/L. In a BID detector, a plasma is generated by applying a high voltage to a quartz dielectric chamber, in the presence of helium. Compounds that elute from the GC column are ionised by this He plasma, then captured with collection electrodes and described as peaks. The detection limit of the BID is approximately 500 ng/L. The most sensitive sensor available is the PDHID, which is shown schematically in Figure 17. The PDHID uses a stable, low powered, pulsed DC discharge in helium as an ionisation source. Compounds coming from the GC are ionised by high-energy photons from the helium discharge. These photons have enough energy (13.5 – 17.5 eV) to ionise all elements and compounds, with the exception of neon. The electrons resulting from this ionisation are focused towards the collector electrode by the bias electrodes. Changes in the measured current constitute the detector response. The helium must be 99.9995 % pure, otherwise impurities quench the ionisation of the helium atoms. The detection limit of the PDHID is 50 ng/L.

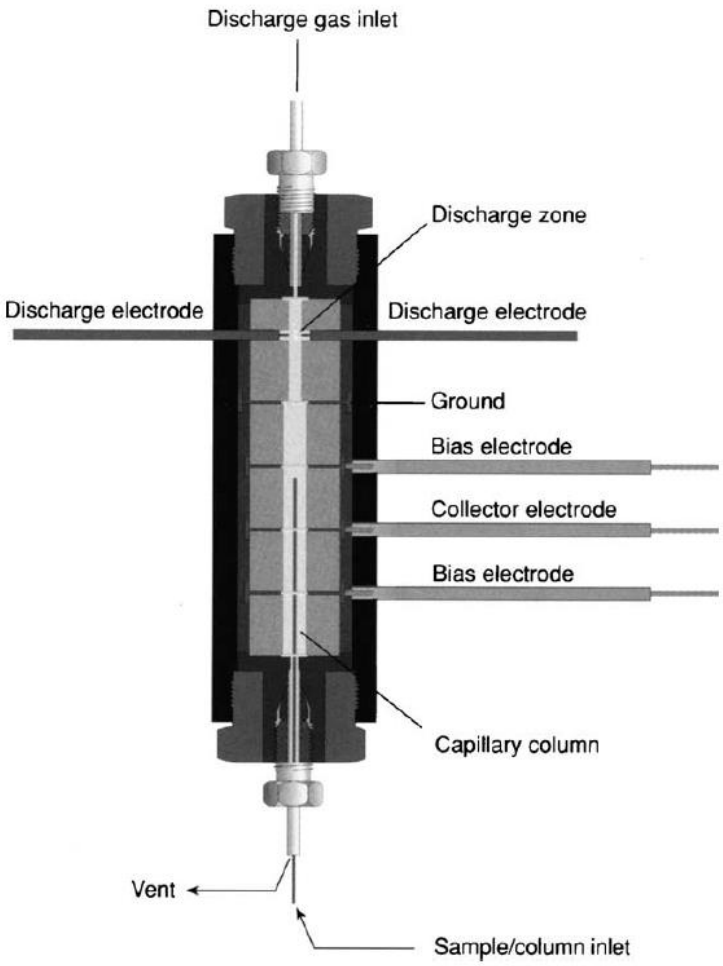

Figure 17. Scheme of a Pulse Discharge Helium Ionization Detector (PDHID).

2.6.1.1 Identification of peaks

The calibration of the GC consisted of two parts: (i) determination of the retention time of the most probable carbon compounds, and (ii) determination of the detection limit for each compound. The retention time is dependent on the type of column and the temperature of the furnace. Therefore it must be determined with calibration gases for each type of column (and furnace temperature). We focused on the most probable carbon-containing corrosion products from Zircaloy: methane, ethane, ethene, propane, propene and carbon dioxide. As both retention time and peak separation depend on the experimental parameters, we

conducted preliminary tests to optimise the peak definition for the above compounds. The results, i.e. the parameter values used for our analyses, are shown in Table 4.

Table 4. Parameters used for GC analysis.

Parameters	Values
Carrier gas pressure	350.5 kPa
Total flow	47.1 mL/min
Column flow	14.38 mL/min
Linear velocity	44.2 cm/sec
Purge flow	4.0 mL/min
Split ratio	2
Detector temperature	200°C
Initial column temperature	35°C
Ramp of temperature	15°C/min until 175°C 10°C/min until 200°C 5°C/min until 215°C 2.5°C/min until 235°C 10 min at 235°C

Figure 18 shows a chromatogram indicating the peaks of the most probable carbon compounds. The broad peak present at a lower retention time than methane can be attributed to nitrogen (matrix gas), to argon (carrier gas), and partially to oxygen (present in air during the injection). The slope in the background signal is due to an increase of temperature of the column.

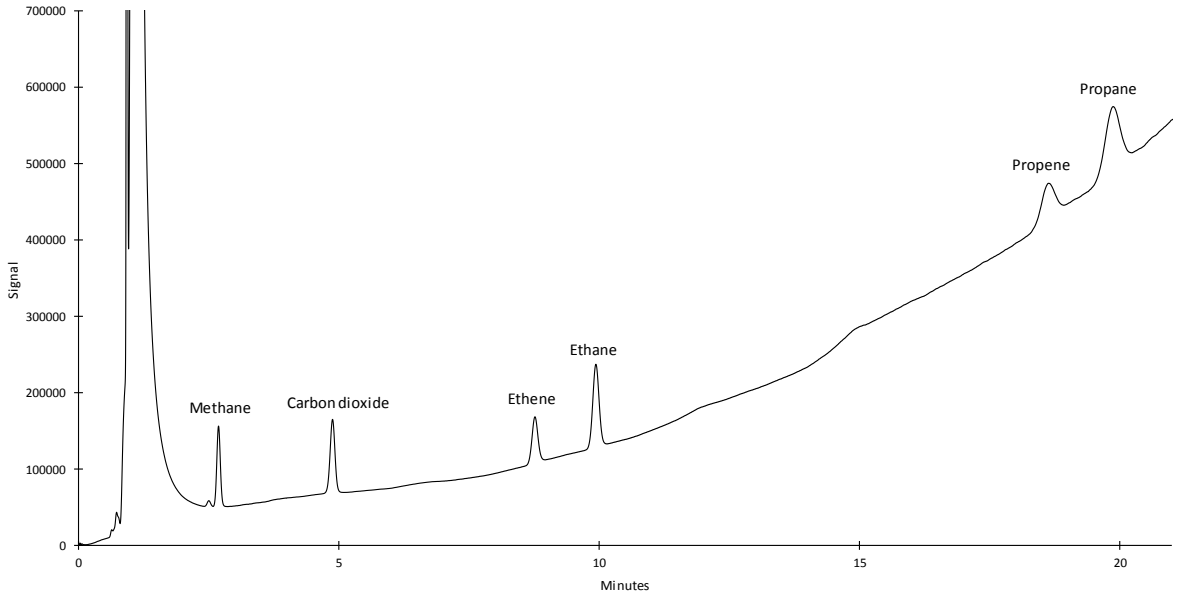

Figure 18. Gas chromatogram of a mixture of methane, carbon dioxide, ethene, ethane, propene and propane at a concentration of 10 µg/g.

Some peaks, besides methane, remain present at retention times between 2 and 3 minutes even when pure nitrogen is injected into the GC, as shown in Figure 19. Those peaks are ghost peaks coming from pressure changes in the injector and one of them appears at the same retention time as methane. To try to remove these peaks, the sample injection was performed exactly 20 seconds after piercing the septum of the injector with the syringe and 20 seconds before removing the syringe from the injector. This procedure resulted in a decrease of the intensity of the ghost peaks. Nevertheless they were still present, leading to an increase of the detection limit of methane. In addition, this procedure created new peaks close to 0.7 minutes of retention. These correspond to peaks of O_2 and N_2 from air accidentally injected during the piercing of the septum.

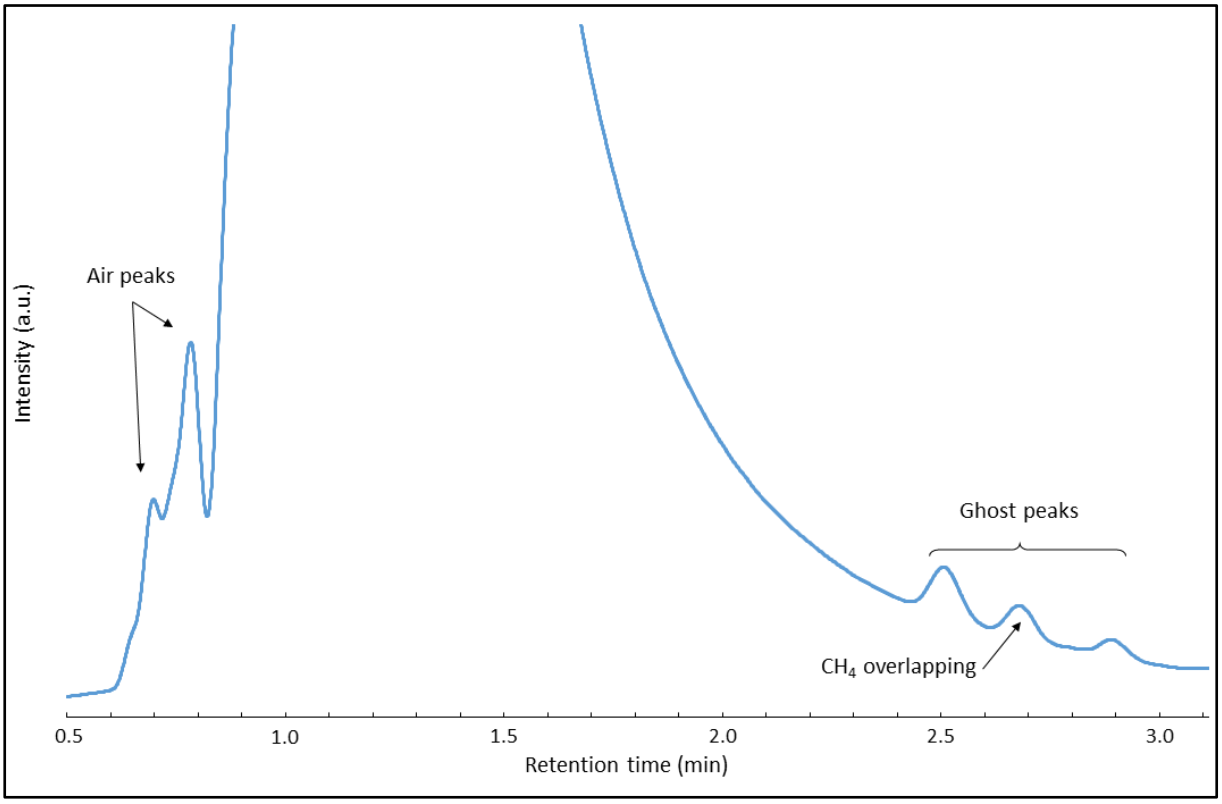

Figure 19. Magnification of the gas chromatogram between 0.5 and 3.1 minutes showing 'ghost peaks'.

2.6.1.2 Determination of the detection limits

The detection limits for the most probable carbon compounds were determined in two ways: (i) by means of the noise in the vicinity of the peak of interest, and (ii) by measuring standards of successive lower concentration until no (clear) peak was observed anymore. More details on the determination of the detection limits can be found in Appendix 2. Table 5 shows the reported limits, taken as the average value (rounded up) of the detection limits determined by means of both methods. The value for carbon dioxide, however, seems to be extremely high and has to be considered with care. In fact, it does not represent the practical detection limit. Because a direct injection technique of the sample is used, some ambient air will inevitably enter the column (and the detector), which results in carbon dioxide contamination.

Table 5. List of analysed gasses and their detection limits using the Shimadzu GC-2010 Plus with the PDHID detector.

Gasses	Reporting limits (µg/g)
Methane	0.4
Carbon dioxide	3
Ethene	0.2
Ethane	0.2
Propene	1.5
Propane	0.75

2.6.2 Techniques used to analyse liquid

2.6.2.1 Total (In)Organic Carbon

TOC (Total Organic Carbon) analysis is usually carried out by measuring total carbon (TC) and total inorganic carbon (TIC). Total organic carbon is then obtained by subtraction of TC and TIC. Total carbon is determined by injection of a small aliquot of sample into a furnace filled with a catalyst. All carbon products are oxidized to carbon dioxide which is detected by an infrared (IR) detector after purification of the gases leaving the furnace. Total inorganic carbon is determined by injection of a small aliquot in a reactor filled with dilute phosphoric acid. All inorganic carbon species are converted to carbon dioxide. These are purged from the reactor and detected by the IR detector.

Instead of TOC, one could also measure NPOC (Non Purgeable Organic Carbon). This is carried out by acidifying and purging the sample with gas so that all carbonates in the samples are converted to carbon dioxide which is then purged. The carbon compounds that remain in solution are supposed to be organic and can be measured directly as TC. This assumption is only true if no volatile organic compounds are present in the solution as these could also be purged from the sample. This approach is very useful for samples with high TIC levels or samples with high pH values because these can quickly absorb carbon dioxide. This gives rise to unstable TIC levels and makes accurate determination of TIC and TOC impossible.

For TIC analysis, the samples were not diluted prior to analysis. Because the samples have high pH values, NPOC measurement is preferred. Samples were acidified and purged and then analysed for TC.

All measurements were carried out with a Skalar Formacs HTi TOC analyser. This instrument is able to analyse liquid aqueous samples with a carbon content of 0.5 mg/L or higher. Calibration of the instrument was carried out in the concentration range 0.5 to 10 mg/L and 10 to 100 mg/L. The appropriate calibration was used for the samples. The injection volume for both TC and TIC was 100 µL and repeated measurements were carried out until the relative standard deviation (RSD) on the replicates was better than 2%.

2.6.2.2 Ion Chromatography (Carboxylic acid analysis)

Ion chromatography was realized to measure the concentration of carboxylic acids, such as formate, acetate and oxalate, using a Dionex IC-25 machine with potassium hydroxide eluent generator. The IC-25 Ion Chromatograph performs isocratic ion analyses using conductivity detection. The IC25 integrates pump and detector functions in a single instrument. 25 µL of sample was injected on a Dionex AS15 column at room temperature.

2.6.2.3 Liquid Scintillation Counting

The ^{14}C activity was detemined by Liquid Scintillation Counting using a Quantulus 1220 counter. The cocktail used is Optiphase Hisafe 3 (Perkin Elmer) which handles a broad range of solutes. It combines good counting efficiency with a very high level of sample acceptance, particularly for high ionic strength solutes. 17 mL of the cocktail was mixed with 2.5 mL sample in super polyethylene vials of 20 mL (Perkin Elmer).

3 Results and Discussion

3.1 *Nitrogen analysis*

The nitrogen content analysis of the unirradiated Zircaloy-4 was performed on two different samples. The results are presented in Table 6.

Table 6. Average nitrogen content (N_{avg}) of the unirradiated Zircaloy-4 samples.

Sample ID	N_{avg} (µg/g)
ZR4 19430	17 ± 3.9
ZR4 M92029	25 ± 2.6

According to the literature [BLOKHIN, 2012] and/or technical specifications [ASTM, 2013], the nitrogen content is usually between 40 and 80 µg/g. Values measured for SCK•CEN samples are 2 to 4 times lower. This result leads to a decrease of the expected amount of ^{14}C inside the sample after irradiation. Indeed, the activation of ^{14}N ($^{14}N(n,p)^{14}C$) is the most probable production of ^{14}C in Zircaloy-4.

3.2 *Metallographic analysis*

Metallographic analysis was performed on both irradiated and unirradiated samples to analyse the influence of radiation on the metallic structure. The unirradiated sample was a part of the Zircaloy-4 rod while the irradiated sample is the F6678-R4-R sample composed of the cladding, representative of samples used for the static corrosion tests and the end-plug, representative of sample used for the accelerated corrosion tests.

3.2.1 Unirradiated sample

According to the specifications, Zircaloy-4 consists of about 98 wt% Zr, 1.2-1.7 wt% Sn, 0.18-0.24 wt% Fe, 0.07-0.13 wt% Cr and 1000-1400 µg/g O. The Sn is uniformly distributed over the bulk material, but Fe and Cr are concentrated in $Zr(Fe,Cr)_2$ intermetallic Laves phases. Carbon has a weakly unfavourable effect on the corrosion behaviour and the amount of carbon is limited to a maximum of 270 µg/g.

The grain structure of Zircaloy-4 is represented in Figure 20. This material consists of small uniform equiaxed grains with a grain size of 11.8, which corresponds to an average grain size of 6 µm with a surface area of 36.4 µm². The small black spots can be attributed to the Laves phases.

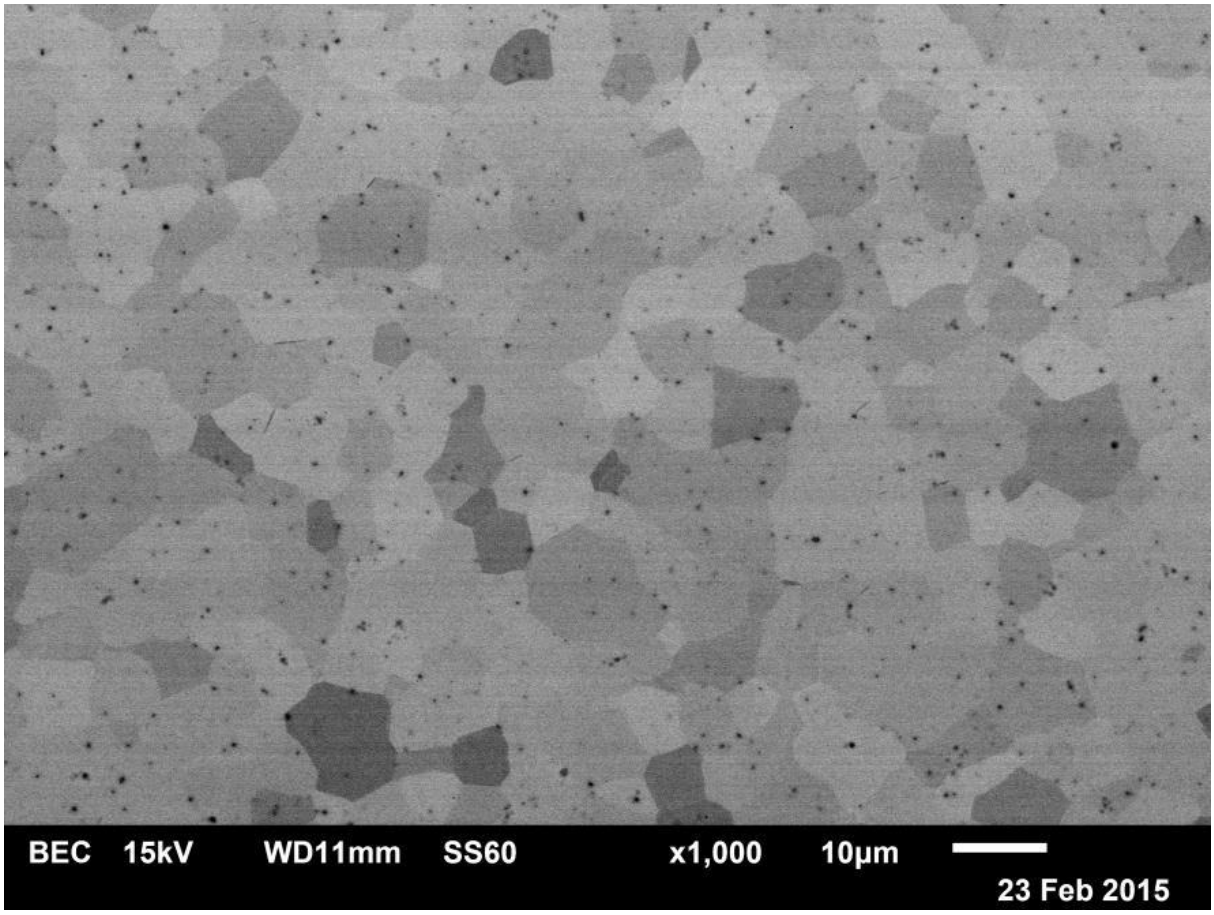

Figure 20. SEM micrographs (BSE) of the unirradiated Zircaloy-4 surface.

Typical images of the defect structure of Zircaloy-4 are shown in Figure 21 (A and B). The main defects that are occurring are line dislocations with a density of $4.1\times10^{13}/m^2$. The grain orientation can be determined from the diffraction pattern as shown in Figure 21 (C). It was found that most grains have a comparable orientation, which was identified as the [1-210] zone axis. It is known that during the manufacturing process, grains become textured, which results in grains having a similar orientation.

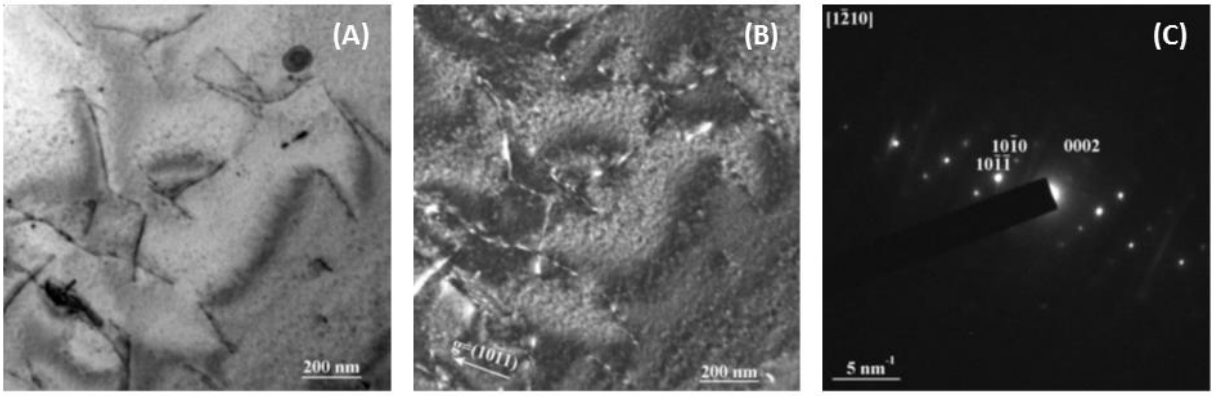

Figure 21. (A) Bright field and (B) dark field micrographs of the typical defect structure in Zircaloy-4. (C) Typical diffraction pattern showing the grain orientation.

Most of the precipitates present in a Zircaloy-4 material are Laves phases. An example of such a precipitate is given in Figure 22 (A and B). These precipitates are partially dissolved during the electrochemical polishing process. This can be seen with the upper right part of the precipitate, which has a higher intensity (less absorption) and therefore shows no diffraction contrast.

The nominal composition of this phase is $Zr(Fe,Cr)_2$. The elemental composition is confirmed by the EDS analysis on this particle, which is shown in Figure 22 (C). Apart from the Zr signal, peaks corresponding to Fe and Cr were observed as well. Any carbon observed in other samples is considered to be the result of a surface contamination during the analysis because it is not present in this sample.

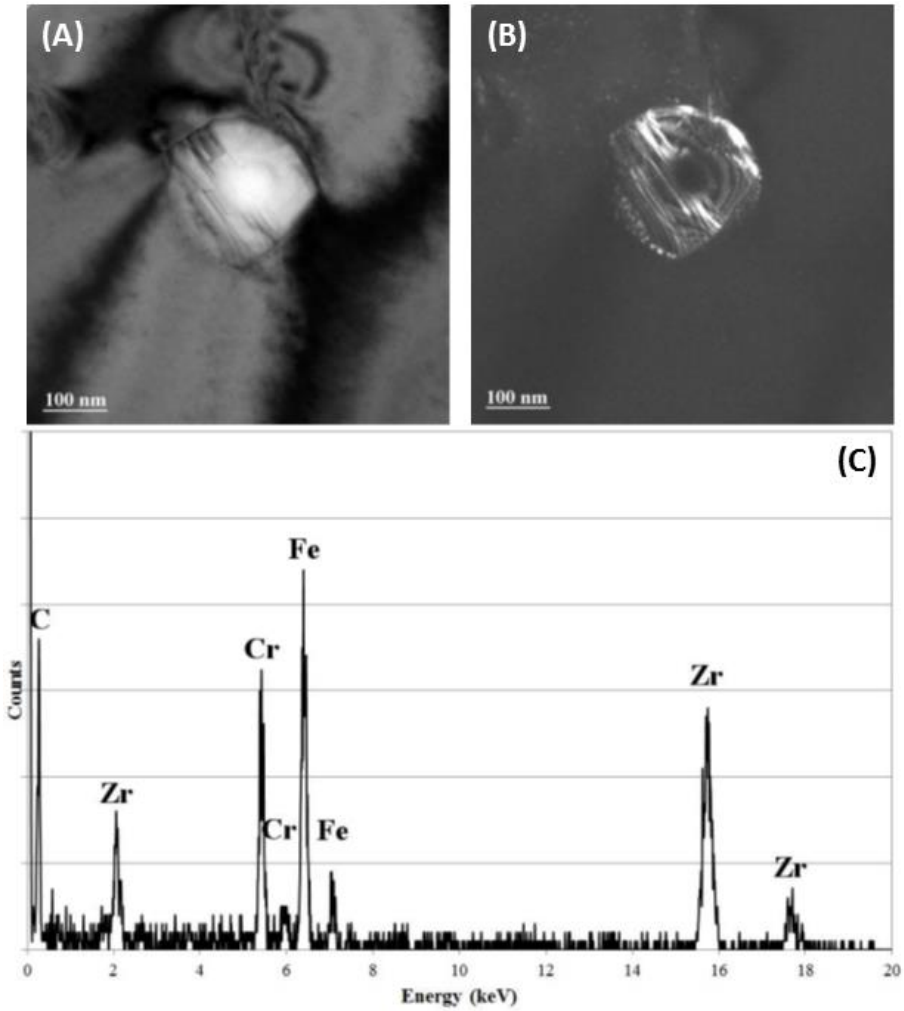

Figure 22. (A) Bright field and (B) dark field micrographs of Laves phase in Zircaloy-4. (C) Corresponding EDS spectrum of the Laves phase.

A second type of precipitate is shown in Figure 23 (A, B and C). The bright field and dark field images show that these precipitates are elongated along the (0002) planes and are needle or platelet shaped. The EDS spectrum in Figure 23 (E) shows the composition of the precipitate in comparison to the spectrum of the bulk of Zircaloy-4. For the visual comparison of Figure 22 (C) and Figure 23 (E), the spectrum of the precipitate is renormalized so that both spectra have the same total number of counts. The bulk metal consists mainly of zirconium. Small amounts of carbon and oxygen are detected as well, which can be attributed to the expected contamination of the surface as well as slight oxidation of the zirconium which is very reactive. When magnifying the spectrum between

2 and 6 keV, a small Sn peak can be found, in agreement with the 1.2 wt.% of Sn added to the Zircaloy-4. No Cr or Fe can be detected as these elements are forming the Laves phases. The spectrum of the precipitate (Figure 23 (E)) only contains Zr and C. The carbon content is significantly higher than in the spectrum of the bulk material. This may be the result of higher local contamination during the recording of this spectrum or it can be an indication that carbon is present in the precipitate.

A second option to identify the precipitate is to determine the crystallographic structure from the diffraction pattern shown in Figure 23 (D). Because of the small size of the precipitate, the appearance of diffraction spots from the bulk Zircaloy-4 could not be avoided and the 0002, -1011 and -1010 reflections, typical for the [1-210] zone, are indicated. The additional reflections agree with the [110] zone axis of a face centered cubic (FCC) structure with a lattice parameter of 4.6 ± 0.2 Å. Several phases, including ZrC, ZrN or ZrH_2, could have the correct crystal structure. In combination with the EDS results, it is most likely that this phase is a ZrC precipitate.

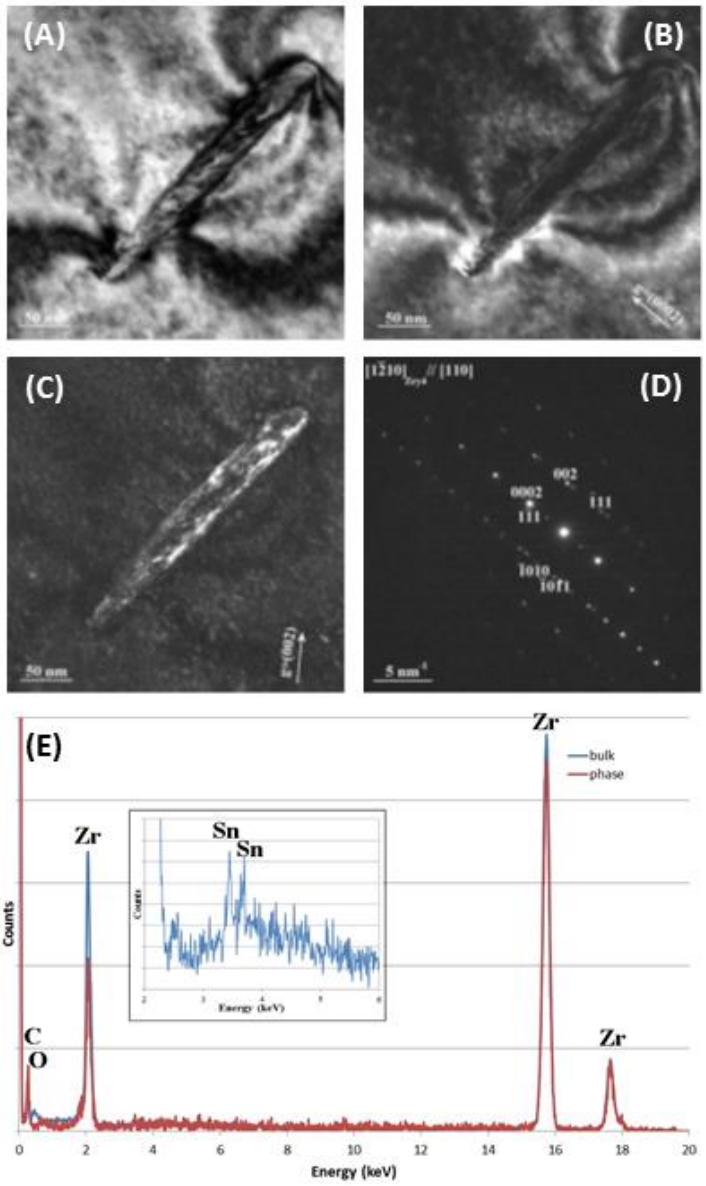

Figure 23. (A) Bright field and (B and C) Dark field micrographs of a second type of precipitate in Zircaloy-4. (D) Corresponding diffraction pattern. (E) Corresponding EDS analysis.

3.2.2 Active sample

After the study of the material before irradiation, the analysis of the microstructure of the irradiated Zircaloy-4 was done. These properties were only studied by Transmission Electron Microscopy. The Zircaloy-4 sample remained in the reactor for a long time during

which it was kept at 300 °C, but the neutron fluence was low. The microstructure is thus representative of the low fluence irradiation microstructure.

3.2.2.1 The cladding

Figure 24 shows the micrographs of the lath grain structure (A) and the dislocation structure (B and C) of the irradiated Zircaloy-4 cladding (cross-section). This direction is perpendicular to the rolling direction of the rod. The rolling process induces texture on the cladding, resulting in a narrow lath structure, that is different from the structure in the Zircaloy-4 rod, studied previously. Line dislocations are present with a dislocation density that is comparable to the Zircaloy-4 rod before irradiation.

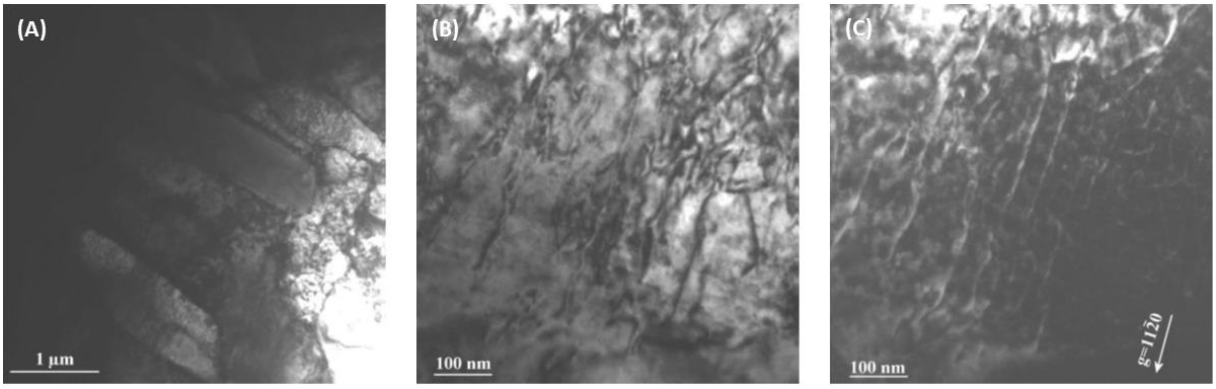

Figure 24. (A) Bright field micrograph of the lath grain structure of the irradiated Zircaloy-4 cladding in cross section, (B) bright field and (C) dark field micrographs of the dislocation structure.

The main effect of the neutron irradiation is shown in Figure 25. A large amount of small black contrast features are observed. The contrast features are related to the presence of small dislocation loops. The nature of the loops was not characterized in detail, but from literature it is known that, at low doses, only a-type loops are formed, while at higher burn-up c-type loops are dominant [ADAMSON, 2000]. The a-loops have a Burgers vector of 1/3[11-20] and are located on the prism planes of the hexagonal unit structure. The majority

are vacancy type loops, but also interstitial loops are reported. The c-loops have a Burgers vector of 1/2[0001] and are located on the basal planes. The diffraction contrast images of Figure 25A and B, show small loops that are inclined with respect to the (0001) basal plane and in the high resolution image of Figure 25C it can be observed that the (0001) planes are not deformed by the dislocation loop. Both observations are in agreement with a-type dislocation loops, which are expected to occur at the low neutron fluence.

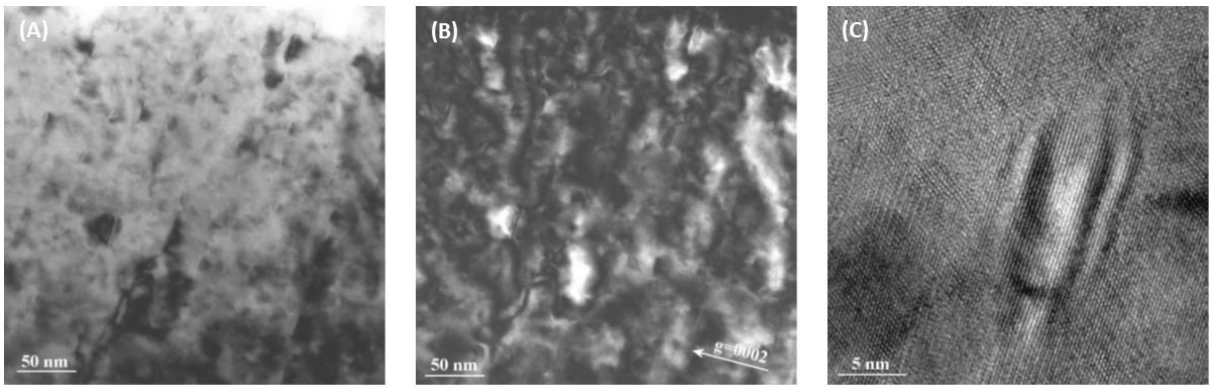

Figure 25. (A) Bright field and (B) dark field micrographs of the radiation induced defects in the cladding. (C) High resolution micrograph of a radiation induced dislocation loop.

3.2.2.2 The end plug

The end plugs are made from the same type of Zircaloy-4 materials as the fuel cladding, but the production process is different. Mainly the rolling stages, which are required to produce cladding tubes, are not required to produce the end plugs. This has a major effect on the texture. The grain structure in the end plug is different from the cladding. In this sample (Figure 26(A)), equiaxed grains are observed instead of lath shaped grains.

The fringe-like defect contrast that can be observed in Figure 26(B-D), is in literature referred to as "Corduroy" contrast and is an artefact of thin foil preparation for TEM samples [ADAMSON, 2000]. Even though the features are parallel to the (0001) basal

planes, the deformation of the lattice causing the contrast is related to stray stress fields induced by an a-type dislocation loops.

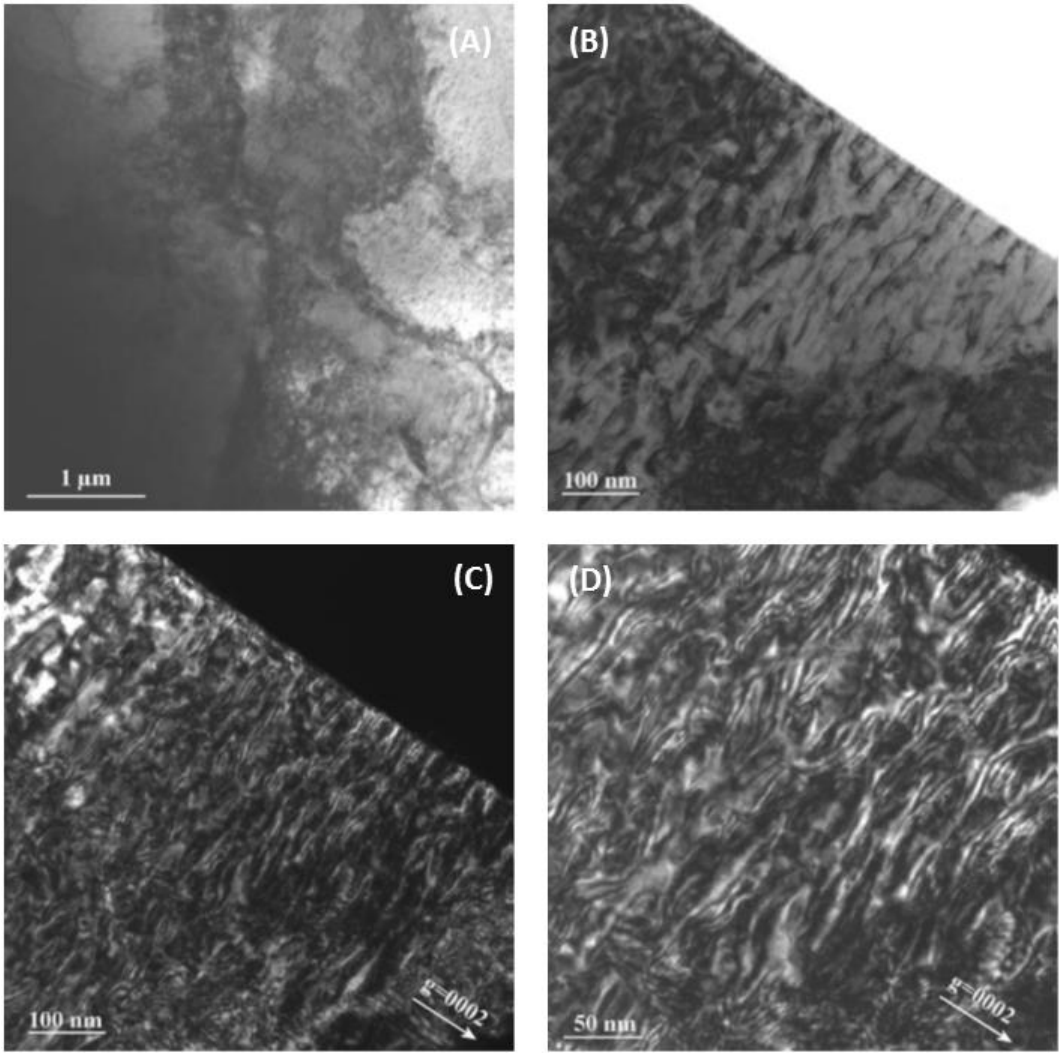

Figure 26. (A) Bright field micrograph of the grain structure in the Zircaloy-4 end plug; (B) bright field and (C-D) dark field micrographs of the radiation induced defects in the Zircaloy-4 end plug.

The Laves phase precipitates are still present in the irradiated sample. Low temperature irradiation of Zircaloy-4 leads to the amorphisation of the precipitates [ADAMSON, 2000; GRIFFITHS, 1994]. The precipitate in Figure 27 is still crystalline, which agrees with the

low neutron irradiation dose of the sample. However, the diffraction spots are getting weaker compared to the unirradiated Zircaloy-4, which is a first indication of the beginning of the amorphisation. The EDS spectrum in Figure 27(C) reveals the presence of Fe and Cr in the precipitate. The concentrations of Fe and Cr are low compared to a similar precipitate before irradiation, but this is probably due to a significant contribution from the Zircaloy-4 matrix to the spectrum, which is proven by the presence of a small Sn signal.

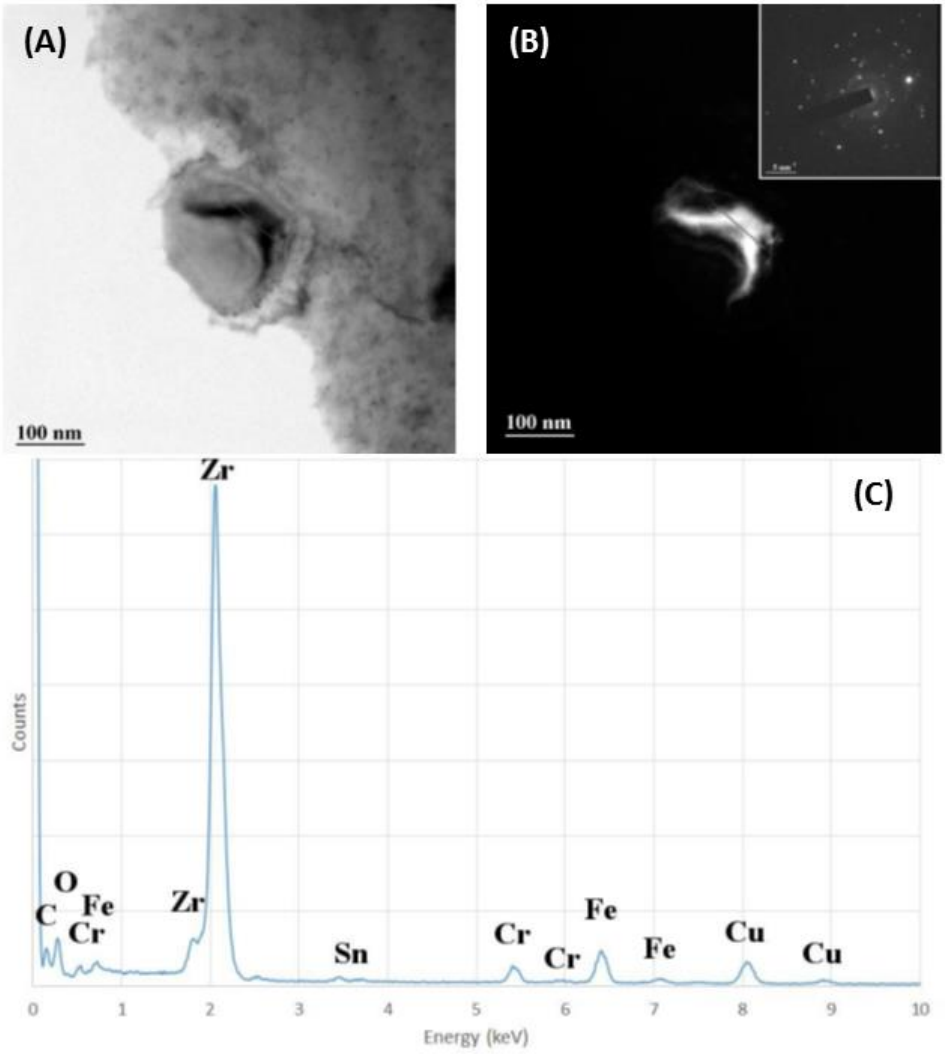

Figure 27. (A) Bright field and (B) dark field micrographs of a Laves type $Zr(Fe, Cr)_2$ precipitate. The inset of (B) shows a complex diffraction pattern consisting of Zircaloy-4 matrix reflections and weak diffraction spots from the precipitate. (C) The EDS spectrum of the precipitate.

3.3 γ-ray spectrometry of active materials

In order to determine the activity of samples and to list radionuclides present in irradiated Zircaloy-4 samples, γ-ray spectrometry was performed on sample F6678-R4-E, used for accelerated corrosion tests, and on sample F6678-R4-A. This last sample possesses the highest dose rate of the samples used for the static corrosion tests and was the closest to the fuel. Its activities will be used as over-estimation for samples FF6678-R4-B and FF6678-R4-C. Radionuclide identification in Zircaloy-4 samples and their activities are listed in Table 7.

Table 7. γ-ray spectrometry of sample F6678-R4-A and F6678-R4-E.

Nuclides	Sample F6678-R4-A		Sample F6678-R4-E	
	Activity (Bq)	Uncertainty (Bq)	Activity (Bq)	Uncertainty (Bq)
^{241}Am	1.13×10^{4}	0.39×10^{4}	-	-
^{144}Ce	4.8×10^{5}	1.7×10^{5}	1.88×10^{3}	0.38×10^{3}
^{60}Co	5.1×10^{4}	1.8×10^{4}	2.78×10^{4}	0.56×10^{4}
^{134}Cs	5.0×10^{3}	1.8×10^{3}	255	89
^{137}Cs	4.6×10^{5}	1.6×10^{5}	1.24×10^{3}	0.25×10^{3}
^{155}Eu	2.26×10^{4}	0.79×10^{4}	-	-
^{54}Mn	6.4×10^{3}	2.2×10^{3}	1.68×10^{3}	0.34×10^{3}
^{95}Nb	2.3×10^{5}	0.81×10^{5}	4.40×10^{4}	0.88×10^{4}
^{106}Ru	9.4×10^{5}	3.3×10^{5}	1.33×10^{3}	0.40×10^{3}
^{125}Sb	4.6×10^{5}	1.6×10^{5}	1.43×10^{5}	0.29×10^{5}
^{113}Sn	2.72×10^{4}	0.95×10^{4}	7.7×10^{3}	1.5×10^{3}
^{95}Zr	9.7×10^{4}	3.4×10^{4}	1.98×10^{4}	0.40×10^{4}

As expected, the activity of the sample F6678-R4-A, which is closest to the fuel compared to F6678-R4-E, is higher. Moreover, this activity is mainly emitted by ^{106}Ru, ^{144}Ce, ^{137}Cs, ^{125}Sb and ^{95}Nb for F6678-R4-A and ^{125}Sb, ^{95}Nb, ^{60}Co and ^{95}Zr for F6678-R4-E.

3.4 Estimation of the ^{14}C content of irradiated samples

Based on the measurement of the nitrogen content in unirradiated Zircaloy-4, an estimation of the ^{14}C amount after irradiation of the metal was obtained using a computer modeling calculation.

The production of ^{14}C through nuclear reaction on nitrogen, carbon and oxygen was evaluated for a PWR representative neutron spectrum, as a literature review shows [WALLACE, 1977] that the following reactions may provide ^{14}C buildup:

$^{13}C(n,\gamma)^{14}C$; $^{14}N(n,p)^{14}C$; $^{15}N(n,d)^{14}C$; $^{16}O(n,^{3}He)^{14}C$; $^{17}O(n,\alpha)^{14}C$

Among these, $^{14}N(n,p)^{14}C$ would bring the dominant contribution.

A simple, single cell model was therefore developed in the SCALE-6.1 code using the 'Triton' depletion sequence. The cladding composition was taken as standard Zircaloy-4, while the fuel is UO_2 with an enrichment of 4.25% in ^{235}U. The evolution of the isotopic composition of both the fuel and the cladding was simulated, assuming a 3-cycle power history of 500 days per cycle, at a constant power of 40 MW/t_U. The final burnup of the fuel is then 60 GWd/t_U, which corresponds to a total neutron fluence of 4.08 $x10^{22}$ n/cm^2 for the cladding.

The calculations were then repeated with a small change in the cladding composition, where nitrogen, carbon or oxygen is added at a concentration of 1000 wt. µg/g, with an isotopic composition reflecting natural abundances. It is an overestimation, although from this calculation, results can be proportionally descaled to any lower concentration.

Differences in ^{14}C compared to the reference case then provide the ^{14}C buildup associated to the sole presence of 1000 wt. µg/g of the considered element, in conditions representative of a PWR neutron spectrum. Considering the low concentration of these trace elements in the cladding, second order effects due to the presence of the trace elements or ^{14}C may be neglected; the ^{14}C concentrations obtained can then be rescaled to reflect the actual cladding material composition and fluence.

From the calculations, it appears that the only significant ^{14}C production arises with the presence of nitrogen: the addition of 1000 µg/g of N (natural abundances) leads to the production of 5 µg/g of ^{14}C at the end of irradiation. The value can be rescaled to other N content in view of the linear buildup of ^{14}C over the irradiation history.

Table 8 shows the concentration of ^{14}C of Zircaloy-4 samples, and its corresponding activity, obtained from the computer simulation depending on the nitrogen concentration previously measured. The corrosion of 1 g of Zircaloy-4 will lead to the release of ~0.1 µg of ^{14}C. Unfortunately, the total activity of the irradiated Zircaloy-4 used couldn't be measured at SCK•CEN and no comparison with the calculation could be done.

Table 8. ^{14}C activity of the irradiated Zircaloy-4 obtained from the computer simulation and its initial nitrogen content.

Sample ID	C_N (wt. µg/g)	Fluence (n/cm²)	Concentration of ^{14}C (wt. µg/g)	Computer simulation of ^{14}C activity (Bq/g)
ZR4 19430	17 ± 3.9	4.08×10^{22}	8.12×10^{-2}	13300
ZR4 M92029	25 ± 2.6	4.08×10^{22}	1.19×10^{-1}	19560

3.5 *Polarisation curves for Zircaloy-4*

In preparation of accelerated corrosion tests, it is necessary to record first potentiodynamic polarisation curves. During these measurements the potential was scanned from the cathodic to the anodic region and the current was recorded. Polarisation curves give information on the behaviour of the metal at different potentials and show the active to passive and/or the passive to transpassive transitions of the metal. This will help to choose the best potential range to apply during the accelerated corrosion tests.

As explained earlier (see Section 2.5.1), accelerated corrosion tests were performed in two different electrolytes. First, a saturated portlandite ($Ca(OH)_2$) pore water solution with a pH of approximately 12.5 was used. In a second phase, chlorides were added to the portlandite

pore water in order to induce pitting corrosion and thus artificially increase the corrosion rate. All polarisation curves were recorded under an anaerobic nitrogen atmosphere.

In this section, polarisation curves for both samples (unirradiated and irradiated) in both electrolytes (portlandite pore water without and with chlorides) are presented.

3.5.1 Unirradiated sample

The polarisation curve of the unirradiated Zircaloy-4 sample in pure saturated $Ca(OH)_2$ aqueous solution is shown in Figure 28. This curve shows a broad passive range starting from -0.7 V (vs. Ag/AgCl); very low or no corrosion will happen in this zone. At lower potential, the curve shows an active corrosion zone. Finally, below -1.04 V, representing the corrosion potential, cathodic current is recorded.

From this polarisation curve, a potential of -0.75 V (vs. Ag/AgCl) was selected for the accelerated corrosion tests. Indeed, even if the current is quite low at this potential (10^{-6} A), it represents the highest current in the active corrosion zone of the curve, which is expected to result in the highest corrosion rate.

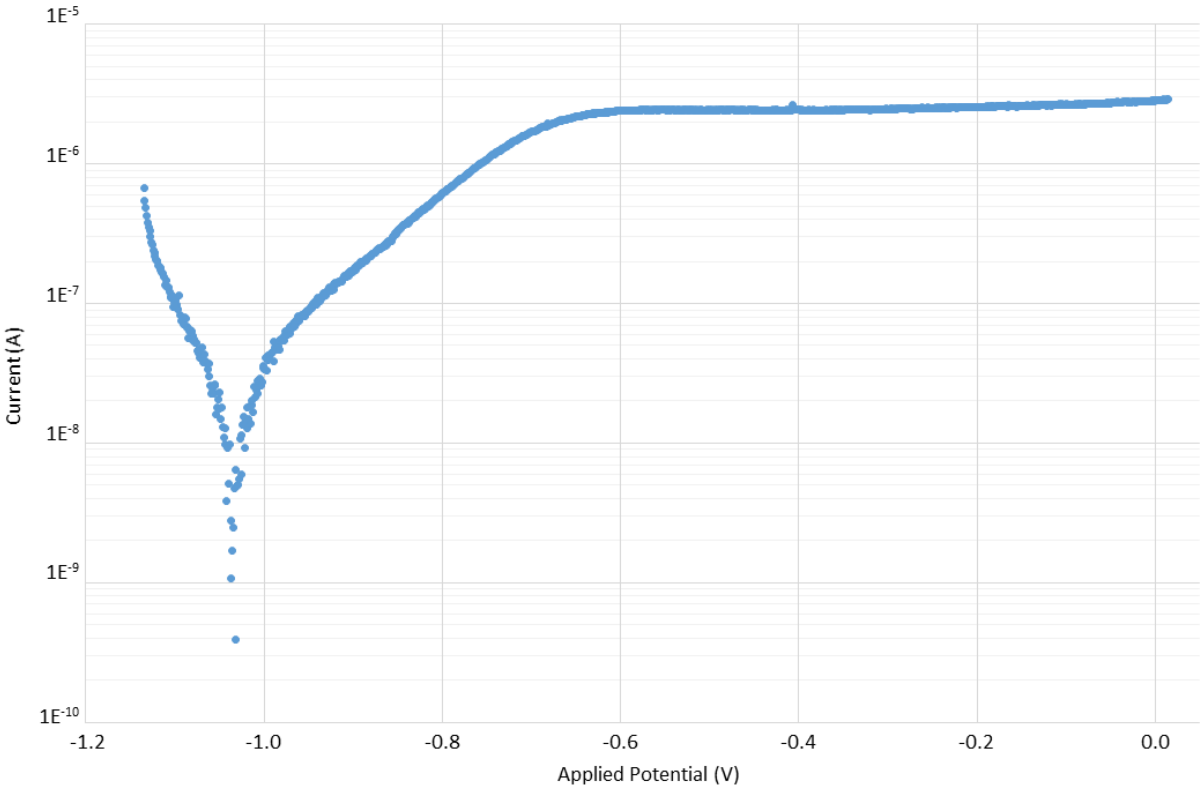

Figure 28. Polarisation curve of the unirradiated Zircaloy-4 sample in saturated $Ca(OH)_2$ aqueous solution.

The same measurement was performed in presence of 0.5 M of $CaCl_2$ (Figure 29). Chloride has a huge influence on the polarisation curve and then, on the corrosion behaviour of the Zircaloy-4 sample. The plateau of the passive zone appears at higher voltage (~0.2 V vs. Ag/AgCl) while the corrosion potential appears at ~-0.72 V (vs. Ag/AgCl). Another difference observed is the presence of pitting corrosion, shown by a sudden sharp increase of the current in the polarisation curve at ~0.55 V (vs. Ag/AgCl) corresponding to pitting potential.

From this polarisation curve, a potential of 0.6 V (vs. Ag/AgCl) was chosen for the accelerated corrosion tests with chlorides. At this potential, pitting corrosion will occur, leading to a much higher corrosion rate than the one observed without chlorides, as shown by the higher current reached: ~4 $x10^{-3}$ A compared to 10^{-6} A without chlorides.

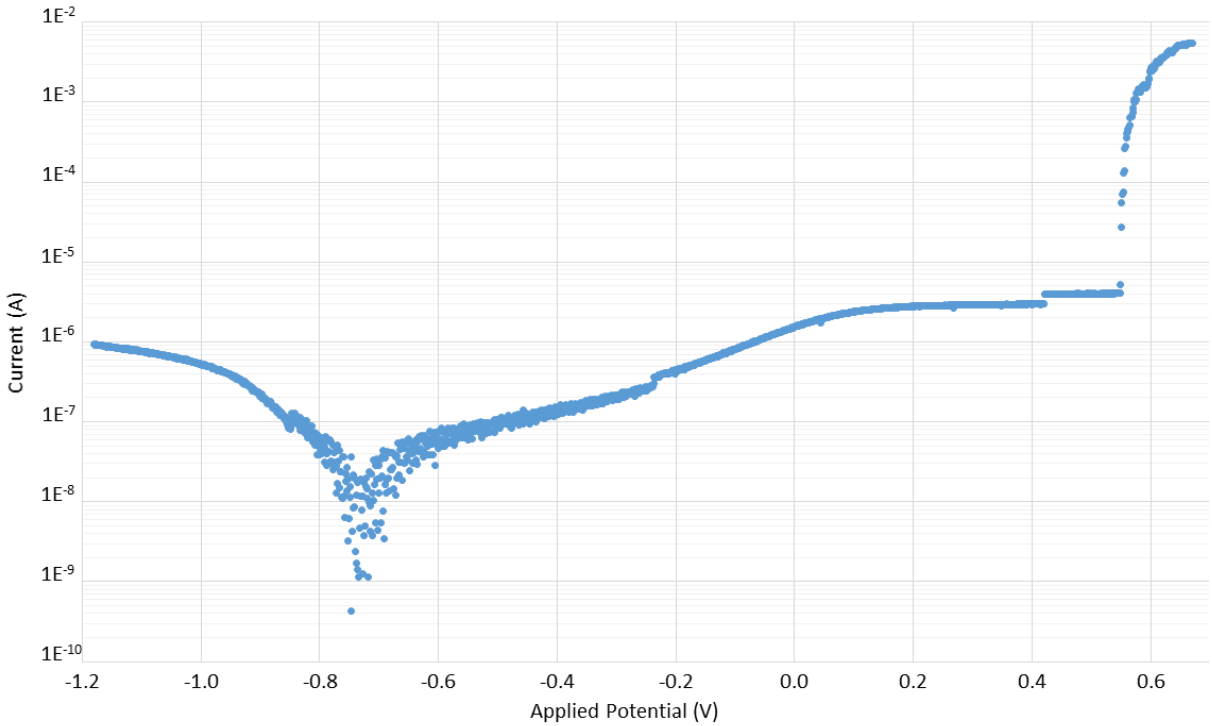

Figure 29. Polarisation curve of the unirradiated Zircaloy-4 sample in saturated $Ca(OH)_2$ + 0.5 M $CaCl_2$ aqueous solution.

3.5.2 Active sample

To perform accelerated corrosion tests on irradiated Zircaloy-4, polarisation curves of this sample in both electrolytes were needed. Even if the material is the same as the unirradiated one, radioactivity could modify the electrochemical behaviour of the material.

Figure 30 shows the polarisation curve of the irradiated Zircaloy-4 in saturated portlandite pore water. Note that the cathodic part of the curve was not recorded because the measurement started at the open circuit potential.

As expected, the curve shows the same kind of behaviour as the one obtained for the unirradiated sample, with the presence of a broad passive range starting from -1V (vs. Ag/AgCl) in the µA current range. Even if results must be taken with care because each

polarisation curve was recorded only once[1], irradiation induced changes on the behaviour of the Zircaloy-4 sample. First, the corrosion potential is shifted from -1.04 V to ~-1.23 V (vs. Ag/AgCl). Secondly, the passive current decreased from ~2.5×10^{-6} A (unirradiated) to ~1.5×10^{-6} A (irradiated), resulting in an improvement of the quality of the passive film, leading maybe to a better corrosion resistance.

In order to stay in the stability domain of water and to compare with the unirradiated sample, a potential of -0.75 V vs. Ag/AgCl was chosen for the accelerated corrosion tests on the irradiated Zircaloy-4 sample.

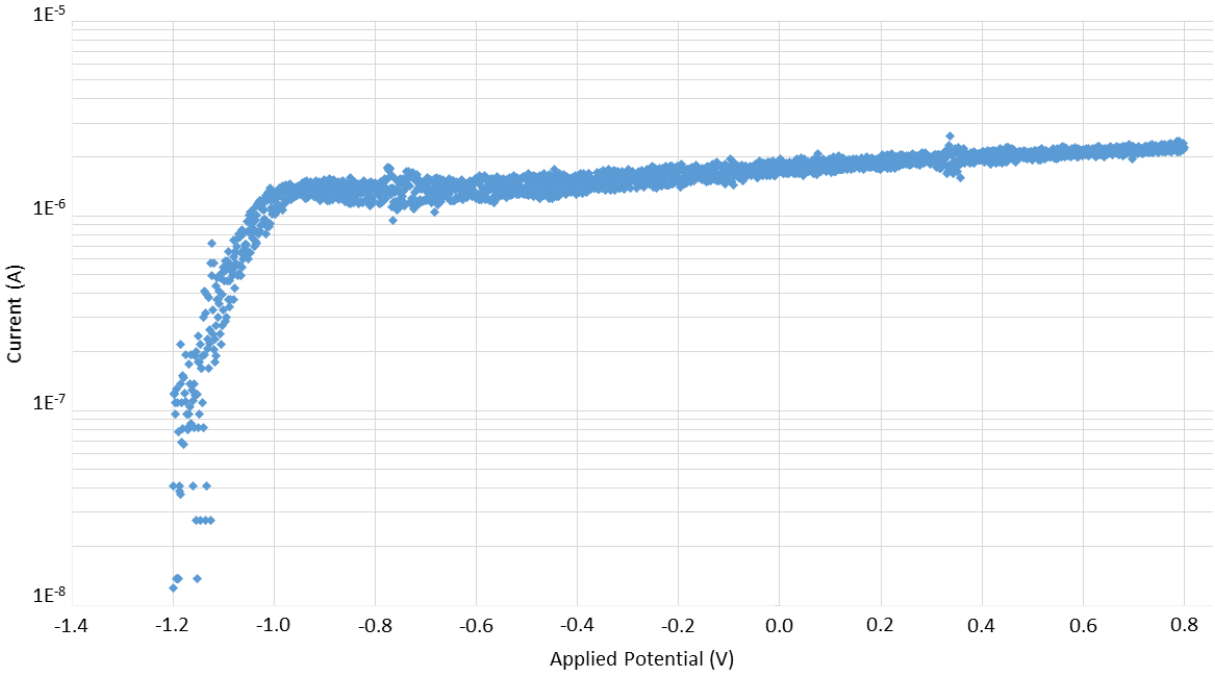

Figure 30. Polarisation curve of the irradiated Zircaloy-4 sample in saturated $Ca(OH)_2$ aqueous solution.

Figure 31 shows the polarisation curve of the irradiated Zircaloy-4 sample in the presence of chlorides (0.5 M $CaCl_2$). Irradiation induced some changes in the behaviour of the sample. The corrosion potential is shifted from ~0.55 V to ~1 V (vs. Ag/AgCl) and the passive

[1] Due to the small size of the sample and to be able to realise all the tests needed for this research, it was not possible to repeat the polarisation tests.

current decreased by a factor of ~2. Also, a broader passive zone of almost 1.9 V was observed, together with an increase of the pitting potential from ~0.55 V to 0.9 V (vs. Ag/AgCl).

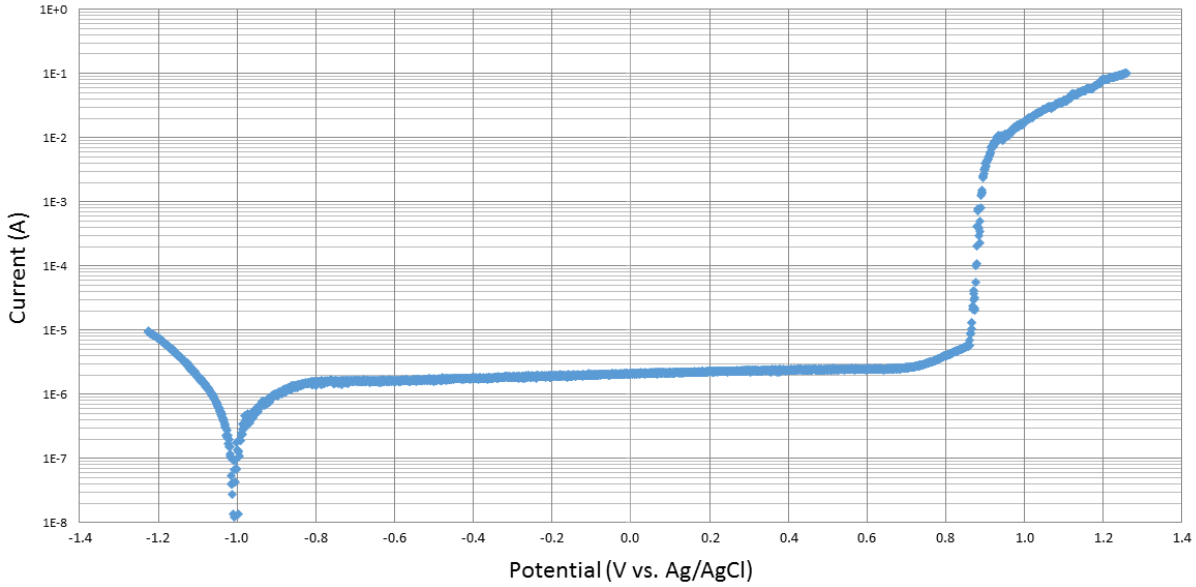

Figure 31. Polarisation curve of the irradiated Zircaloy-4 sample in saturated $Ca(OH)_2$ + 0.5 M $CaCl_2$ aqueous solution.

From this polarisation curve, a potential of 1.0 V (vs. Ag/AgCl) was chosen for the accelerated corrosion tests with chloride on the irradiated Zircaloy-4 samples. At this potential, pitting corrosion will occur, leading to a much higher corrosion rate than the one observed without chlorides. Nevertheless, at such high potential, hydrolysis of water is also present leading to the production of high amounts of O_2 and H_2 in the experimental vial.

3.6 *Carbon speciation after static and accelerated corrosion tests*

While static corrosion tests were performed to obtain information on the behaviour of Zircaloy-4 in real geological conditions, accelerated corrosion tests were performed to

obtain some indication of the corrosion mechanism and the light carbon-based molecules formation – such as methane, ethane, ethene – in a shorter reaction time. So, accelerated corrosion will provide qualitative results while static corrosion tests should give more realistic and quantitative results on the corrosion rate.

The carbon speciation of the gas phase was determined by gas chromatography. The carbon speciation of the liquid phase was determined by total Inorganic/Organic Compounds analysis (TIC/TOC), ion chromatography of carboxylic acids (IC) and Liquid Scintillation Counting (LSC) to determine ^{14}C activity. Results are reported in this section.

3.6.1 Analysis of the gas phase by gas chromatography

3.6.1.1 Accelerated corrosion tests

Accelerated corrosion tests are potentiostatic tests where a fixed potential is applied to the working electrode during the test while the obtained current is recorded. The potential applied to the working electrode was chosen based on the outcome of the corresponding polarisation curve, as explained in the previous section.

Accelerated corrosion tests were performed on both irradiated and unirradiated samples in two different electrolytes. The first electrolyte was the saturated portlandite $Ca(OH)_2$ solution simulating conditions met in the Belgian supercontainer in the underground repository. The second electrolyte was saturated portlandite $Ca(OH)_2$ solution with 0.5 M of $CaCl_2$. The presence of chloride induces the pitting corrosion of metals, leading to higher corrosion rates. So, even if chemical conditions induced by this second electrolyte are much more harsh than the real conditions compared to the first one, information could be obtained much faster.

3.6.1.1.1 Unirradiated samples

3.6.1.1.1.1 Saturated $Ca(OH)_2$ aqueous electrolyte

Figures 32 and 33 show chromatograms for Zircaloy-4 in pure portlandite pore water as a function of time. The applied potential was -750 mV vs. Ag/AgCl (0.1 M KCl). This potential was chosen based on the corresponding polarisation curve (see Figure 28 in Section 3.5.1). As explained earlier, this potential corresponds to the higher current in the active corrosion zone of the curve, leading to the highest corrosion rate.

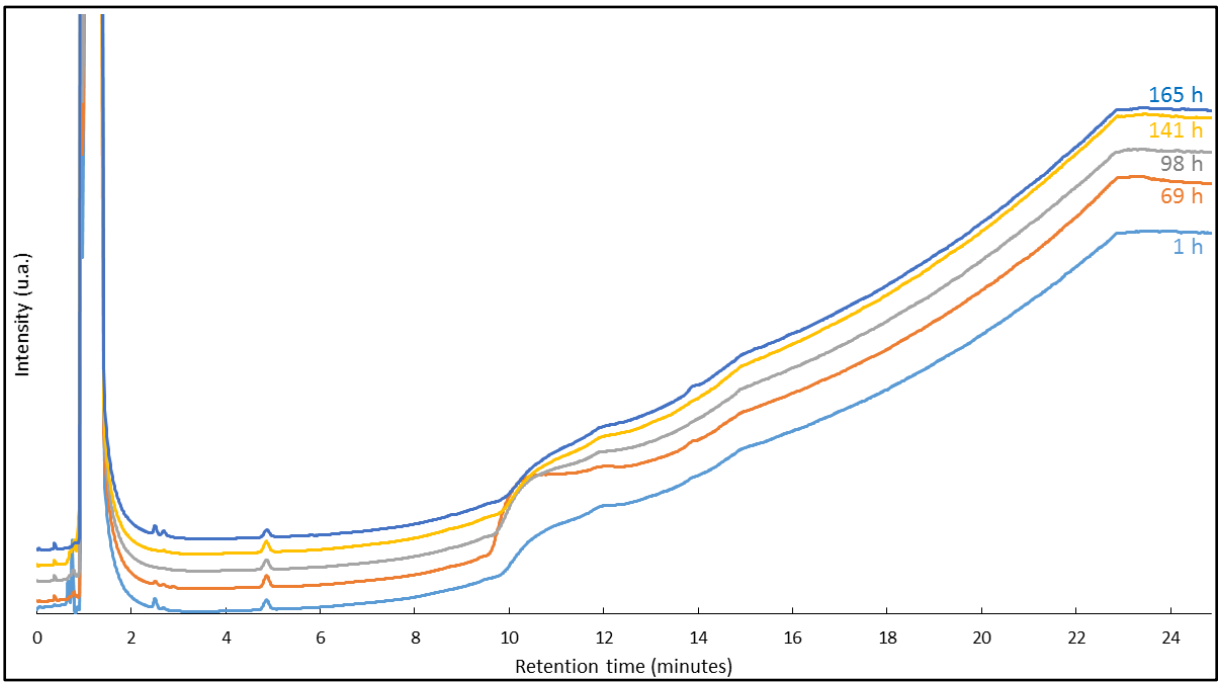

Figure 32. Gas chromatograms of gas sampling from the headspace of the accelerated corrosion vial at different corrosion times of the unirradiated Zircaloy-4 sample in $Ca(OH)_2$ electrolyte.

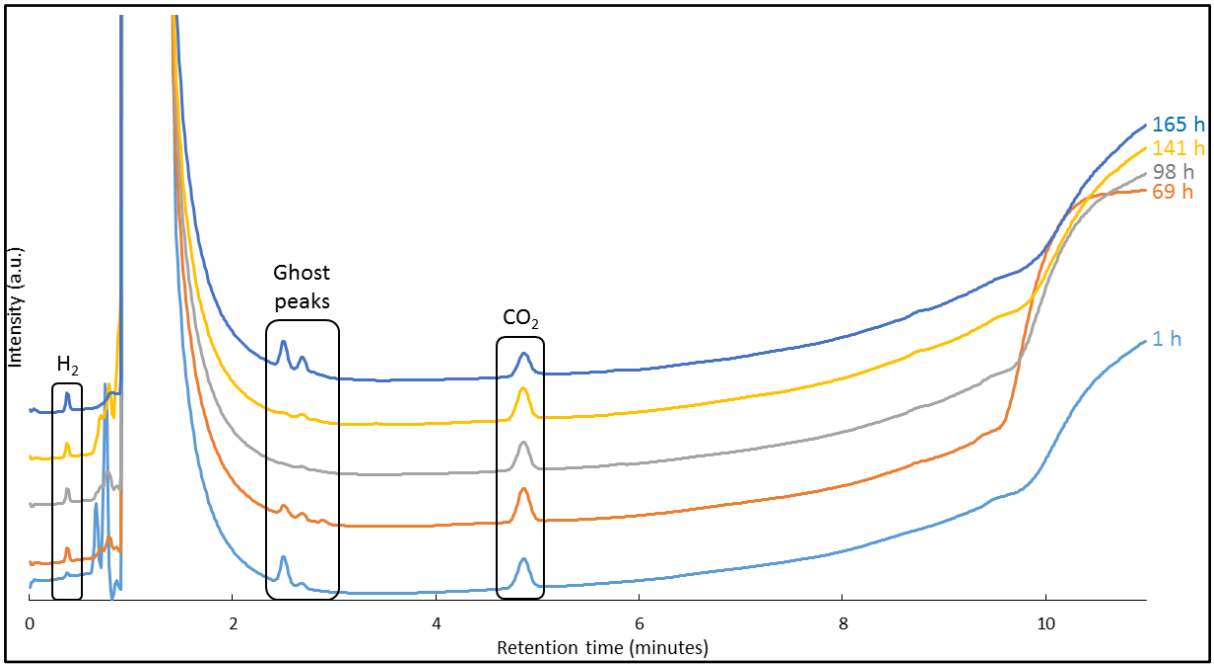

Figure 33. Gas chromatograms of gas sampling from the headspace of the accelerated corrosion vial at different corrosion times of the unirradiated Zircaloy-4 sample in $Ca(OH)_2$ electrolyte (Zoom from 0 to 11 min of Figure 32).

The analysis of the gas chromatograms presented in Figures 32 and 33 show the presence of ghost peaks at ~2.5 minutes of retention time. These peaks possess different intensities depending on the chromatogram. Despite their presence, there is no peak with a higher intensity than the detection limit, meaning that no or very little methane gas was produced during this test. The same conclusion can be made for other hydrocarbon gasses analysed during the calibration of the column (CO_2, ethene, ethane, propene and propane). Nevertheless, at ~0.4 minutes of retention, the presence of a peak resulting from the detection of H_2 is observed. Figure 34 shows that the intensity of this peak slightly increases with corrosion time up to 69 hours. After 69 hours, the intensity of the H_2 peak remained stable. Indeed, the corrosion of Zircaloy-4 at high pH is initially represented by a parabolic law [KATO, 2013]. Figure 35 also shows a decrease of the current until a few nanoAmpère or less after only a few hours of corrosion, confirming this parabolic law.

Finally, a bump at ~10 minutes of retention time is also observed due to the presence of water in the headspace of the corrosion vial (Figure 33). This bump appears at the retention time of ethane leading to difficulties to detect the presence of this gas.

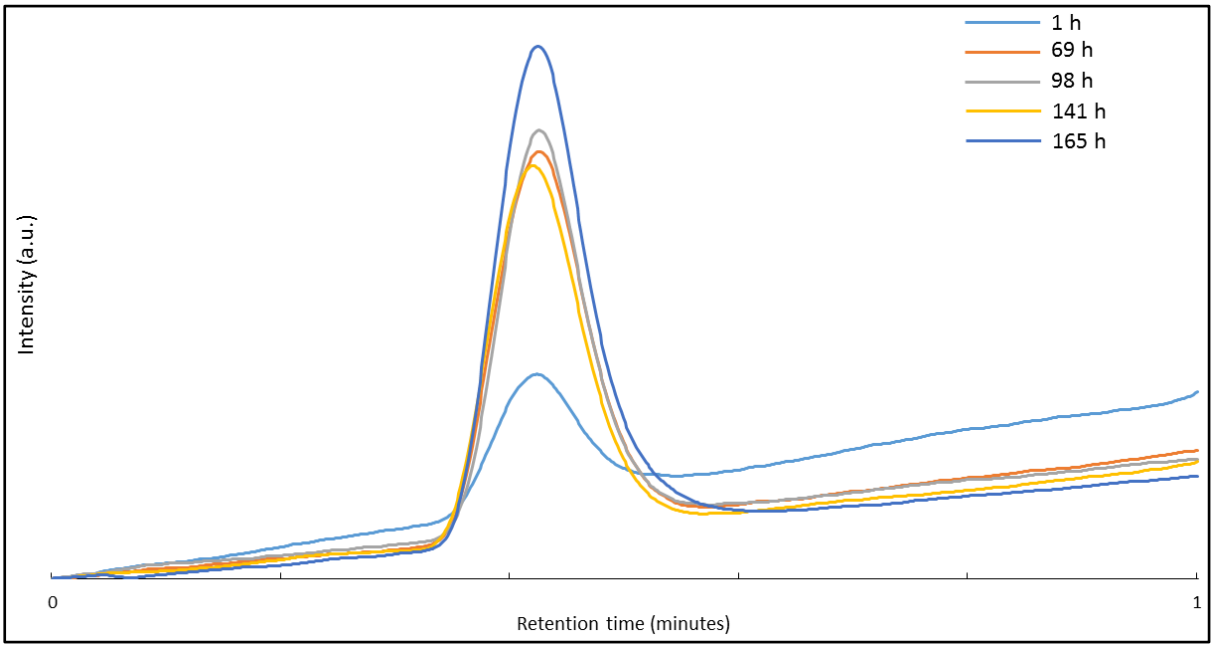

Figure 34. Gas chromatograms of gas sampling from the headspace of the accelerated corrosion vial at different corrosion times of the unirradiated Zircaloy-4 sample in $Ca(OH)_2$ electrolyte (Zoom from 0.2 to 0.6 minute of Figure 32).

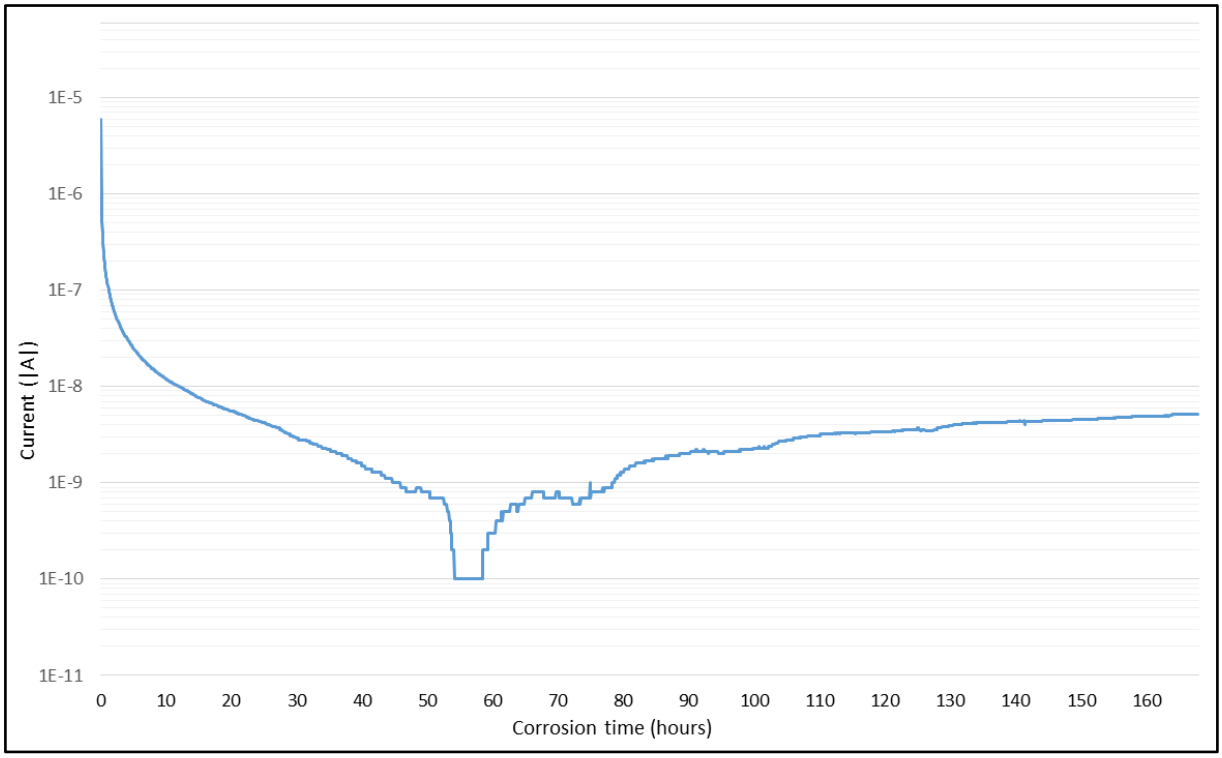

Figure 35. Current as a function of corrosion time of the unirradiated Zircaloy-4 sample in $Ca(OH)_2$

From Figure 35, it was also possible to calculate the total charge as well as the amount of corroded metal (see calculation in Appendix 3). It appeared that a corrosion rate of ~54 nm/year is obtained if all the recorded current came from the corrosion of the Zircaloy-4. This value looks very high compared to the corrosion rate of 10 nm per year suggested by IAEA [IAEA, 1998 ; IAEA 2006].

3.6.1.1.1.2 Saturated $Ca(OH)_2$ aqueous electrolyte in presence of chloride ($CaCl_2$)

Looking at the accelerated corrosion test in saturated portlandite, nearly no corrosion happened even after 7 days of testing. To increase the corrosion rate, 1 mole of chloride (0.5 M $CaCl_2$) was added to the electrolyte solution. This addition led to a decrease of the pH from ~12.5 to ~11.7.

These conditions are more harsh than the ones encountered in geological storage but they offer the possibility to hasten the release of Zr (and other alloying elements from the bulk metal matrix) by inducing pitting corrosion which should lead to an increase of the gas formation.

The applied potential was 600 mV vs. Ag/AgCl (0.1 KCl). This potential was chosen based on the corresponding polarisation curve (see Figure 29 in Section 3.5.1). As explained earlier, pitting corrosion happens at this potential leading to a higher release of Zr (and other elements). Indeed, only a few seconds after applying the chosen potential, pitting occurred and grey precipitation products were formed abundantly from the metal surface. Figures 36 and 37 show chromatograms obtained from the analysis of the headspace of the corrosion vial after 1 hour and 5 hours of corrosion.

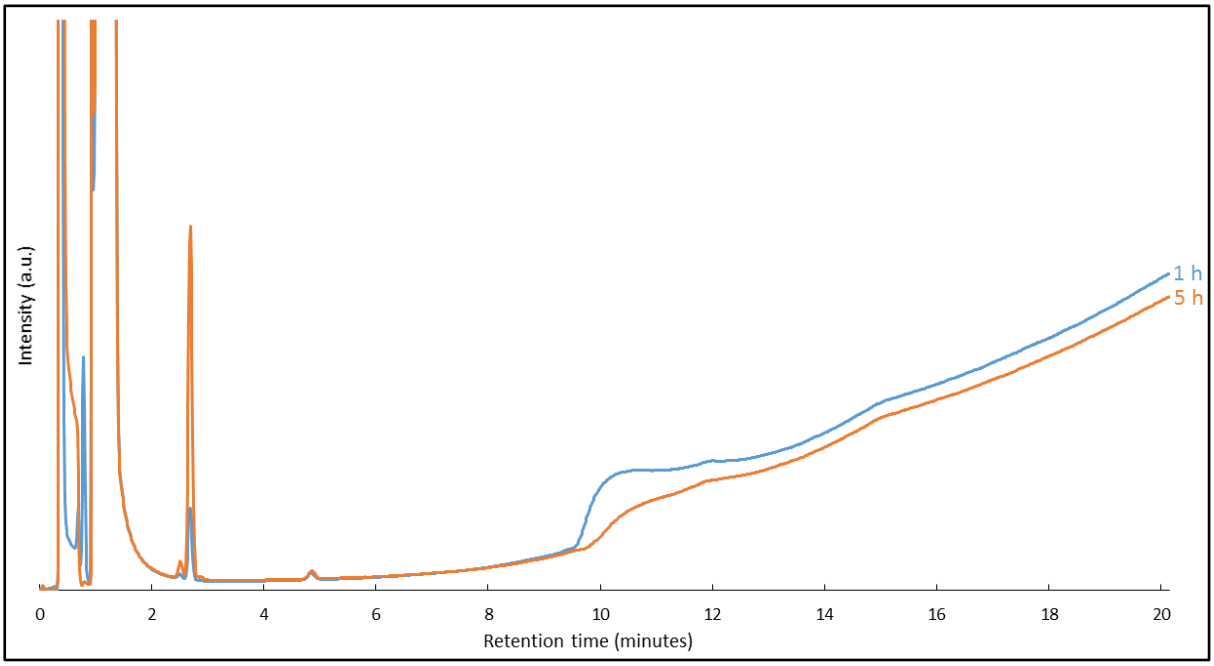

Figure 36. Gas chromatograms of gas sampling from the headspace of the accelerated corrosion vial at different corrosion times of the unirradiated Zircaloy-4 sample in $Ca(OH)_2$ + $CaCl_2$ electrolyte.

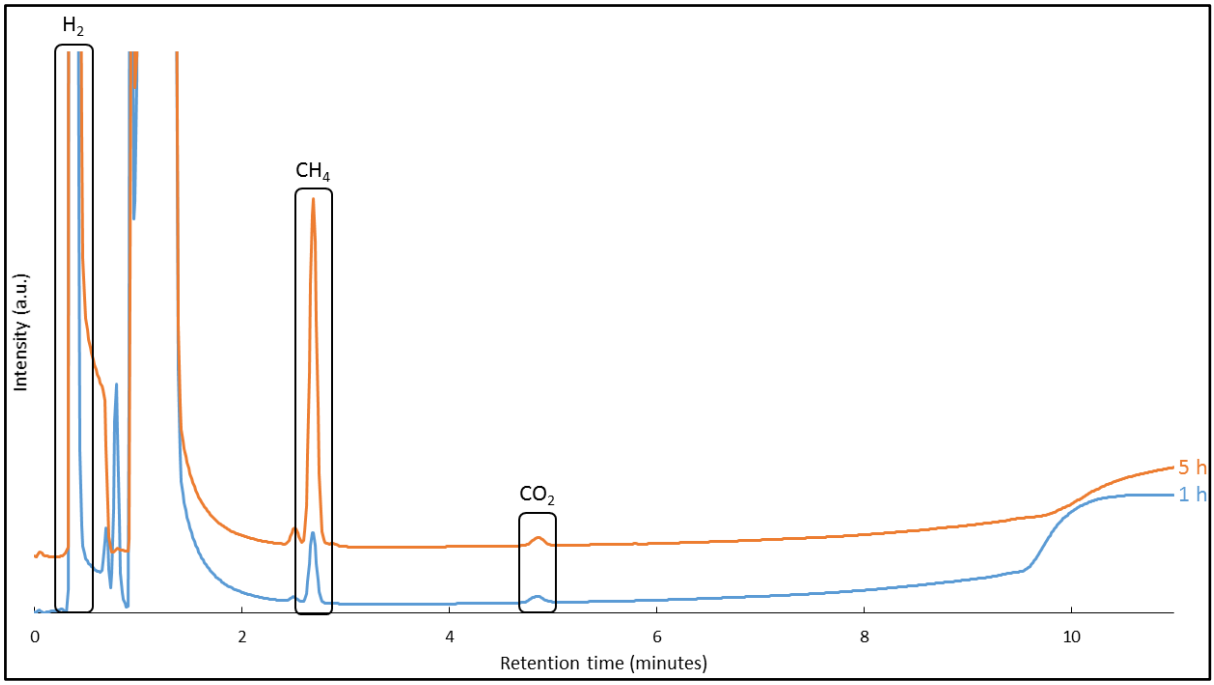

Figure 37. Gas chromatograms of gas sampling from the headspace of the accelerated corrosion vial at different corrosion times of the unirradiated Zircaloy-4 sample in $Ca(OH)_2$ + $CaCl_2$ electrolyte (zoom of Figure 36).

Figures 36 and 37 show a huge production of methane and hydrogen. Concentrations of 13.1 ± 0.7 µg/g and 66.4 ± 3.4 µg/g (calculated using the validation presented in Appendix 2) of methane were obtained after 1 and 5 hours of corrosion, respectively, in the presence of chloride. These values look very high, but by analysing the depth of the corroded Zircaloy-4 and taking into account the concentration of carbon in the Zircaloy-4 bulk (270 µg/g; see Table 1) and considering the hypothesis that all the carbon reacts to form methane, this concentration is plausible (calculation shown in Appendix 4). Note that this hypothesis is credible in view of the chromatograms. Indeed, except for the intense peak at ~0.4 minutes of retention time, resulting from the formation of hydrogen during corrosion of Zircaloy-4, no other peaks could be detected.

3.6.1.1.2 Irradiated samples

The same kind of corrosion tests than the ones realised on unirradiated samples were performed on the irradiated one in order to study the effect of irradiation.

3.6.1.1.2.1 Saturated $Ca(OH)_2$ aqueous electrolyte

Figures 38 and 39 show chromatograms obtained from the analysis of the headspace of the corrosion vial as a function of time. As for the unirradiated sample, the applied potential is -750 mV vs. Ag/AgCl (0.1 M KCl).

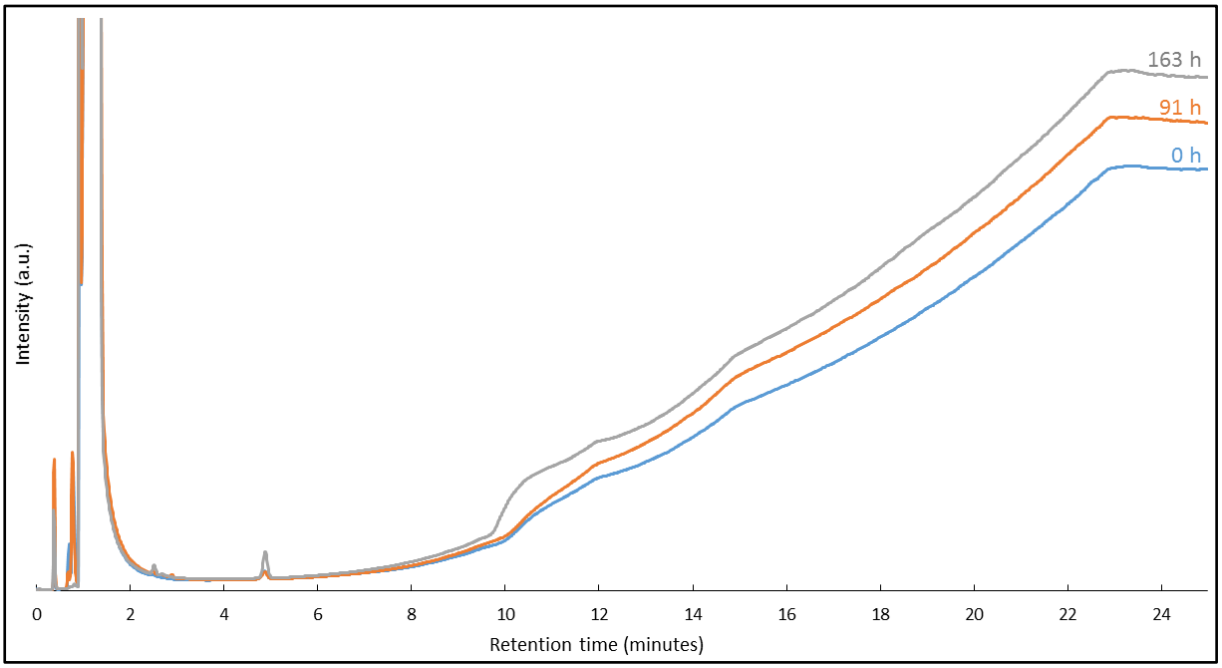

Figure 38. Gas chromatograms of gas sampling from the headspace of the accelerated corrosion vial at different corrosion times of the irradiated Zircaloy-4 sample in $Ca(OH)_2$ electrolyte.

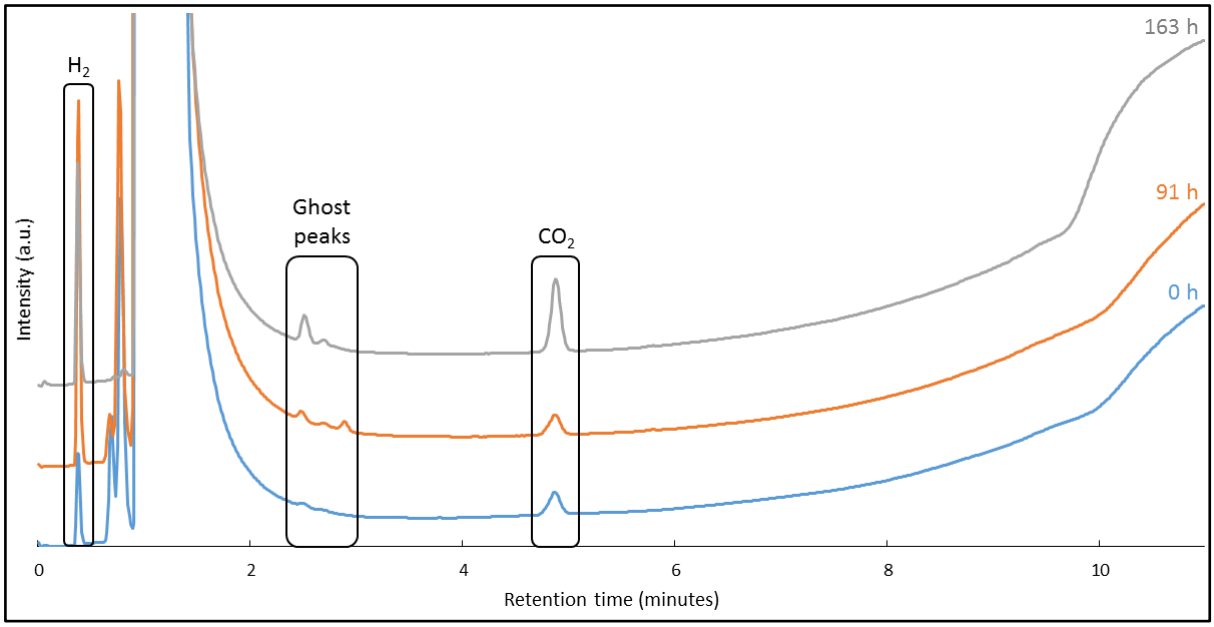

Figure 39. Gas chromatograms of gas sampling from the headspace of the accelerated corrosion vial at different corrosion times of the irradiated Zircaloy-4 sample in $Ca(OH)_2$ electrolyte (zoom of Figure 38).

No carbon-based molecules could be measured even after nearly 7 days of testing. Nevertheless, the peak of hydrogen is a little more intense than the ones observed for the unirradiated Zircaloy-4 corrosion. This phenomenon could be due to a higher corrosion, although this is not confirmed by the low current (between 10^{-10} A and 10^{-9} A) recorded throughout the entire test (Figure 40).

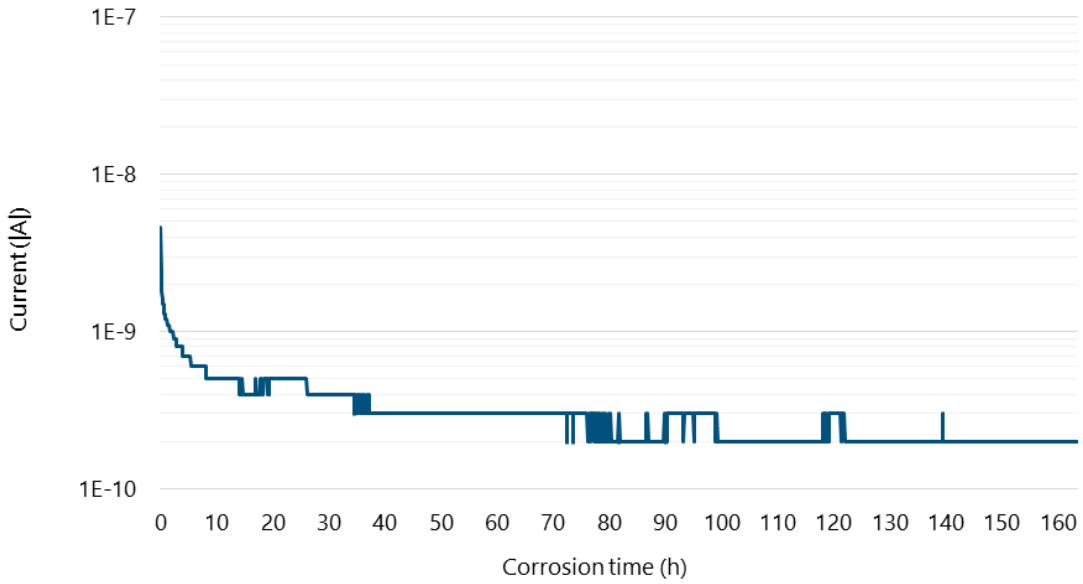

Figure 40. Current as a function of corrosion time of the irradiated Zircaloy-4 sample in $Ca(OH)_2$

Here again, the total charge as well as the estimated corrosion rate were calculated from the I vs. t curve (Figure 40). A corrosion rate of ~4 nm/year is obtained if all the recorded current came from the corrosion of the Zircaloy-4. This value is lower than the one obtained for the unirradiated sample and looks more at the value suggested by IAEA [IAEA, 1998; IAEA 2006]. This could have resulted from a better corrosion resistance, as suggested by the improvement of the quality of the passive film or from the fact that the passive layer was already present at the beginning of this test. Indeed, the potentiostatic test was performed directly after recording the polarisation curve. This was done to avoid an extra polishing step and to keep enough material for the following corrosion tests that had to be realised on this sample.

3.6.1.1.2.2 Saturated $Ca(OH)_2$ aqueous electrolyte in presence of chloride ($CaCl_2$)

The applied potential was 1 V vs. Ag/AgCl (0.1 M KCl). This potential was chosen based on the corresponding polarisation curve (see Figure 31 in Section 3.5.2). As explained earlier, pitting corrosion occurred at this potential. However, this high potential led also to the hydrolysis of water and thus the production of hydrogen and oxygen in the corrosion vial. Figures 41 and 42 show chromatograms obtained from the analysis of the headspace of the corrosion vial after a corrosion of 2 hours 20 minutes and 4 hours 30 minutes.

The irradiated sample showed a similar behaviour to the unirradiated sample, with respect to the production of hydrogen and methane. Hydrogen is produced via the corrosion of the Zircaloy-4 sample but also via water hydrolysis, as explained above. Concentrations of 59.4 ± 3.0 µg/g and 93.8 ± 4.7 µg/g (calculated using the validation presented in Appendix 2) of methane were obtained after 2 hours 20 minutes and 4 hours 30 minutes of corrosion, respectively, in the presence of chloride. This methane concentration is higher than the one obtained after the analysis of the unirradiated sample. This could be due to the higher concentration of carbon inside the irradiated sample by the activation of ^{14}N ($^{14}N(n,p)^{14}C$). However, the most probable reason is the change of the applied potential, which changes the corrosion conditions. Moreover, in these conditions, there is a production of hydrogen from water hydrolysis and this higher hydrogen concentration could enhance the reaction with the released carbon to produce methane.

Note that the intensity of the CO_2 peak is higher after 2 hours 20 minutes of corrosion than after 4 hours 30 minutes of corrosion. This could be explained by a small leak observed at the connection between the needle and the syringe during this injection in the GC, leading to an air contamination.

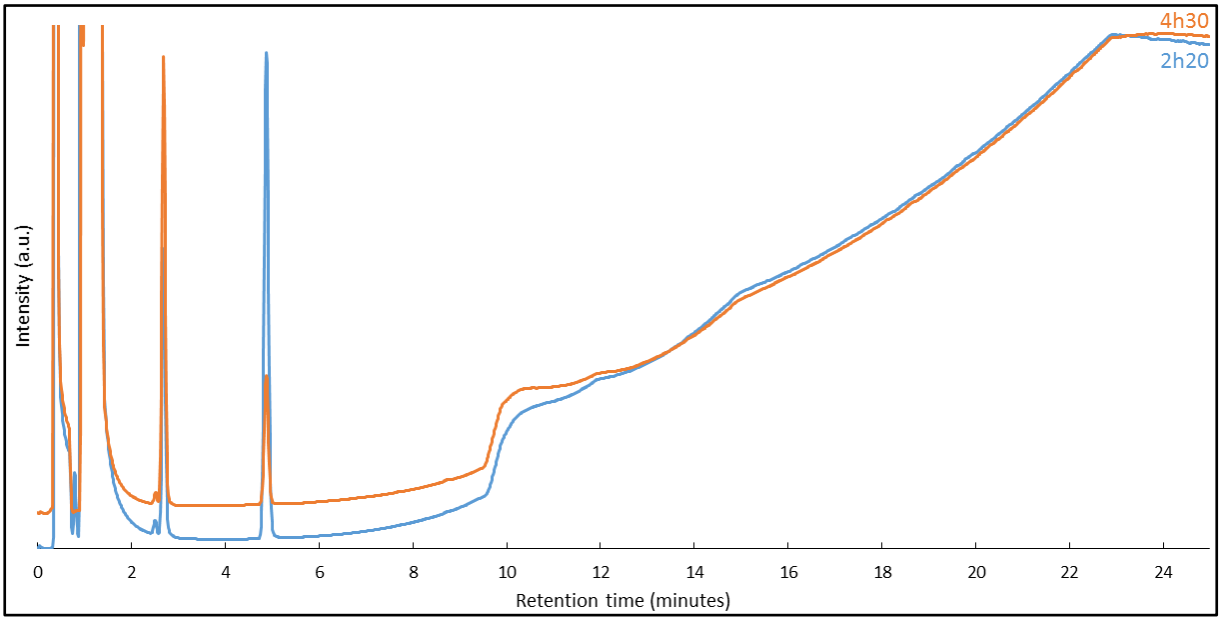

Figure 41. Gas chromatograms of gas sampling from the headspace of the accelerated corrosion vial at different corrosion times of the irradiated Zircaloy-4 sample in $Ca(OH)_2$ + $CaCl_2$ electrolyte.

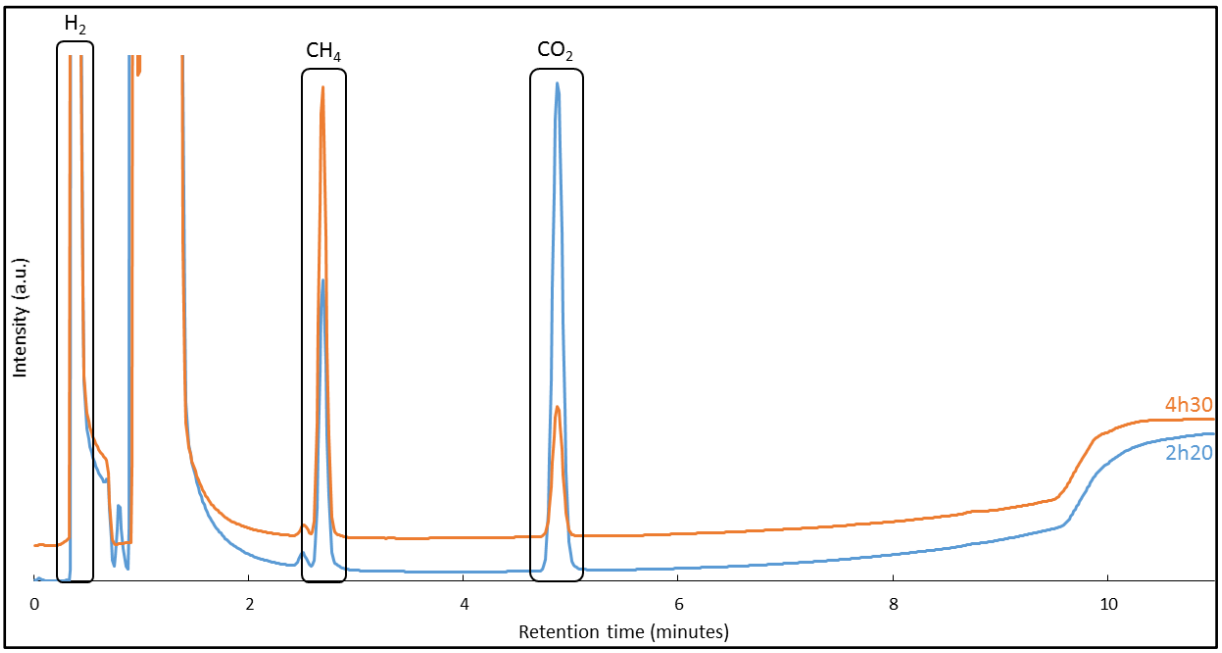

Figure 42. Gas chromatograms of gas sampling from the headspace of the accelerated corrosion vial at different corrosion times of the irradiated Zircaloy-4 sample in $Ca(OH)_2$ + $CaCl_2$ electrolyte (zoom of Figure 41).

3.6.1.2 Static corrosion tests

As mentioned in Section 2.1.2.1, static corrosion tests were performed on sample F6678-R4-A, F6678-R4-B and F6678-R4-C. Unirradiated samples were not tested. Table 9 gives the dose rate of these samples just after cutting (14/07/2016), just before the start of the static corrosion tests (09/09/2016) and after the end of the static tests (23/03/2017).

Table 9. Dose rate after cutting the samples and just before to start static corrosion tests of irradiated Zircaloy-4 samples.

Sample ID	Dose rate (µSv/h)		
	14/07/2016 (in contact)	09/09/2016 (in contact through a plastic flask)	23/03/2017 (in contact through a plastic flask)
F6678-R4-A	900	450	240
F6678-R4-B	450	270	130
F6678-R4-C	400	200	110

A decrease of the sample activity in time was observed. This decay can be partly attributed to the corrosion process. It is believed to be also due to the natural radionuclide decay (Radionuclide elements are listed in Table 7). Indeed, the dose rate was already decreasing before to start the tests, as shown in Table 9. This decay before the test was also measured on the sample used for the accelerated corrosion tests. In this case, the dose rate in direct contact (without the presence of plastic flask) decreased from 270 µSv/h to 113 µSv/h in seven months (from 14/07/2016 to 15/02/2017).

After 195 days (~6.5 months), gas and liquid samples were taken. The corresponding chromatograms are compared in Figures 43 and 44.

Figure 43 shows a broad peak corresponding to the presence of oxygen. This high concentration did not come from the accidental injection of air in the column because its presence is recurrent to the three samples. Moreover, it was not due to a leak in the static test vials because the intensity of the peak corresponding to the presence of CO_2 (Figure 44)

is comparable to the intensities measured during the calibration procedure. So, it is believed that oxygen should come from water radiolysis.

Figure 44 shows a zoom of Figure 43. Peaks for hydrogen, methane, carbon dioxide and ethene can clearly be distinguished. Between 9 and 10 minutes of retention, a bump in the GC chromatograms is observed, which can be attributed to water. Unfortunately, this bump can interfere with the ethane peak. Therefore, it becomes impossible to know if this gas was formed (or not) during the corrosion of Zircaloy-4 samples. The signals for the carbon compounds were quantified using the calibration curves shown in Appendix 2. The results are shown in Table 10. The measured concentrations are low, but are well above the detection limit, except for carbon dioxide.

No calibration curve was available for hydrogen and the concentration could not be determined quantitatively.

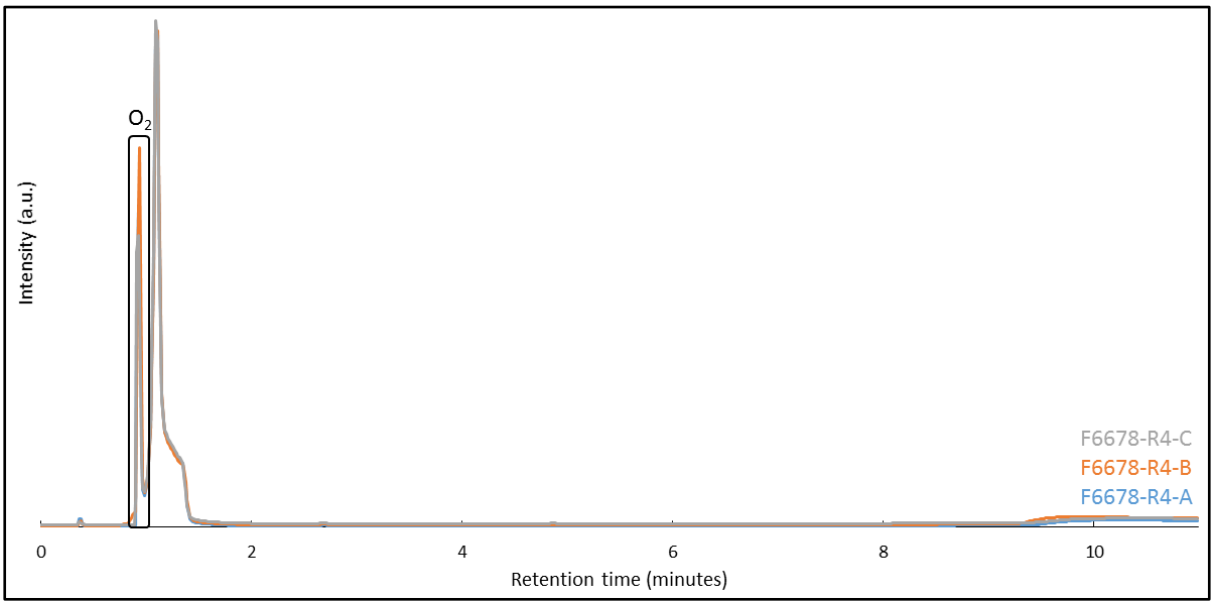

Figure 43. Gas chromatograms of gas sampling from the headspace of the static corrosion vials of the irradiated Zircaloy-4 sample in $Ca(OH)_2$ after 195 days.

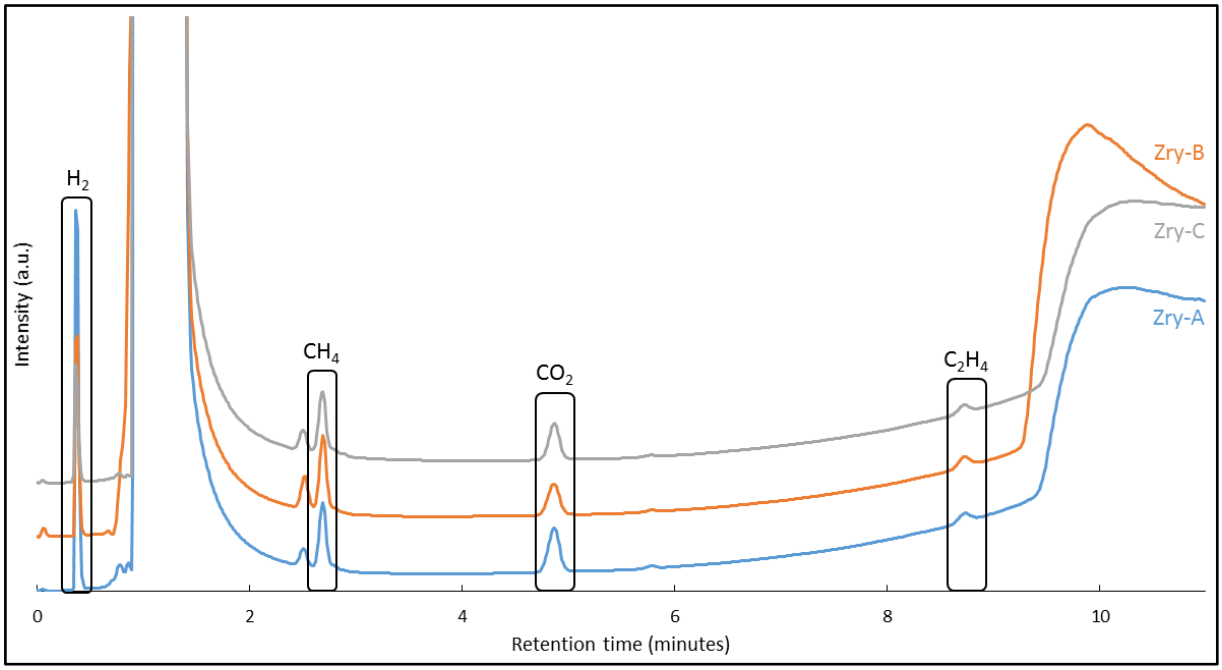

Figure 44. Gas chromatograms of gas sampling from the headspace of the static corrosion vials of the irradiated Zircaloy-4 sample in $Ca(OH)_2$ after 195 days (Zoom of Figure 43).

Table 10. Calculated concentrations of methane, ethene and carbon dioxide in the gas phase after static corrosion tests of Zircaloy-4 in portlandite pore water (duration 195 days).

Samples	Methane		Ethene		Carbon dioxide	
	Measured peak area	Calculated concentration (µL/L)	Measured peak area	Calculated concentration (µL/L)	Measured peak area	Calculated concentration (µL/L)
F6678-R4-A	445448	6.4 ± 0.3	87015	1.0 ± 0.1	461671	5.0 ± 2.0
F6678-R4-B	481731	7.0 ± 0.4	104984	1.2 ± 0.1	341713	3.2 ± 2.0
F6678-R4-C	410637	5.9 ± 0.3	72075	0.8 ± 0.1	364723	3.6 ± 2.0
Mean value		6.4 ± 0.3		1.0 ± 0.1		3.9 ± 2.0

Thanks to the calculated carbon-based gas production and the carbon concentration in the bulk, an approximation of the corrosion rate could be determined (details are given in Appendix 5). Under the simplified hypothesis that all the carbon present in the bulk, and released during the corrosion, was transformed in carbon-based gas, the corrosion depth reached 45 nm after 195 days, which corresponds to a corrosion rate of 84 nm per year. Due to the high uncertainties on the CO_2 concentration, we also calculated the corrosion rate

without taking into account the CO_2 contribution. In these conditions, the calculated corrosion rate equals 57 nm/year.

These values look very high compared to the corrosion rate of 10 nm per year suggested by IAEA [IAEA, 1998 ; IAEA 2006] but they are in good agreement with the corrosion rate calculated from the I vs. t curve (Figure 35 and Appendix 3). Even if the corrosion was reproducible on our 3 tests, this value should be considered with caution. Indeed, due to the washing step, initially performed to reduce the activity of those samples, the oxide layer formed at the surface of the Zircaloy-4 sample was changed, which might have led to possible changes in the corrosion rate.

3.6.2 Analysis of the liquid phase

The previous sections gave an overview of the carbon speciation in the gas phase determined by gas chromatography. In this section the carbon speciation of the liquid phase is discussed. This carbon speciation was realised by total organic / inorganic carbon analysis (TIC/TOC) and by ion chromatography (IC) to determine the presence of carboxylic acids. The ^{14}C determination was analysed by liquid scintillation counting (LSC), while the whole activity of the solutions was measured by γ-ray spectrometry.

3.6.2.1 Carbon speciation by total organic / inorganic carbon analysis and by ion chromatography

Carbon speciation analysed by total organic / inorganic carbon (TIC/TOC) was realised on blank electrolytes and on all leachate solutions after static and accelerated corrosion tests. Results are shown in Table 11. TIC and TOC values of Zircaloy-4 leachate solutions were corrected for the TIC and TOC content present in the blank solution. Non corrected values are presented in Appendix 7. It has to be mentioned that the analysis of solutions obtained after the corrosion of active samples or inactive samples was performed with two different apparatus. To be able to compare all results, blank solutions were analysed by both TIC/TOC machines and gave very similar results.

Analysis of the blanks showed that some inorganic and organic carbon was already present in solution before the start of the corrosion tests. Even if the solutions were prepared in a glove box under inert atmosphere, inorganic carbon could come from the reaction of CO_2 (still present in the glove box atmosphere, albeit in a very low concentration) with the high pH solution, producing carbonates. A small contamination with atmospheric CO_2 may also have happened during the measurement of the solution, although this should have led to a higher TIC concentration in the leachate solutions as well. However, the corrosion of Zircaloy-4 released some Zr^{4+} ions in solution, even if in low concentration, which could have led to the precipitation of $Zr(CO_3)_2$. Indeed, the K_{sp} of $Zr(CO_3)_2$ ($3.6x10^{-10}$ $(mol/L)^3$) is lower than the one of $CaCO_3$ ($4.95x10^{-9}$ $(mol/L)^2$) and its precipitation is favored compared to the one of $CaCO_3$. This precipitation could then decrease the TIC content in solution. The organic carbon probably came from a degradation of the sample holder resin due to a combination of the high pH solution and sample radiation. The organic carbon could also come from the polypropylene recipient into which the solution was poured after its preparation to avoid the increase of Si due to glass dissolution at high pH, which would chang the composition of the solution and maybe the corrosion behaviour.

No inorganic carbon was found after the accelerated corrosion tests in saturated portlandite solution while approximately 4 mg/L of organic carbon was obtained for the accelerated corrosion of unirradiated samples and more than 19 mg/L for the accelerated corrosion of the irradiated sample in saturated portlandite solution. This last result is surprising because neither the GC analysis nor I vs. t curves recorded during the corrosion test could explain such a high concentration. Furthermore, this organic carbon should not come from a contamination of the electrolyte used for this analysis because electrolyte from the same batch was also used for the analysis of the blank (Blank-$Ca(OH)_2$). As explain earlier, organic carbon could then come from the polypropylene recipient or sample holder resin.

The analysis of the accelerated corrosion tests electrolyte in the presence of chloride showed the presence of inorganic and organic carbon after the corrosion of the unirradiated sample. This was expected due to pitting corrosion. However, only a small amount of inorganic and organic carbon was detected after the corrosion of the irradiated material (see Table A7-1 in

Appendix 7). Due to pitting corrosion, heavy particles were released in solution. Some carbon could have been adsorbed and/or precipitated with these particles.

Finally, after the static corrosion tests, no inorganic carbon was detected in the saturated portlandite solution while only little organic carbon was detected (under the blank level; Tables 11 and A7-1). These results were expected because of the low corrosion rate expected for those tests. Moreover, the lower organic carbon concentration in leachates from static corrosion tests than in the blank solution supports our hypothesis that organic carbon maybe came from the polypropylene recipient. Indeed, for the static corrosion tests, the solution was used directly after its preparation and hence it was not stored in plastic bottles for a long time, as done for the accelerated tests. Indeed, the large batch of solution was realised for all the accelerated tests realised in this study.

Table 11. Results from total organic / inorganic carbon analysis of blank electrolytes and the Zircaloy-4 leachates (blank value substracted from leachate concentration).

Sample-ID	Electrolyte/Material	TIC (mg/L)	TOC (mg/L)
Blank-$Ca(OH)_2$	Saturated portlandite water solution	6.4 ± 0.8	4.4 ± 0.5
Blank-$CaCl_2$	Saturated $Ca(OH)_2$ water solution + 0.5 M $CaCl_2$	7.4 ± 0.7	7.4 ± 0.7
Inactive-Zry-4_ $Ca(OH)_2$	Unirradiated Zircaloy-4 / Accelerated test / $Ca(OH)_2$ water solution	< 0.5	3.9 ± 0.8
Inactive-Zry-4_ $CaCl_2$	Unirradiated Zircaloy-4 / Accelerated test / $Ca(OH)_2$ + $CaCl_2$ water solution	10.8 ± 0.5	4.1 ± 1.1
Active-Zry-4_ $Ca(OH)_2$	Irradiated Zircaloy-4 / Accelerated test / $Ca(OH)_2$ water solution	< 0.5	19.4 ± 2.4
Active-Zry-4_ $CaCl_2$	Irradiated Zircaloy-4 / Accelerated test / $Ca(OH)_2$ + $CaCl_2$ water solution	< 0.5	< 0.5
Sol-F6678-R4-A	Irradiated Zircaloy-4 / Static test / $Ca(OH)_2$ water solution	< 0.5	< 0.5
Sol-F6678-R4-B	Irradiated Zircaloy-4 / Static test / $Ca(OH)_2$ water solution	< 0.5	< 0.5
Sol-F6678-R4-C	Irradiated Zircaloy-4 / Static test / $Ca(OH)_2$ water solution	< 0.5	< 0.5

Ion chromatography was also performed to analyse the carboxylic acid content such as formate, acetate and oxalate in the leachate solutions (Table 12). The analysis of the blank solutions showed that no carboxylic acids were detected in presence of chloride, while some formate and acetate were already present in saturated portlandite solution in low concentration. The presence of these molecules is surprising because both electrolytes were prepared in the same conditions. One of the differences between both electrolytes is the higher pH obtained for the saturated portlandite solution (~12.5 compared to ~11.7 in the presence of chloride) which could influence the solution stored in polypropylene bottles. The second difference is the presence of 0.5 mol/L of Ca^{2+}, which could bind formate and acetate, resulting in their precipitation, removed after filtration over 0.45 µm before the ion chromatography analysis. Finally, in none of the solutions was oxalate found. This may mean that the formation of molecules with two carboxylic acid functions is less favourable in the conditions met during these corrosion tests.

After the accelerated corrosion tests in saturated portlandite solution (without chloride), formate and acetate were detected. This was unexpected for accelerated corrosion because tests were running for only one week in 400 mL solution volume, leading to a very low corrosion of the Zircaloy-4 sample and an even more lower carbon-based molecule concentration. Therefore, these molecules could also come from impurities, as the ones measured in the blank.

After the accelerated corrosion tests in the presence of chloride, no carboxylic acids were detected. Either the organic carbon-based compounds were entirely present in the gas phase as CH_4, as shown by GC, or they are present in the precipitate formed during pitting corrosion or they could be adsorbed on the vial wall.

For the static corrosion tests, formate and acetate were detected (Tables 12 and A7-2). Thanks to this information, the approximation of the corrosion rate, calculated in Appendix 5, could be adjusted. The new calculation (Appendix 6) gave a mean corrosion rate of ~1.7 µm after 195 days of corrosion. This simple calculation clearly showed that formate and acetate detected after static corrosion did not come only from the corrosion but also from contamination of the saturated portlandite solution used to perform the corrosion tests.

Again, this contamination could maybe come from the polypropylene vials used to transfer the solution or from the ion chromatograph during the measurement of our sample. Indeed, the visual effect of such a high corrosion (1.7 µm) would be easily seen without microscope (obtaining a matt surface, difference in colour before and after the corrosion test, etc). Yet no specific sample changes were observed at the end of the static corrosion test.

Table 12. Carboxylic acid content analysis by ion chromatography for Zircaloy-4 leachates and blank electrolytes *(blank value substracted from leachate concentration).*

Sample ID	Electrolyte / Material	Formate (mg/L)	Acetate (mg/L)	Oxalate (mg/L)
Blank-$Ca(OH)_2$	Saturated portlandite water solution	0.16 ± 0.02	0.14 ± 0.01	< 0.1
Blank-$CaCl_2$	Saturated $Ca(OH)_2$ water solution + 0.5 M $CaCl_2$	< 0.1	< 0.1	< 0.1
Inactive-Zry-4_$Ca(OH)_2$	Unirradiated Zircaloy-4 / Accelerated test / $Ca(OH)_2$ water solution	< 0.1	0.19 ± 0.03	< 0.1
Inactive-Zry-4_$CaCl_2$	Unirradiated Zircaloy-4 / Accelerated test / $Ca(OH)_2$ + $CaCl_2$ water solution	< 0.1	< 0.1	< 0.1
Active-Zry-4_$Ca(OH)_2$	Irradiated Zircaloy-4 / Accelerated test / $Ca(OH)_2$ water solution	0.12 ± 0.03	0.13 ± 0.03	< 0.1
Active-Zry-4_$CaCl_2$	Irradiated Zircaloy-4 / Accelerated test / $Ca(OH)_2$ + $CaCl_2$ water solution	< 0.1	< 0.1	< 0.1
Sol-F6678-R4-A	Irradiated Zircaloy-4 / Static test / $Ca(OH)_2$ water solution	0.35 ± 0.05	< 0.1	< 0.1
Sol-F6678-R4-B	Irradiated Zircaloy-4 / Static test / $Ca(OH)_2$ water solution	0.28 ± 0.04	< 0.1	< 0.1
Sol-F6678-R4-C	Irradiated Zircaloy-4 / Static test / $Ca(OH)_2$ water solution	0.15 ± 0.03	0.10 ± 0.02	< 0.1

In conclusion, the interpretation of the TIC/TOC and ion chromatography analyses is not easy and many hypotheses were formulated to try to explain the results. To check these hypotheses, more experimental work is ongoing such as the analysis of possible adsorbed

carbon-based molecules on the corrosion cell walls and the release of organic carbon from the resin used to embed the test specimens. However, the uncertainties on these TIC/TOC and ion chromatography analyses should remain high.

3.6.2.2 Liquid Scintillation Counting

To determine the total ^{14}C activity released in solution by corrosion, Liquid Scintillation Counting (LSC) was performed on all leachates of irradiated Zircaloy-4 (static and accelerated corrosion tests). Looking at the ^{14}C concentration in the Zircaloy-4 sample calculated in Section 3.4 and the possible mass weight of Zircaloy-4 corroded during static tests (see Appendix 5), the activity of the released ^{14}C should be ~7 Bq in 35 mL of solution and 15 mL for the gas head space.

Unfortunately, due to the contamination of solutions with other higher energetic radionuclides (e.g. ^{60}Co), it was not possible to calculate the ^{14}C activity of leachates from static corrosion tests and accelerated tests in presence of chloride. The only measurable solution was the leachate from the accelerated corrosion test in saturated portlandite solution. LSC gave an activity below 12.4 Bq/L, which is considered as the background. This value was expected due to the very low corrosion rate occurring during this test.

3.6.2.3 γ-ray spectometry

Finally, γ-ray spectrometry was also performed on the electrolyte solutions after static corrosion of sample F6678-R4-B (Table 14) and accelerated corrosion of the irradiated Zircaloy-4 in the presence of chloride (Table 15). These solutions were chosen because F6678-R4-B released more carbon species than F6678-R4-A and F6678-R4-C. In addition, during the accelerated corrosion tests, the sample corroded more intensively in the chloride-containing solution compared to the saturated portlandite solution.

Tables 14 and 15 show that, indeed, a small percentage (0.1-1%) of radionuclides present in the Zircaloy-4 samples are dissolved in solution due to their corrosion. Moreover, for both

tests, radionuclides possessing higher activity in solution also possessed higher activity in the bulk sample. This could mean that radionuclides are homogeneously present inside the sample.

Finally, the activity of the solution from the static test is lower than the one from the accelerated corrosion tests in presence of chloride, confirming that, as expected, the pitting corrosion induced a higher corrosion than the static corrosion.

Unfortunately, SCK•CEN has no expertise in the separation of ^{14}C from other radionuclides in solution. So, as explained in the previous section, the determination of the ^{14}C activity was not possible.

Table 14. γ-ray spectrometry of the electrolyte solution after the static corrosion of sample F6678-R4-B.

F6678-R4-B	
Nuclides	Activity (Bq/L)
^{54}Mn	< 11
^{60}Co	53 ± 5
^{95}Nb	141 ± 17
^{95}Zr	< 23
^{106}Ru	3700 ± 400
^{113}Sn	< 19
^{125}Sb	1950 ± 250
^{134}Cs	620 ± 70
^{137}Cs	3090 ± 340
^{144}Ce	240 ± 40

Table 15. γ-ray spectrometry of the electrolyte solution after the accelerated corrosion of sample F6678-R4-E in the presence of $CaCl_2$.

Active-Zry-4_$CaCl_2$	
Nuclides	Activity (Bq/L)
^{54}Mn	630 ± 70
^{60}Co	18000 ± 1200
^{95}Nb	4200 ± 500
^{95}Zr	1560 ± 120
^{106}Ru	220 ± 100
^{113}Sn	2340 ± 330
^{125}Sb	37000 ± 5000
^{134}Cs	< 60
^{137}Cs	287 ± 35
^{144}Ce	180 ± 50

4 Conclusions

The aim of the work at SCK•CEN in the framework of Work Package 3 of the CAST project was to investigate the release of ^{14}C from Zircaloys representative for the claddings of the fuel of Belgian nuclear power plants and the ^{14}C speciation in a cementitious environment, which is relevant for the Belgian Supercontainer design, as perceived for the geological disposal of high level waste.

Both irradiated and unirradiated Zircaloy-4 samples, representative of the fuel cell claddings of Belgian nuclear power plants, were studied at the SCK•CEN.

The unirradiated sample was a rod of Zircaloy-4 which was cut in smaller pellets. The total nitrogen content of this sample showed the presence of 17 to 25 µg/g in the bulk, which is 2 to 4 times lower than the 40 to 80 µg/g expected from the specification sheets. Calculation showed that this would lead, after irradiation, to a ^{14}C activity of 13300 to 19600 Bq/g in the irradiated Zircaloy-4.

Metallographic analysis was performed on both irradiated and unirradiated samples to analyse the influence of radiation on the metallic structure. The structure of the samples possessed dislocation line defects and, $Zr(Fe,Cr)_2$ Laves phases and needle- or platelet-like

ZrC phase precipitates. The main effect of the neutron irradiation was the presence of small dislocation loops and a low amorphisation of the Laves phase precipitates.

To obtain information on the behaviour of Zircaloy-4 in real geological conditions, long-running static (leaching) corrosion tests were performed. Accelerated (polarised) corrosion tests were performed to obtain some indication of the corrosion mechanism and the formation of lower carbon molecules in a shorter reaction time. The electrolyte used was a saturated portlandite $Ca(OH)_2$ aqueous solution of pH 12.5, representative of the geological disposal conditions. In addition, for a second batch of accelerated tests, 0.5 M of $CaCl_2$ was added to the portlandite solution, stimulating pitting corrosion in order to obtain a higher yield of corrosion products.

The accelerated tests were performed under a nitrogen atmosphere in glass test cells equipped with a standard three-electrode setup, using a home-made Ag/AgCl electrode as reference electrode, a platinum mesh as counter electrode, and an embedded and polished Zircaloy-4 sample as working electrode. Before starting the accelerated corrosion tests, polarisation curves were recorded to have information on the electrochemical behaviour of the Zircaloy-4 samples. Irradiation seemed to induce some difference in the sample behaviour such as the stabilisation of the passivation layer or the shift of the corrosion potential to more a reductive potential. The addition of chloride led to a huge increase of the current at a potential called pitting potential, where pitting corrosion commences.

The static (leaching) tests were performed in PEEK-lined steel vials with an internal volume of 50 cm^3 filled with 35 cm^3 of electrolyte under a nitrogen atmosphere. After closing the cell gastight with a lid, the whole setup was left behind a lead wall for 195 days.

Carbon speciation was analysed by total organic / inorganic carbon content (TIC/TOC), ion chromatography (IC) and liquid scintillation counting (LSC) for the liquid phase and by gas chromatography for the gas phase. Unfortunately, it was difficult to obtain reliable information of the total inorganic and organic compounds in solution due to the very low concentration of carbon-based compounds coming from corrosion process and due to the presence of some contamination which were very difficult to avoid. The activity of ^{14}C was

also difficult to obtain due to the presence of other radionuclides and due to the low concentration of ^{14}C released during corrosion.

Gas chromatography analysis showed that no carbon-based compounds were detected after the accelerated corrosion tests in saturated portlandite, while methane was observed in the presence of chloride. For the static corrosion tests, methane, ethene and maybe CO_2 were produced. Methane is the main carbon-based gas present in the gas phase.

5 References

[ADAMSON, 2000] ADAMSON, R.B. [2000]. *Zirconium in the Nuclear industry: Twelfth international symposium, ASTM STP, Vol.* 1354, eds. G.P. Sabol and G.D. Moan, American Society for Testing and Materials, 15-31.

[ASTM, 2002] ASTM B353-02. [2002]. Standard specification for wrought zirconium and zirconium alloy seamless and welded tubes for nuclear service.

[ASTM, 2013] ASTM B811-13. [2013]. Standard specification for wrought zirconium alloy seamless tubes for nuclear reactor fuel cladding, *ASTM International*, West Conshohocken, PA. DOI: 10.1520/B0811-13, Available from http://www.astm.org

[BLOKHIN, 2012] BLOKHIN, D.A., CHERNOV, V.M., BLOKHIN, A.I., DENIM, N.A., and SIPACHEV, I.V. [2012]. Nuclear physical properties of zirconium alloys E110 and E635 under long-term neutron irradiation in VVER-1000 reactor, *Inorganic Materials: Applied Research*, vol. 3, 124-128.

[GRIFFITHS, 1994] GRIFFITHS, M., MECKE, J.F., and WINEGAR, J.E. [1994]. *Zirconium in the Nuclear Industry: Eleventh International Symposium, ASTM STP*, Vol. 1295, Eds. E.R. Bradley and G.P. Sabol, American Society for Testing and Materials, 580-602.

[IAEA, 1998] IAEA. [1998]. Durability of spent nuclear fuels and facility components in wet storage, *IAEA-TECDOC-1012*.

[IAEA, 2006] IAEA. [2006]. Understanding and managing ageing of material in spent fuel storage facilities, *IAEA Technical Reports Series n°443*, p. 26.

[KATO, 2013] KATO, O. TANABE, H., SAKURAGI, T. NISHIMURA, T., and TATEISHI, T. [2013]. Corrosion tests of Zircaloy hull waste to confirm applicability of corrosion model and to evaluate influence factors on corrosion rate under geological disposal conditions, *Scientific Basis for Nuclear Waste Management XXXVII*, Barcelona, Spain, 29 September – 3 October 2013, Mat. Res. Soc. Symp. Proc. 1518.

[TAIT, 1994] TAIT, W.S. [1994]. *An introduction to electrochemical corrosion testing for practicing engineers and scientists*, (USA: Pair O Docs Publications).

[WALLACE, 1977] WALLACE, D. [1977]. Carbon-14 production in nuclear reactors, Oak Ridge National Laboratory, Tennessee, USA, Available from http://web.ornl.gov/info/reports/1977/3445605743782.pdf

Appendix 1: Precipitation probability of $CaCO_3$ (calcite) at pH 12.5

What is the solubility of $CaCO_3$ at 25°C?

$K_{ps} = 4.95\ 10^{-9}\ M^2 = [Ca^{2+}].[CO_3^{2-}]$

In a $Ca(OH)_2$ aqueous solution at a pH of 12.5, the concentration of Ca^{2+} is:

Strong base pH formula: $pH = 14 + \log [base]$

$=> 12.5 = 14 + \log [OH^-]$

$=> [OH^-] = 0.032\ M$

So, $[Ca^{2+}] = [OH^-]/2 = 0.016\ M$

Then, precipitation of $CaCO_3$ will start when the concentration of CO_3^{2-} reaches:

$[CO_3^{2-}] > K_{ps} / [Ca^{2+}] = 4.95\ 10^{-9} / 0.016$

$[CO_3^{2-}] > 3.1\ 10^{-7}\ M$ or $1.86\ 10^{-5}\ g/L$

Appendix 2: Validation of the measurement of methane, carbon dioxide, ethene, ethane, propene and propane in gas samples by the *GC-2010 Plus* gas chromatograph

1. Summary

In the Table A2-1, a summary of the validation results is given. More details can be found in the next chapters.

Table A2-1. *Summary of the validation results.*

Reporting limits	Methane: 0.4 µg/g Carbon dioxide: 3µg/g Ethene: 0.2 µg/g Ethane: 0.2 µg/g Propene: 1.5 µg/g Propane: 0.75µg/g
Linearity	From reporting limit to 10 µg/g (when a regression with weights 1/concentration is used)
Measurement uncertainty(*)	Methane: 0.2 µg/g or 5% of concentration (largest of both) Carbon dioxide: 2 µg/g or 5% of concentration (largest of both) Other gases: 1/3 of reporting limit or 5% of concentration (largest of both)

(*) Only a rough estimate of the measurement uncertainty can be given.

Note: The measurements for the validation study took place from December 2016 till February 2017 and chromatograms were acquired by means of the method *Method Cast- No headspace.gcm* (see SOP *Measurement of methane, carbon dioxide, ethene, ethane, propene and propane in gas samples by the GC-2010 plus A gas chromatograph* for more information).

2. Detection limits

Initially, detection limits were calculated by means of the noise in the proximity of the peak of interest as follows (Figure A2-1):

- A background section with width (time interval) at least equal to the width of the near peak (peak width at baseline) is determined.

- The slope of the approximated linear line for the data points within this section is calculated by the least square method.
- Two parallel lines are drawn by shifting the slope upward and downward, so that all data points within the section fall between two lines.
- The distance between the two parallel lines in the Y axis direction is the noise width for the section.
- The noise width is multiplied by 3 and this result is transformed to concentration (µg/g) via a calibration.

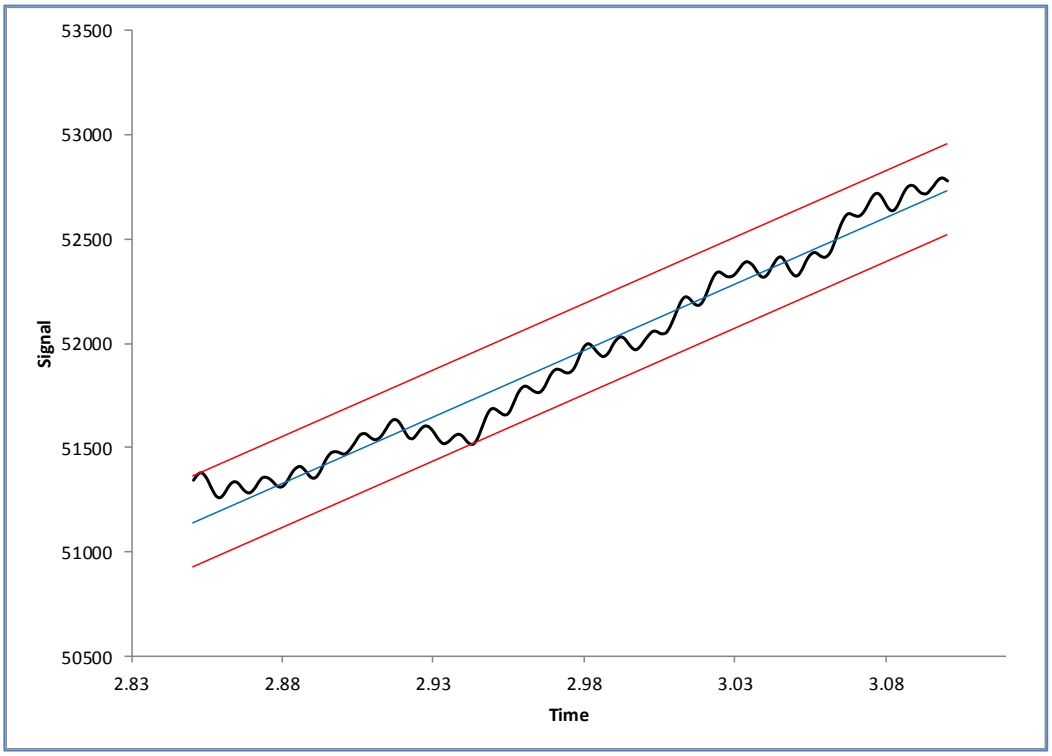

Figure A2-1. *Determination of detection limit by means of noise.*

Secondly, detection limits were also determined in a more practical way by measuring standards of successive lower concentrations (difference in concentration between successive standards was maximum a factor 2) until no (clear) peak was observed anymore.

Results of both methods are given in the Table A2-2:

Table A2-2. *Detection limits of analysed gases by gas chromatography*

	Detection limit (in µg/g) determined by means of the noise	**Detection limit (in µg/g) determined by measuring standards of successive lower concentrations**
Methane	0.11	0.10
Carbon dioxide	(0.11)	---
Ethene	0.19	0.10
Ethane	0.17	0.10
Propene	0.65	1.5
Propane	0.61	0.75

For carbon dioxide however, the above methods give no realistic value of the practical detection limit: because a direct injection technique of the sample is used, some air will always enter the column (and the detector), which results in carbon dioxide contamination. This of course influences the practical detection limit of carbon dioxide and must be taken into account.

Therefore, 59 blanks were measured over a period of 2 weeks. These blanks consisted of pure nitrogen or other standard gases in which no carbon dioxide was present. Approximately half of them were taken directly from the gas bottle and the other half from the gas mouse that was filled with the standard gas. No systematical difference in carbon dioxide concentration was observed between blanks from the bottle as compared to blanks from the gas mouse, from which it can be concluded that use of the gas mouse causes no further carbon dioxide contamination. The observed peak areas of the carbon dioxide in the blanks varied between 62 $x10^3$ and 299 $x10^3$, the average value was 180 $x10^3$ and the standard deviation 56 $x10^3$. For the calibration (see also further), all peak areas of the standards are corrected for the mean value of the blank (from all measured peak areas a value of 180 $x10^3$ is subtracted) and also when samples are measured, the carbon dioxide peak areas are corrected by this value. This implies that the detection limit can be defined as 3 times the standard deviation of the blank values, which means that the carbon dioxide detection limit equals a peak area of 168 $x10^3$ (3 times 56 $x10^3$), corresponding to a concentration of 3 µg/g.

Also it was noticed that sometimes a 'ghost peak' appeared at the retention time of methane. To investigate this further, 15 blanks were taken over a period of two weeks. These blanks were taken directly from the gas bottle with pure nitrogen as well as from the glove bag in which the experimental setups are placed (glove bag filled with nitrogen). Evaluation of these blank measurements revealed no systematic difference between blanks from the bottle compared to blanks from the glove bag, and in blanks corresponding methane concentrations between 0 and 0.40 µg/g were found, with an average of 0.13 µg/g and a standard deviation of 0.10 µg/g. As the average blank concentration (coming from the ghost peak) is very low and a ghost peak not always appeared, correction for the blank is not advisable. However, the detection limit will be influenced by the (occasional) appearance of a ghost peak and can be taken as the average corresponding methane concentration plus three times the standard deviation of the blank measurements, thus 0.4 µg/g.

The Table A2-3 gives the reporting limits, which are taken as the maximum (rounded up) of the detection limits determined by means of the different methods.

Table A2-3. *Reporting limits for the carbon-based gas by gas chromatography.*

	Reporting limits (µg/g)
Methane	0.4
Carbon dioxide	3
Ethene	0.2
Ethane	0.2
Propene	1.5
Propane	0.75

Remark concerning samples from the CAST project:

As samples in the framework of the CAST project are taken in a bag placed in a fume hood, which is flushed with pure nitrogen, a possible additional carbon dioxide contamination can occur when the nitrogen does not flush all air out of the bag. This was investigated by taking several samples (blanks) from the flushed bag and the results are given in Table A2-4. From these data we can see that, apart from the first measurement, peak areas do not significantly differ from the 'environmental/apparatus blank' that is described above. So, no additional correction seems needed. However, when it turns out that sample carbon

dioxide concentrations around the reporting limit (3 µg/g) are important (depends on the outcome of the CAST experiments), further investigation is advised.

Table A2-4. *Investigation of the additional carbon dioxide contamination.*

Date of measurement	Carbon dioxide peak area	Corresponding carbon dioxide concentration (µg/g) (*)
2017-01-18	521970	6
2017-01-19	183197	1
2017-02-06	256666	2
2017-02-07	205673	1
2017-02-08	157470	0
2017-02-14	122227	0

(*) Concentrations are calculated using the calibration curve described further in § 3 (peak areas are corrected for 'environmental/apparatus blank' of 180414 and concentrations are calculated using the corrected peak areas and an intercept of -57275 and a slope of 67721).

3. Linearity

Of each gas several standards with concentrations from the detection limit up to 10 µg/g were measured.

Different linear regression models were evaluated: unweighted, weighted with weights equal to 1/C (C = concentration) and weighted with weights equal to $1/C^2$. From these evaluations, it appeared that the models with weights equal to 1/C gave the best results, so these will be used for further routine measurements.

In the following figures, the calibration curves are presented and in the tables below some regression statistics are given. From the graphs and the values of the residuals, it can be concluded that for all gasses a linear relationship exists from the detection limit to 10 µg/g (when a regression with weights 1/C is used).

Note: All measured peak areas for carbon dioxide are corrected for the average blank (signal of 180 000, see §1). This means that peak areas from samples also have to be corrected for the blank, before the concentration is calculated by means of the

calibration curve. For example, a carbon dioxide peak area in a sample of 500 000 corresponds to a concentration of 5.6 µg/g:

[(500 000 - 180 000) - (-57275)] / 67721 = 5.6 (-57275 is the intercept of the calibration curve and 67721 the slope)

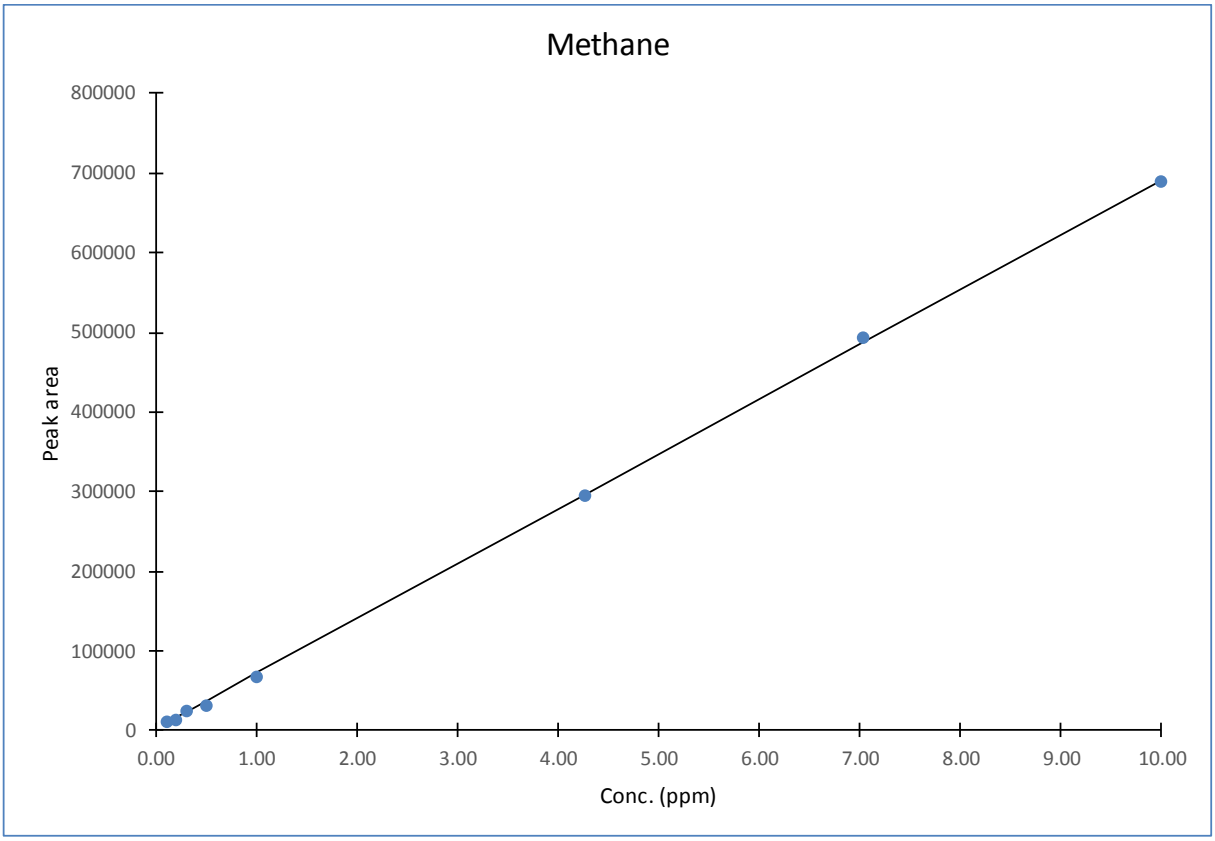

Methane

Conc. (µg/g)	Measured peak area	Calculated conc.	Residual in µg/g	Residual in %
0.10	12397	0.13	0.03	34
0.20	14171	0.16	-0.04	-21
0.30	24625	0.31	0.02	5
0.50	32860	0.43	-0.07	-14
1.00	67962	0.94	-0.06	-6
4.27	296015	4.27	-0.01	0
7.04	495056	7.17	0.12	2
10.00	689973	10.01	0.01	0

Intercept	3233
Slope	68640

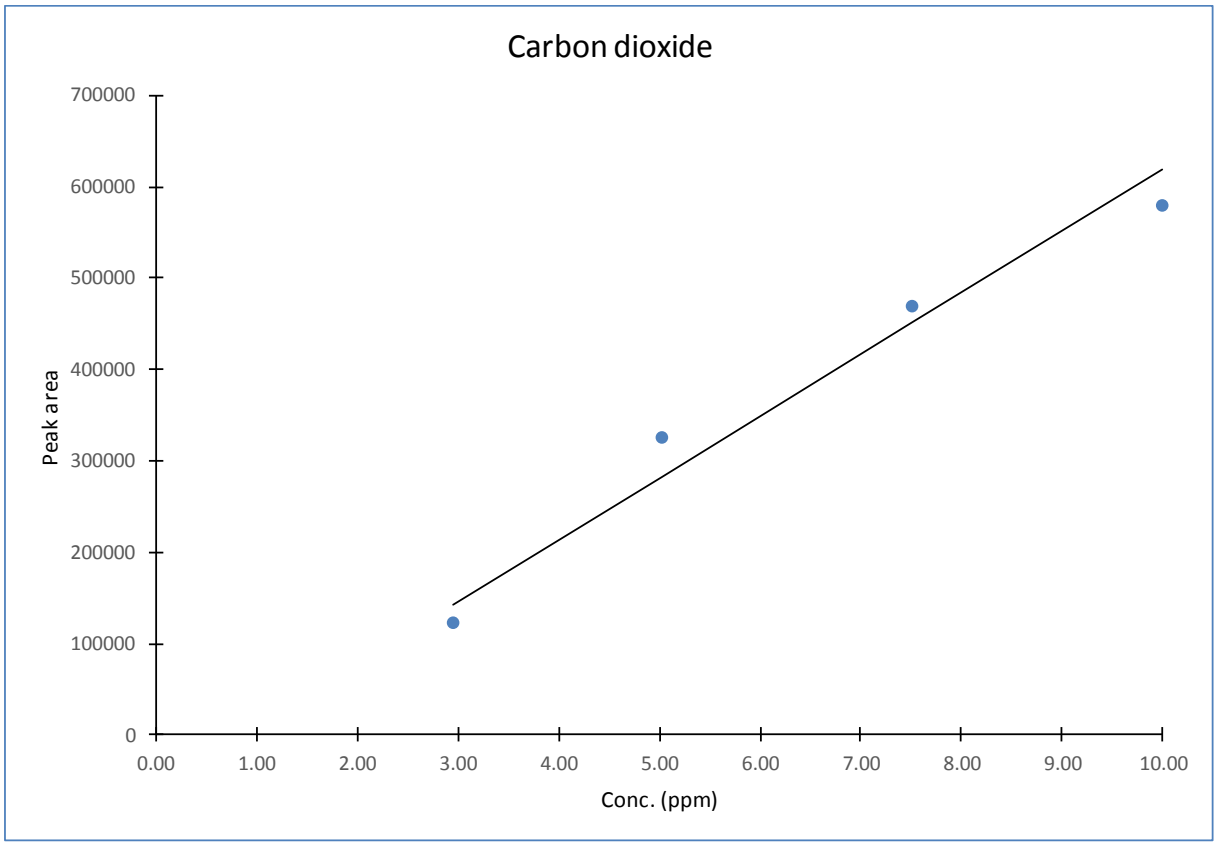

Carbon dioxide

Conc. (µg/g)	Measured peak area (corrected for blank)	Calculated conc.	Residual in µg/g	Residual in %
2.95	122174	2.65	-0.30	-10
5.03	326044	5.66	0.64	13
7.52	470022	7.79	0.27	4
10.00	579125	9.40	-0.60	-6

Intercept	-57275
Slope	67721

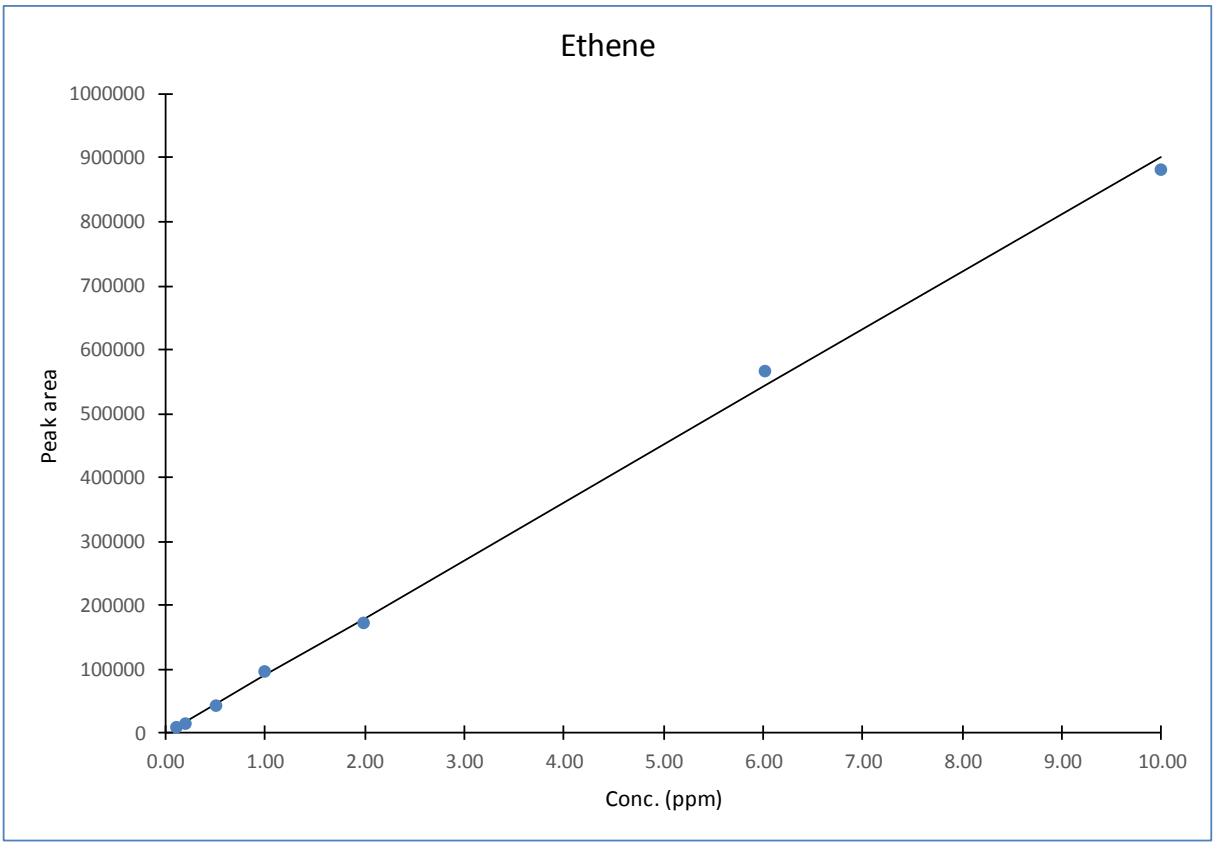

Ethene

Conc. (µg/g)	Measured peak area	Calculated conc.	Residual in µg/g	Residual in %
0.10	10485	0.11	0.01	14
0.20	15204	0.17	-0.03	-16
0.50	43173	0.48	-0.02	-4
1.00	96210	1.07	0.07	7
1.99	173095	1.92	-0.07	-3
6.02	566638	6.29	0.26	4
10.00	880847	9.77	-0.23	-2

Intercept	192
Slope	90093

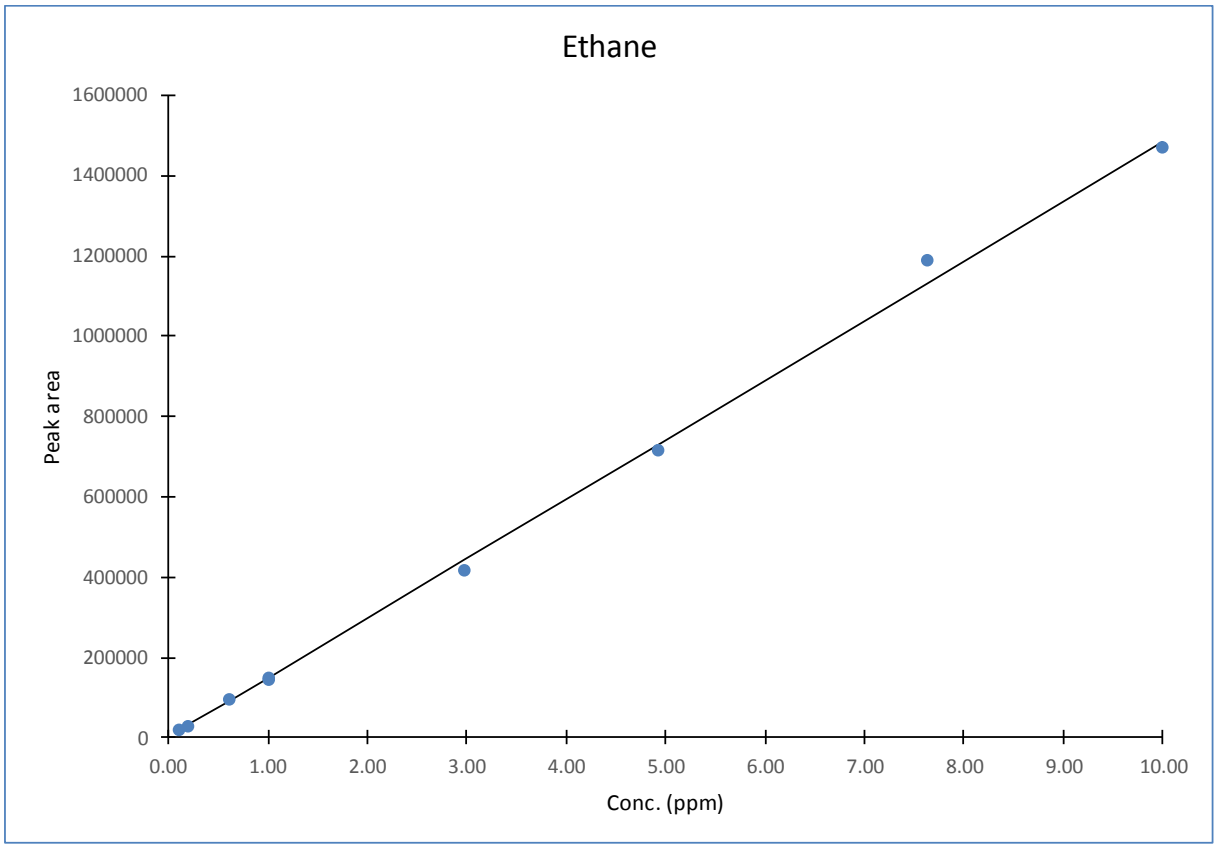

Ethane

Conc. (µg/g)	Measured peak area	Calculated conc.	Residual in µg/g	Residual in %
0.10	19021	0.11	0.01	15
0.20	30038	0.19	-0.01	-7
0.61	92870	0.61	0.01	1
1.00	143101	0.95	-0.05	-5
1.00	147592	0.98	-0.02	-2
2.98	418263	2.81	-0.16	-5
4.93	717848	4.84	-0.09	-2
7.63	1189578	8.02	0.39	5
10.00	1469406	9.92	-0.08	-1

Intercept	2004
Slope	147990

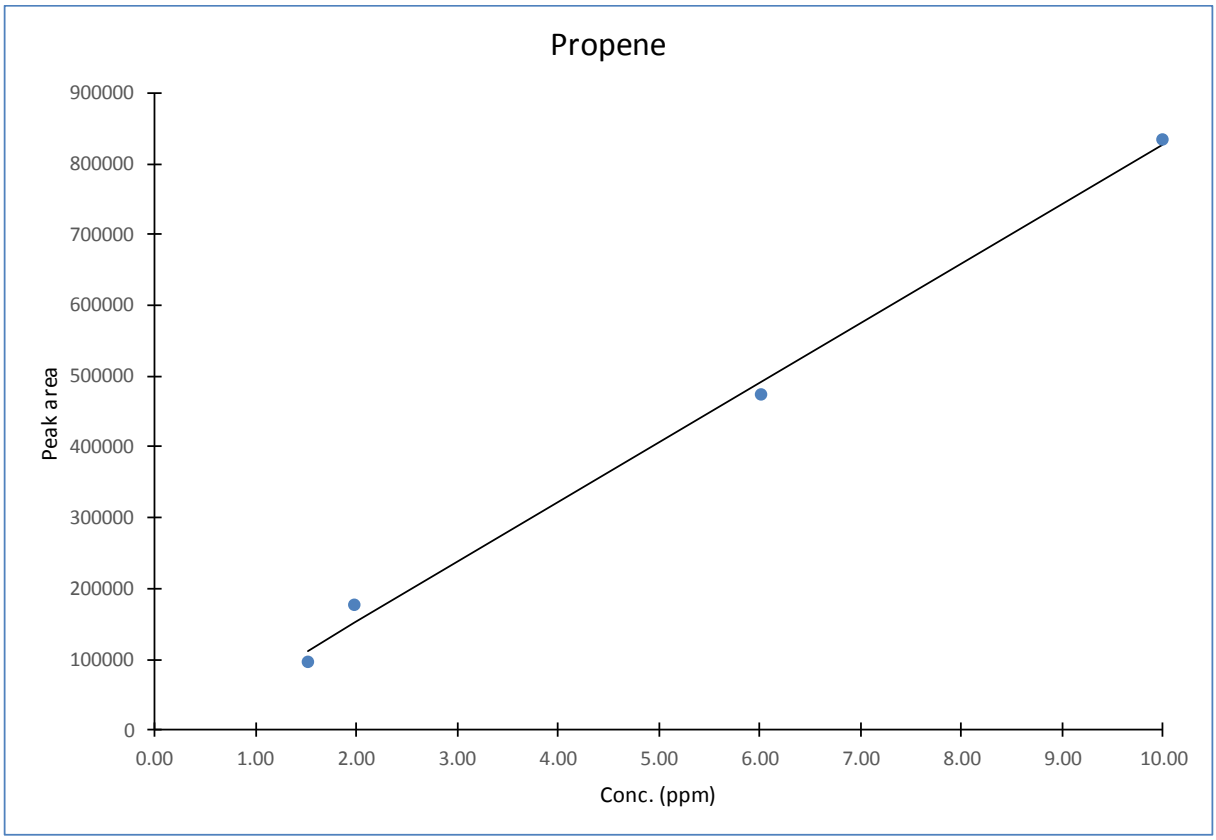

Propene

Conc. (µg/g)	Measured peak area	Calculated conc.	Residual in µg/g	Residual in %
1.53	96329	1.33	-0.20	-13
1.98	176171	2.28	0.30	15
6.02	474245	5.82	-0.20	-3
10.00	834735	10.10	0.10	1

Intercept	-15991
Slope	84238

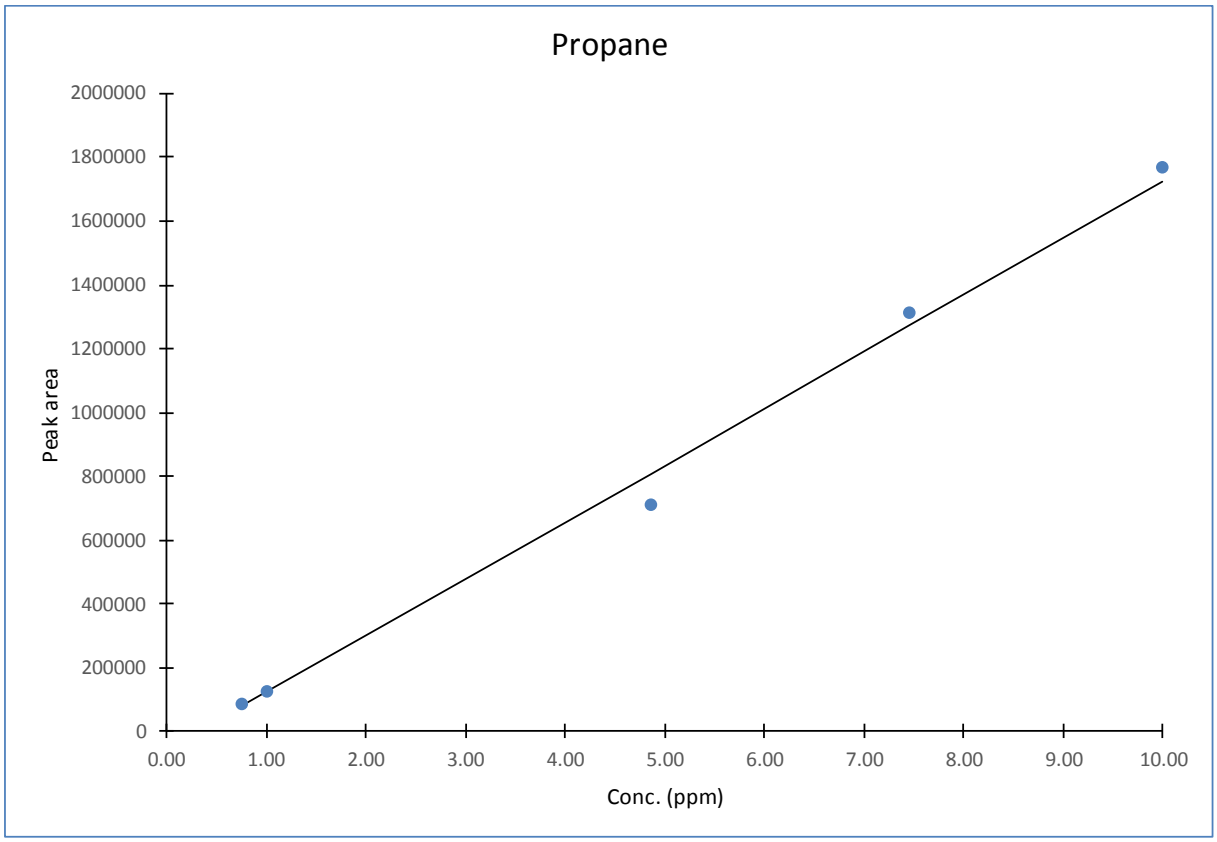

Propane

Conc. (µg/g)	Measured peak area	Calculated conc.	Residual in µg/g	Residual in %
0.76	86775	0.79	0.03	4
1.00	125659	1.01	0.01	1
4.85	709554	4.30	-0.56	-11
7.46	1314673	7.70	0.24	3
10.00	1770776	10.27	0.27	3

Intercept	-53835
Slope	177640

4. Measurement uncertainty

The calculated residuals (see § 2) can give us an idea of the measurement uncertainty: apart from one outlier (propane 4.85 µg/g), all residuals are less than or equal to one third of the reporting limit or 5 % of the concentration. So these values can be used as a (rough) estimate of the measurement uncertainty (95 % confidence interval).

The above applies to all gases, except to carbon dioxide at low concentrations (less than 40 µg/g) and methane at low concentrations (less than 4 µg/g):

- As the reporting limit of carbon dioxide is mainly determined by fluctuations in the 'environmental/apparatus blank', we need to take as measurement uncertainty for low concentrations a value of 2 times the standard deviation of the blank measurements, being 2 µg/g.

- As the reporting limit of methane is mainly determined by the occasional appearance of a ghost peak, we need to take as measurement uncertainty for low concentrations a value of 2 times the standard deviation of the methane concentrations that correspond to the peak areas of the ghost peak, being 0.2 µg/g.

Note: The procedure thus consists of calculating the value of 5 % of the concentration (in µg/g) and if this value is larger than 1/3 of the reporting limit (or 2 µg/g for carbon dioxide and 0.2 µg/g for methane), this is the measurement uncertainty. Else, the measurement uncertainty equals 1/3 of the reporting limit (or 2 µg/g for carbon dioxide and 0.2 µg/g for methane).

Example 1: In a sample, an ethane peak area of 400 000 is measured. From the calibration, it is calculated that this peak area corresponds to a concentration of 2.69 µg/g. 5 % of 2.69 µg/g is 0.13 µg/g, which is larger than 1/3 of the reporting limit of ethane (1/3 of the reporting limit is 0.07 µg/g). So, the measurement uncertainty is 0.13 µg/g and the result is expressed as: 2.69 µg/g ± 0.13 µg/g.

Example 2: In a sample, a propene peak area of 200 000 is measured. From the calibration, it is calculated that this peak area corresponds to a concentration of 2.56 µg/g. 5 % of 2.56 µg/g is 0.13 µg/g, which is lower than 1/3 of the reporting limit of propene (1/3 of the reporting limit is 0.5 µg/g). So, the measurement uncertainty is 0.5 µg/g and the result is expressed as: 2.6 µg/g ± 0.5 µg/g.

Example 3: In a sample, a carbon dioxide peak area of 500 000 is measured. This value is corrected for the blank (180 000, see § 1), which gives a corrected peak area of 320 000. From the calibration, it is calculated that a (corrected) peak area of 320 000 corresponds to a concentration of 5.6 µg/g. 5 % of 5.6 µg/g is 0.28 µg/g, which is lower than 2 µg/g. So, the measurement uncertainty is 2 µg/g and the result is expressed as: 5.6 µg/g ± 2.0 µg/g.

An important remark is that the above derived measurement uncertainties strictly speaking only apply to standards (only measurements of standards were used). This however is the best we can do: determination of the measurement uncertainties for real samples requires at least multiple measurements of the same samples, which is impossible as we have very little amounts of the real samples. On the other hand, because it is known that in gas chromatography matrix effects are very limited, the measurement uncertainties of standards can be considered as representative for real samples (to a certain extent).

Appendix 3. Corrosion rate calculation from the I vs. t plot

Hypotheses:

- All the recorded current come from the corrosion of the Zircaloy-4 sample

- Only the oxydation of Zr° in Zr^{4+} is considered

Taking into account:

Parameters	Parameter symbol	Values
Corrosion time, unirradiated Zircaloy-4	$t_{corr,unirr}$	604510 seconds
Corrosion time, irradiated Zircaloy-4	$t_{corr,irr}$	587880 seconds
Density of Zircaloy-4	ρ_{Zry-4}	6.56 g/cm³
Mean specific surface of unirradiated Zircaloy-4	$A_{corr,unirr}$	1.13 cm²
Mean specific surface of irradiated Zircaloy-4	$A_{corr,irr}$	0.73 cm²
Molecular weight	MM_{Zr}	91.224 g/mol
Avogadro number	N_A	6.023×10^{23} mol^{-1}

Unirradiated Zircaloy-4 sample

Thanks to the potentiostatic I vs. t plot, the mean current (<I>) was calculated:

$<I> = 5.4 \times 10^{-9}$ A

Knowing the corrosion time ($t_{corr,unirr}$), it is possible to calculate the total charge (Q):

$Q = <I> \times t_{corr,unirr} = 5.4 \times 10^{-9} \times 604510 = 3.27 \times 10^{-3}$ C

Knowing that 1C is equivalent to the charge of approximately 6.2415×10^{18} electrons, the number of electrons involved (N_{e-}) is:

$N_{e-} = Q \times 6.2415 \times 10^{18} = 3.27 \times 6.2415 \times 10^{18} = 2.04 \times 10^{16}$ e^-

Four electrons are involved in the corrosion of one atom of iron ($Zr° \rightarrow Zr^{4+} + 4e^-$). So, the number of iron atoms involved (N_{Zr}) is:

$N_{Zr} = N_{e-} / 4 = 2.04 \times 10^{16} / 4 = 5.1 \times 10^{15}$ zirconium atoms

And the number of mol of iron (n_{Zr}) is:

$n_{Zr} = N_{Zr} / N_A = 5.1 \times 10^{15} / 6.023 \times 10^{23} = 8.5 \times 10^{-9}$ mol of Zr

Making the approximation that the Zircaloy-4 is only composed of zirconium, the weight of corroded Zircaloy-4 (W_{Zry-4}) is:

$W_{Zry-4} = n_{Zr} \times MM_{Zr} = 8.5 \times 10^{-9} \times 91.224 = 7.7 \times 10^{-7}$ g of zirconium

$= 7.7 \times 10^{-7}$ g of Zircaloy-4

Finally, knowing the specific surface of Zircaloy-4 ($A_{corr,unirr}$) and the Zircaloy-4 density (ρ_{Zry-4}), the corrosion depth (Corr. Depth) is:

Corr. Depth = $(W_{Zry-4} / \rho_{Zry-4}) / A_{corr} = (7.7 \times 10^{-7} / 6.56) / 1.13 = 1.04 \times 10^{-7}$ cm = 1.04 nm

And the corrosion rate (per year) is:

1.04 / 604510 x (365.25 x 24 x 60 x 60) = **54 nm/year**

Irradiated Zircaloy-4 sample

The same calculation was made for the corrosion of the irradiated Zircaloy-4 sample and the corrosion rate is **4 nm/year**.

Appendix 4. Formation of methane from static corrosion of Zircaloy-4

Hypothesis:

- All the carbon is used to form methane during corrosion.

- The carbon is homogeneously present in the bulk

Taking into account:

Parameter	Parameter symbol	Values
Concentration of carbon in Zircaloy-4	$C_{content}$	270 µg/g
Density of Zircaloy-4	ρ_{Zry-4}	6.56 g/cm³
Density of methane	ρ_{CH4}	$6.56x10^{-4}$ g/cm³
Corroded surface of Zircaloy-4	A_{corr}	1.13 cm²
Corroded depth of Zircaloy-4	D_{corr}	0.02 cm
Molecular weight of Carbon	MW_C	12.011 g/mol
Molecular weight of Methane	MW_{CH4}	16.142 g/mol
Headspace corrosion vial	V_{HS}	1.045 L

Calculation:

The weight of corroded Zircaloy-4 (W_{Zry-4}) equals:

$W_{Zry-4} = A_{corr} \times D_{corr} \times \rho_{Zry-4} = 1.13 \times 0.02 \times 6.56 = 0.148$ g

The concentration of carbon in Zircaloy-4 is 270 µg/g (270 ppm).

In 0.148 g, there is 40 µg of carbon, which corresponds to a number of moles (n_C) of

$N_C = 4x10^{-5}/12.011$ mol C $= 3.327x10^{-6}$ mol C

Considering that all the carbon that is removed from the bulk during corrosion is transformed in methane, $3.327x10^{-6}$ mol of methane (n_{CH4}) will be produced. The weight of methane (W_{CH4}) produced can then be calculated:

$W_{CH4} = n_{CH4} \times MW_{CH4} = 3.327x10^{-6} \times 16.142 = 5.37x10^{-5}$ g = 53.7 µg of methane.

And the volume of methane produced is:

$V_{CH4} = W_{CH4} / \rho_{CH4} = 5.37x10^{-5} / 6.56x10^{-4} = 8.19x10^{-2}$ cm³ = 81.9 µL of methane.

So, taking into account the volume of the headspace (1.045 L), the concentration in µg/g of produced methane (C_{CH4}) is:

$C_{CH4} = 81.9 / 1.045 = 78.34$ µg/g

Appendix 5. Corrosion rate calculation from the carbon-based gas production during the static tests

Hypothesis:

- All the carbon is used to form methane, ethene or carbon dioxide during corrosion.
- The carbon is homogeneously present in the bulk

Taking into account:

Parameter	Parameter symbol	Values
Concentration of carbon in Zircaloy-4	$C_{content}$	270 µg/g
Density of Zircaloy-4	ρ_{Zry}	6.56 g/cm³
Density of methane	ρ_{CH4}	6.56 x10^{-4} g/cm³
Density of ethene	ρ_{C2H4}	1.18 x10^{-3} g/cm³
Density of carbon dioxide	ρ_{CO2}	1.87 x10^{-3} g/cm³
Mean specific surface of Zircaloy-4	A_{corr}	11.58 cm²
Head Space volume	V_{HS}	15 cm³
Molecular weight of methane	MW_{CH4}	16.043 g/mol
Molecular weight of ethene	MW_{C2H4}	28.054 g/mol
Molecular weight of carbon dioxide	MW_{CO2}	44.01 g/mol
Molecular weight of carbon	MW_{C}	12.011 g/mol
Mean concentration of methane	C_{CH4}	6.45 µL/L (µg/g)
Mean concentration of ethene	C_{C2H4}	0.97 µL/L (µg/g)
Mean concentration of carbon dioxide	C_{CO2}	3.93 µL/L (µg/g)

Calculation:

Methane:

The volume of methane (V_{CH4}) produced during corrosion equals:

$V_{CH4} = C_{CH4} \times V_{HS} = 6.45 \times 0.015 = 0.097$ µL $= 9.68 \times 10^{-5}$ cm³

Knowing the density of methane (ρ_{CH4}), the weight of methane (W_{CH4}) produced can be calculated as follows :

$W_{CH4} = V_{CH4} \times \rho_{CH4} = 9.68 \times 10^{-5} \times 6.56 \times 10^{-4} = 6.35 \times 10^{-8}$ g

Which corresponds to a number of mole (n_{CH4}) of:

$n_{CH4} = W_{CH4} / MW_{CH4} = 6.35 \times 10^{-8} / 16.043 = 3.96 \times 10^{-9}$ moles of $CH_4 = 3.96 \times 10^{-9}$ moles of carbon

Ethene:

The volume of ethene (V_{C2H4}) produced during corrosion equals:

$V_{C2H4} = C_{C2H4} \times V_{HS} = 0.97 \times 0.015 = 0.0146$ µL $= 1.46 \times 10^{-5}$ cm³

Knowing the density of ethene (ρ_{C2H4}), the weight of ethene (W_{C2H4}) produced can be calculated as follows :

$W_{C2H4} = V_{C2H4} \times \rho_{C2H4} = 1.46 \times 10^{-5} \times 1.18 \times 10^{-3} = 1.72 \times 10^{-8}$ g

Which corresponds to a number of mole (n_{C2H4}) of:

$n_{C2H4} = W_{C2H4} / MW_{C2H4} = 1.72 \times 10^{-8} / 28.054 = 6.12 \times 10^{-10}$ moles of $C_2H_4 = 1.224 \times 10^{-9}$ moles of carbon

Carbon dioxide:

The volume of carbon dioxide (V_{CO2}) produced during corrosion equals:

$V_{CO2} = C_{CO2} \times V_{HS} = 3.93 \times 0.015 = 0.059$ µL $= 5.9 \times 10^{-5}$ cm³

Knowing the density of carbon dioxide (ρ_{CO2}), the weight of carbon dioxide (W_{CO2}) produced can be calculated as follows:

$W_{CO2} = V_{CO2} \times \rho_{CO2} = 5.9 \times 10^{-5} \times 1.87 \times 10^{-3} = 1.1 \times 10^{-7}$ g

Which corresponds to a number of mole (n_{CO2}) of:

$n_{CO2} = W_{CO2} / MW_{CO2} = 1.1 \times 10^{-7} / 44.01 = 2.505 \times 10^{-9}$ moles of $CO_2 = 2.505 \times 10^{-9}$ moles of carbon

Taking into account the above calculations, the total mole amount of carbon released ($C_{released}$) is:

$C_{released} = n_{CH4} + 2x\, n_{C2H4} + n_{CO2} = 3.96 \times 10^{-9} + 1.224 \times 10^{-9} + 2.505 \times 10^{-9} = 7.69 \times 10^{-9}$ mol

Considering the molecular weight of carbon (MW_C), it is possible to calculate the weight of carbon released (W_C)

$W_C = C_{released} \times MW_C = 7.69 \times 10^{-9} \times 12.011 = 9.24 \times 10^{-8}$ g = 92.4 ng

And with the concentration of carbon in the Zircaloy-4 bulk ($C_{content}$), it is possible to calculate the weight of corroded metal ($W_{Zry\text{-}corr}$):

$W_{Zry\text{-}corr} = W_C / C_{content} = 9.24 \times 10^{-8} / 0.00027 = 3.42 \times 10^{-4}$ g = 341.6 µg

Finally, knowing the specific surface of Zircaloy-4 (A_{corr}) and the Zircaloy-4 density (ρ_{Zry}), the corrosion depth (Corr. Depth) after 195 days is:

Corr. Depth = $(W_{Zry\text{-}corr} / \rho_{Zry}) / A_{corr} = (3.42 \times 10^{-4} / 6.56) / 11.58 = 4.5 \times 10^{-6}$ cm = 45 nm

And the corrosion rate (per year) is:

45 / 195 x 365 = **84 nm/year**

Due to the high uncertainties on the CO_2 concentration, we also calculated the corrosion rate without taking into account the CO_2 contribution. In these conditions, the calculated corrosion rate equals **57 nm/year.**

Appendix 6. Corrosion rate calculation from the carbon-based production (gas and liquid phase) during the static tests (adjusted calculation from Appendix 5)

Hypothesis:

- All the carbon is used to form methane, ethene and carbon dioxide from the gas phase and, from formate and acetate from the liquid phase during corrosion.

- The carbon is homogeneously present in the bulk

Taking into account:

Parameter	Parameter symbol	Values
Concentration of carbon in Zircaloy-4	$C_{content}$	270 µg/g
Density of Zircaloy-4	ρ_{Zry}	6.56 g/cm³
Mole of C realised in the gas phase	$C_{released,\ gas\ phase}$	7.69 x10^{-9} mol
Mean specific surface of Zircaloy-4	A_{corr}	11.58 cm²
Head Space volume	V_{HS}	15 cm³
Liquid volume	V_L	35 cm³ (0.035 L)
Molecular weight of formate	MW_{HCO2}	45.018 g/mol
Molecular weight of acetate	MW_{H3C2O2}	59.045 g/mol
Molecular weight of carbon	MW_C	12.011 g/mol
Mean concentration of formate	C_{HCO2}	2.6 x10^{-4} g/L
Mean concentration of acetate	C_{H3C2O2}	7.2 x10^{-5} g/L

Calculation:

Formate:

The number of mol of formate in 35 mL of solution (n_{HCO2}) produced during corrosion equals:

$$n_{HCO2} = (C_{HCO2} / MW_{HCO2}) \times V_L = (2.6 \times 10^{-4} / 45.018) \times 0.035 = 2.02 \times 10^{-7} \text{ mol of } HCO_2$$

$$= 2.02 \times 10^{-7} \text{ mol of C}$$

Acetate:

The number of mol of formate in 35 mL of solution (n_{H3C2O2}) produced during corrosion equals:

$$n_{H3C2O2} = (C_{H3C2O2} / MW_{H3C2O2}) \times V_L = (7.2 \times 10^{-5} / 59.045) \times 0.035$$

$$= 4.27 \times 10^{-8} \text{ mol of } H_3C_2O_2$$

$$= 8.54 \times 10^{-8} \text{ mol of C}$$

Taking into account calculation hereunder, the total mole amount of carbon released in the liquid phase under the formate and acetate form ($C_{released, liq. phase}$) is:

$$C_{released, liq. phase} = n_{HCO2} + 2x\, n_{H3C2O2} = 2.02 \times 10^{-7} + 8.54 \times 10^{-8} = 2.87 \times 10^{-7} \text{ mol}$$

And, knowing the amount of mole of C realised in the gas phase ($C_{released,\ gas\ phase}$) (obtained from Appendix 6), the total amount of carbon released ($C_{released}$) is:

$C_{released} = C_{released,liq.phase} + C_{released,\ gas\ phase} = 2.87 \times 10^{-7} + 7.69 \times 10^{-9} = 2.95 \times 10^{-7}$ mol

Considering the molecular weight of carbon (MW_C), it is possible to know the weight of carbon released (W_C)

$W_C = C_{released} \times M_{WC} = 2.95 \times 10^{-7} \times 12.011 = 3.54 \times 10^{-6}$ g

And with the concentration of carbon in the Zircaloy-4 bulk ($C_{content}$), it is possible to know the weight of corroded metal ($W_{Zry\text{-}corr}$):

$W_{Zry\text{-}corr} = W_C / C_{content} = 3.54 \times 10^{-6} / 0.00027 = 1.31 \times 10^{-2}$ g

Finally, knowing the specific surface of Zircaloy-4 (A_{corr}) and the Zircaloy-4 density (ρ_{Zry}), the corrosion depth (Corr. Depth) after 195 days is:

Corr. Depth = $(W_{CS\text{-}corr} / \rho_{Zry}) / A_{corr} = (1.31 \times 10^{-2} / 6.56) / 11.58 = 1.73 \times 10^{-4}$ cm = **1.73 µm** after 195 days !

This simple calculation clearly show that formate and acetate detected after static corrosion did not come only from the corrosion but also from contamination of the saturated portlandite solution use to make the corrosion tests.

Appendix 7. Total inorganic / organic carbon content and ion chromatography results

Table A7-1 and A7-2 present the results of respectively the total inorganic / organic carbon content and the concentration of carboxylic acids (formate, acetate and oxalate) realised on blank electrolytes and on all leachate solutions after static and accelerated corrosion tests without substraction of the blank values.

Table A7-1. *Results from total organic / inorganic carbon analysis of blank electrolytes and the Zircaloy-4 leachates.*

Sample-ID	Electrolyte/Material	TIC (mg/L)	TOC (mg/L)
Blank-$Ca(OH)_2$	Saturated portlandite water solution	6.4 ± 0.8	4.4 ± 0.5
Blank-$CaCl_2$	Saturated $Ca(OH)_2$ water solution + 0.5 M $CaCl_2$	7.4 ± 0.7	7.4 ± 0.7
Inactive-Zry-4_ $Ca(OH)_2$	Unirradiated Zircaloy-4 / Accelerated test / $Ca(OH)_2$ water solution	6.6 ± 0.2	8.3 ± 0.8
Inactive-Zry-4_ $CaCl_2$	Unirradiated Zircaloy-4 / Accelerated test / $Ca(OH)_2$ + $CaCl_2$ water solution	18.2 ± 0.5	11.5 ± 1.1
Active-Zry-4_ $Ca(OH)_2$	Irradiated Zircaloy-4 / Accelerated test / $Ca(OH)_2$ water solution	< 0.5	23.8 ± 2.4
Active-Zry-4_ $CaCl_2$	Irradiated Zircaloy-4 / Accelerated test / $Ca(OH)_2$ + $CaCl_2$ water solution	1.0 ± 0.5	2.1 ± 0.5
Sol-F6678-R4-A	Irradiated Zircaloy-4 / Static test / $Ca(OH)_2$ water solution	< 0.5	1.8 ± 0.5
Sol-F6678-R4-B	Irradiated Zircaloy-4 / Static test / $Ca(OH)_2$ water solution	< 0.5	2.0 ± 0.5
Sol-F6678-R4-C	Irradiated Zircaloy-4 / Static test / $Ca(OH)_2$ water solution	< 0.5	2.0 ± 0.5

Table A7-2. *Carboxylic acid content analysis by ion chromatography results of the Zircaloy-4 leachates and blank electrolytes.*

Sample ID	Electrolyte / Material	Formate (mg/L)	Acetate (mg/L)	Oxalate (mg/L)
Blank-$Ca(OH)_2$	Saturated portlandite water solution	0.16 ± 0.02	0.14 ± 0.01	< 0.1
Blank-$CaCl_2$	Saturated $Ca(OH)_2$ water solution + 0.5 M $CaCl_2$	< 0.1	< 0.1	< 0.1
Inactive-Zry-4_$Ca(OH)_2$	Unirradiated Zircaloy-4 / Accelerated test / $Ca(OH)_2$ water solution	0.14 ± 0.1	0.32 ± 0.03	< 0.1
Inactive-Zry-4_$CaCl_2$	Unirradiated Zircaloy-4 / Accelerated test / $Ca(OH)_2$ + $CaCl_2$ water solution	< 0.1	< 0.1	< 0.1
Active-Zry-4_$Ca(OH)_2$	Irradiated Zircaloy-4 / Accelerated test / $Ca(OH)_2$ water solution	0.28 ± 0.03	0.27 ± 0.03	< 0.1
Active-Zry-4_$CaCl_2$	Irradiated Zircaloy-4 / Accelerated test / $Ca(OH)_2$ + $CaCl_2$ water solution	< 0.1	< 0.1	< 0.1
Sol-F6678-R4-A	Irradiated Zircaloy-4 / Static test / $Ca(OH)_2$ water solution	0.51 ± 0.05	0.20 ± 0.02	< 0.1
Sol-F6678-R4-B	Irradiated Zircaloy-4 / Static test / $Ca(OH)_2$ water solution	0.44 ± 0.04	0.20 ± 0.02	< 0.1
Sol-F6678-R4-C	Irradiated Zircaloy-4 / Static test / $Ca(OH)_2$ water solution	0.31 ± 0.03	0.24 ± 0.02	< 0.1